AD-A108 762 ANALYTICAL TECHNOLOGY APPLICATIONS CORP SUNNYVALE CA F/G 12/1
AMBIGUITY SURFACE STATISTICS AND OVERCONTAINMENT.(U)
SEP 81 J LAPOINTE N00014-80-C-0698
UNCLASSIFIED ATAC-SV8007-1 NL

1 OF 2
AD A
108762

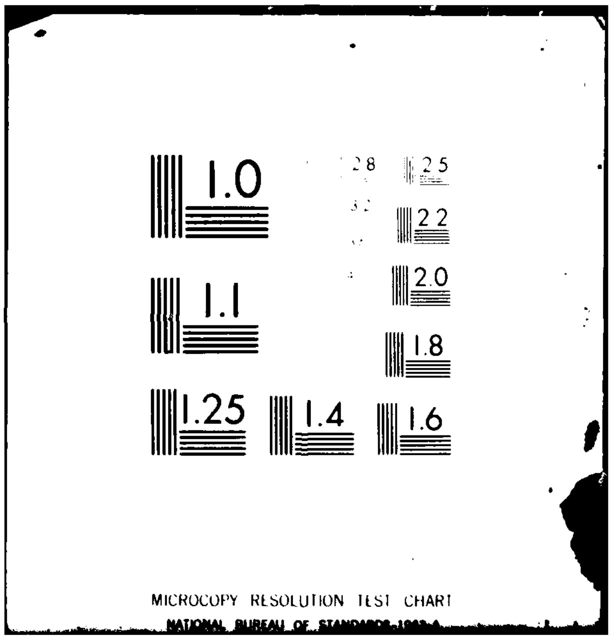
1.0
2.8
2.5
3.2
2.2
3.6
2.0
4.0
1.1
1.8
1.25
1.4
1.6
MICROCOPY RESOLUTION TEST CHART
NATIONAL BUREAU OF STANDARDS-1963-A

ANALYTICAL TECHNOLOGY APPLICATIONS CORPORATION

P.O. BOX 62199 • SUNNYVALE, CA 94088 • (408) 736-8200

Final Report SV8007-1

12

30 September 1981

LEVEL II

AD A108762

AMBIGUITY SURFACE STATISTICS AND OVERCONTAINMENT

117

Prepared for:

Statistics and Probability Program
(Code 411SP)
Office of Naval Research
Arlington, VA 22217

Contract No. N00014-80-C-0698

Prepared by:

Joseph LaPointe, Jr.

Approved for public release; distribution unlimited.

UNCLASSIFIED

SECURITY CLASSIFICATION OF THIS PAGE (When Data Entered)

REPORT DOCUMENTATION PAGE

READ INSTRUCTIONS BEFORE COMPLETING FORM

1. REPORT NUMBER SV8007-1	2. GOVT ACCESSION NO. AD-A11 8762	3. RECIPIENT'S CATALOG NUMBER
4. TITLE (and Subtitle) Ambiguity Surface Statistics and Overcontainment		5. TYPE OF REPORT & PERIOD COVERED Final Report
		6. PERFORMING ORG. REPORT NUMBER ATAC Recport No. SV8007-1
7. AUTHOR(s) Joseph LaPointe, Jr.		8. CONTRACT OR GRANT NUMBER(s) N00014-80-C-0698
9. PERFORMING ORGANIZATION NAME AND ADDRESS Analytical Technology Applications Corporation 491 Macara Avenue, Suite 1011 Sunnyvale, CA 94086		10. PROGRAM ELEMENT, PROJECT, TASK AREA & WORK UNIT NUMBERS 61153N RR 014-05-01 NR 042-471
11. CONTROLLING OFFICE NAME AND ADDRESS Statistics and Probability Program (Code 411SP) Office of Naval Research Arlington, VA 22217		12. REPORT DATE 30 September 1981
		13. NUMBER OF PAGES 120
14. MONITORING AGENCY NAME & ADDRESS (if different from Controlling Office) N/A		15. SECURITY CLASS. (of this report) UNCLASSIFIED
		15a. DECLASSIFICATION DOWNGRADING SCHEDULE N/A

16. DISTRIBUTION STATEMENT (of this Report)

"Approved for Public Release; Distribution Unlimited"

17. DISTRIBUTION STATEMENT (of the abstract entered in Block 20, if different from Report)

N/A

18. SUPPLEMENTARY NOTES

19. KEY WORDS (Continue on reverse side if necessary and identify by block number)

Correlation detection, Signal overcontainment, Ambiguity surface statistics, Surface filtering

20. ABSTRACT (Continue on reverse side if necessary and identify by block number)

Cross-correlation algorithms can be used to detect a signal that is common to both channels. The current understanding of the performance of cross-correlation algorithms is based on the assumption that the processing and signal bandwidths are equal. Under these conditions, it is well known that the signal-to-noise power ratio (SNR) required to achieve a desired performance decreases as the integration time increases. However, in practice,

DD FORM 1473, 1 JAN 73 — EDITION OF 1 NOV 65 IS OBSOLETE

UNCLASSIFIED

SECURITY CLASSIFICATION OF THIS PAGE (When Data Entered)

20. (continued)

it is usually necessary to use a processing bandwidth that is larger than the signal bandwidth (called signal overcontainment) because the signal bandwidth or the signal center frequency are only known approximately. The detection performance of cross-correlation algorithms is derived for the signal overcontainment case. It is shown that the SNR can be decreased by increasing the signal overcontainment for small signal "time-bandwidth" products. It is also shown that for moderate to large signal "time-bandwidth" products, the SNR increases with increasing signal overcontainment, but that the SNR increases very slowly with increasing signal overcontainment.

Image filtering algorithms can be used to enhance the features of an ambiguity surface and thereby improve the detection performance. The P_{FA} at the output of these filters is easily related to the single cell threshold when the noise cells are independent. However, ambiguity surfaces are oversampled to magnify features of the surface when signal is present. It is shown that the P_{FA} at the output of the filters is no longer simply related to the single cell threshold when the surface is oversampled.

EXECUTIVE SUMMARY

The use of cross-correlation for detecting and tracking the source of signals received at spatially separated receiving sites has occupied considerable attention in the research community during recent years. It is necessary to understand the statistical nature of ambiguity surfaces and the interdependence of the cells in the surface under conditions of signal level fluctuation and signal overcontainment in order to accurately evaluate the tracking accuracies and the detection performance of single-cell detectors and surface filters. The current understnding of the statistical nature of ambiguity surfaces is based on the probability density function (PDF) of a single cell for matched containment where the processing and signal bandwidths are equal. However, in actual practice, signals are overcontained because the processing bandwidth is usually larger than the signal bandwidth and the data is oversampled to magnify the surface features. In this study, the current understanding of the statistical nature of ambiguity surfaces is extended to include (1) the effects of overcontainment on detection performance and (2) the dependency between cells of a surface.

The signal-to-noise power ratio (SNR) needed to achieve a specified P_D and P_{FA} can be reduced by overcontaining the signal when the signal time-bandwidth product (N_S) is small ($N_S < 12$). This gain is caused by increasing the noise time-bandwidth product (N_P) through overcontainment which, in effect, produces a better estimate of the background noise. However, for $N_S \geq 12$, there is no gain and the SNR increases with overcontainment because the increase in noise power dominates the effects of increased N_P.

An approximation to the exact detection performance was developed because the exact performance equations are difficult to evaluate. The approximation is based on using the matched containment performance equations and the true magnitude-squared correlation coefficient in the processing band. The approximate performance is very close to the exact performance for overcontainments of practical interest, though the approximate SNRs are slightly smaller than the exact SNRs. However, the approximation should be used with care for large overcontainments because the approximate and exact SNRs differ significantly.

The joint probability density function (PDF) of two cells in a surface was derived for the matched containment case. The cells in a surface are independent only if the surface is not oversampled. Oversampling is defined as cells of width less than $1/2W_p$ sec. in time delay and $1/T$ Hz in Doppler shift, where T is the observation time and $2W_p$ is the processing bandwidth. This has an impact on surface filters because surfaces are sometimes oversampled to magnify the features. When surfaces are oversampled, there is no longer a simple analytical expression for selecting the cell threshold to achieve a desired P_{FA} at the filter output.

ACKNOWLEDGEMENTS

The support of Mr. R. Trueblood of the DARPA Acoustic Research Center (ARC) is gratefully acknowledged. Mr. Trueblood provided computer time at the ARC for evaluating the performance equations and access to real ocean acoustic data.

The support of many other individuals in the ARC community is also gratefully acknowledged. These individuals are too numerous to name, but they provided support in the form of technical discussions and overcoming problems encountered at the ARC. In particular, Mr. G. Godshalk of ENSCO, Inc., provided invaluable support by keeping me abreast of the simulation results for the ENSCO "M out of N" sufrace filter and allowing me to participate in the Minimum Detectable Signal Experiment with the ENSCO team.

CONTENTS

PRECEDING PAGE BLANK-NOT FILMED

CONTENTS (continued)

LIST OF FIGURES

LIST OF FIGURES (continued)

I. INTRODUCTION

The use of cross-correlation for detecting and tracking the source of signals received at spatially separated receiving sites has received considerable attention in the research community during recent years. It is necessary to understand the statistical nature of ambiguity surfaces and the interdependence of the cells in the surface under realistic operational conditions in order to accurately evaluate the tracking accuracies and the detection performance achievable with cross-correlation. The limited understanding of the statistical nature of ambiguity surfaces is based on the statistics of a single cell in the absence of signal-power fluctuation and for equal signal and processing bandwidths (herein called matched containment (ref. 1-4)). The effects of signal-power level fluctuations and signal overcontainment, where the processing bandwidth is larger than the signal bandwidth, must be quantified in order to fully understand the statistical nature of ambiguity surfaces under realistic opertional conditions. The study results presented in this report address the effects of signal overcontainment on detection performance and the correlation between the cells in a surface in the absence of signal-level fluctuations.

An ambiguity surface is a two-dimensional function, $\gamma^2(\tau, f_D)$, which is the sample magnitude-squared of the normalized cross-correlation between the observations received at two spatially separated sites as a function of the relative time delay (τ) and relative Doppler shift (f_D) between the observations. The surface is generated for a specific integration time (T) and processing bandwidth ($2W_P$) as shown in Figure 1-1. In actual practice, the processing bandwidth is always larger than or equal to the signal bandwidth. Since the ambiguity surface is usually computed digitally, the ambiguity surface is quantized into cells of width $\Delta\tau$ seconds in the delay dimension and Δf_D Hz in the Doppler shift dimension, where $\Delta\tau \leq 1/2W_P$ and $\Delta f_D \leq 1/T$.

The actual structure and statistics of the surface can be controlled through the selection of the integration time, processing bandwidth, and surface cell quantization. The accuracy with which the time delay and Doppler shift can be estimated and the ability to detect a signal is in turn controlled by the structure of the surface. The surface can also be considered

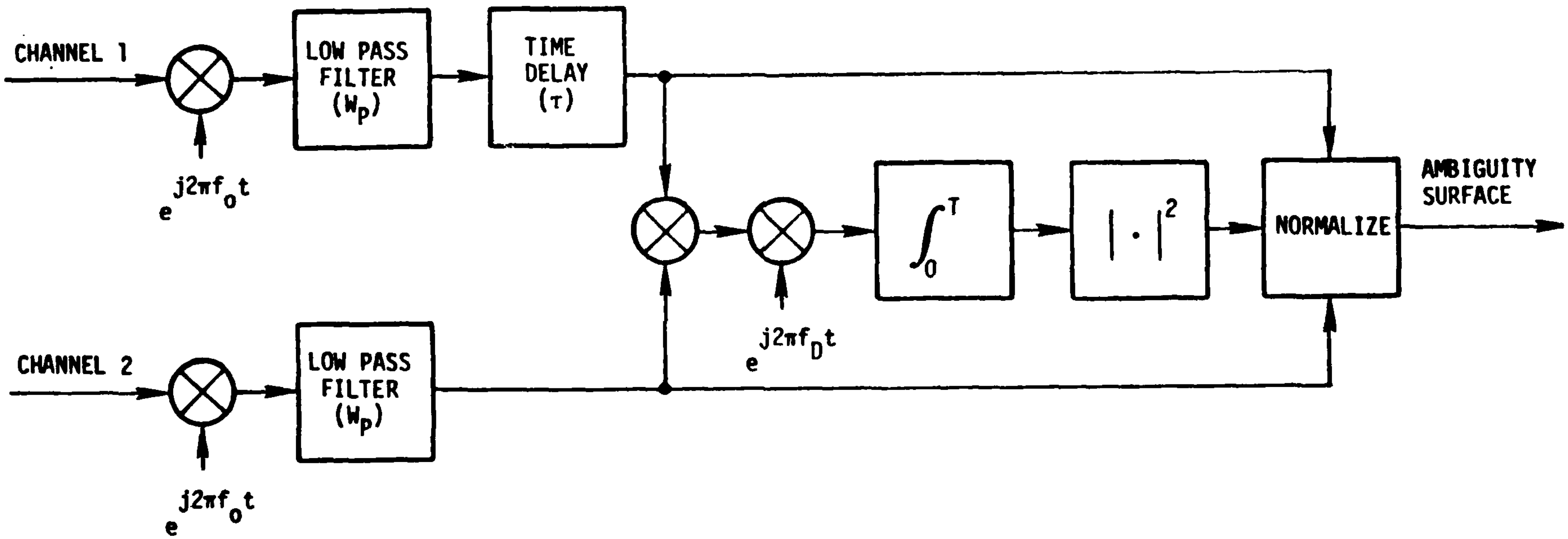

Figure 1-1. Schematic for Generating Ambiguity Surfaces with a Narrowband Correlation Algorithm

an image, and image-processing algorithms, such as "M out of N" algorithms where at least M cells out of a total of N cells must cross a threshold, can be used to detect the presence of a signal (ref. 5). Such surface filtering algorithms are sensitive to the surface structure and the correlation between cells.

The single-cell detection is a detector that detects a signal based on a threshold crossing of a single cell in the surface. The single-cell detection performance for the overcontainment case is presented in Chapter II, where the probability density function (PDF) and cumulative density function (CDF) of a single cell are derived and evaluated. The performance equations for the overcontainment case are complex and difficult to evaluate. An approximation to the single-cell PDF and CDF is derived and the detection performance quantified in Chapter III. The joint statistics between cells is derived and evaluated for the matched containment case in Chapter IV. The results are summarized in Chapter V.

II. DETECTION PERFORMANCE OF THE SAMPLE MAGNITUDE-SQUARED CORRELATION COEFFICIENT

The sample magnitude-squared correlation coefficient (MSCC) is derived and quantified for the signal overcontainment case under the following assumptions: (1) the signal- and noise-power spectra are known and flat, and (2) the noise is spatially uncorrelated. The detection performance is easily quantified once the probability density function (PDF) and the cumulative density function (CDF) are known. The PDF is derived by generalizing the approach used by Goodman to derive the sample MSCC PDF from the PDF of the autocorrelation matrix for matched containment (ref. 1).

Notation is established, and the computation of the sample correlation matrix in the time and frequency domains is discussed in Section 2.1. The derivation of the sample MSCC PDF and CDF is outlined in Section 2.2. Sample plots of the PDF and CDF for various correlations and overcontainments are also presented in Section 2.2. The detection performance is presented in Section 2.3 for the equal- and unequal-channel SNR cases. The results are summarized, and the implications discussed in Section 2.4.

2.1 RELATIONSHIP BETWEEN THE SAMPLE AUTO-CORRELATION MATRIX AND THE SAMPLE MAGNITUDE-SQUARED CORRELATION COEFFICIENT

Let $Z(\ell)$ be a two-dimensional zero mean complex Gaussian random column vector with elements $z_1(\ell)$ and $z_2(\ell)$ representing samples from channels 1 and 2 at time ℓT_S for $\ell = 1,2,\ldots,N_T$. T_S is the sampling interval, and $T = N_T T_S$ is the observation interval. The cross-covariance matrix of $Z(\ell)$ is defined as:

$$R_z(\ell,k) = E\{Z(\ell)\, Z'(k)\} \tag{2.1}$$

where $E\{\cdot\}$ denotes statistical expectation and ' is the complex conjugate of the transpose. Let $Z(\ell)$ contain spatially uncorrelated noise under the H_0 hypothesis and contain correlated signal plus spatially uncorrelated noise under the H_1 hypothesis. Then

PRECEDING PAGE BLANK-NOT FILMED

$$Z(\ell) = \begin{cases} N(\ell) & , \quad H_o \\ S(\ell) + N(\ell) & , \quad H_1 \end{cases} \tag{2.2}$$

and

$$R_Z(\ell,k) = \begin{cases} R_N(\ell,k) & , \quad H_o \\ R_S(\ell,k) + R_N(\ell,k) & , \quad H_1 \end{cases} \tag{2.3}$$

where $R_S(\ell,k)$ is the cross-covariance matrix of the signal $S(\ell)$ and $R_N(\ell,k)$ is the cross-covariance matrix of the noise $N(\ell)$. Finally, assume that the signal- and noise-power spectra are band-limited and flat and that the processing bandwidth ($2W_P$) is larger than the signal bandwidth ($2W_S$) as shown in Figure 2-1. Define the overcontainment ratio

$$OVC = W_P/W_S \quad . \tag{2.4}$$

The signal is overcontained when OVC > 1. Matched containment occurs when OVC = 1.

The sample magnitude-squared correlation coefficient (MSCC) can be computed from the sample auto-correlation matrix. The two-dimensional positive definite Hermetian sample auto-correlation matrix is

$$A = \sum_{\ell=1}^{N_T} Z(\ell)\, Z'(\ell) \quad . \tag{2.5}$$

Let

$$A = \begin{bmatrix} a_{11} & a_{12} \\ a_{12}^* & a_{22} \end{bmatrix} \quad . \tag{2.6}$$

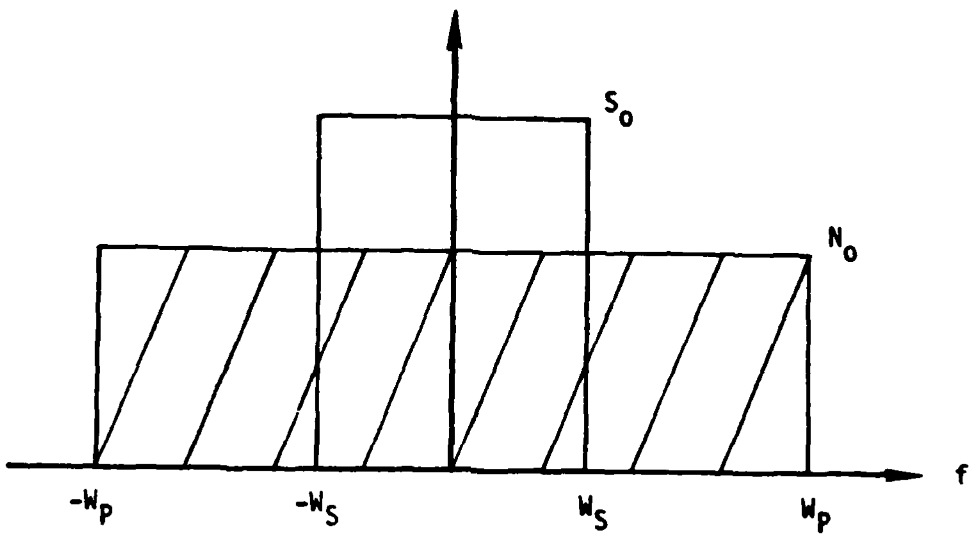

OVERCONTAINMENT RATIO (OVC) $= W_p/W_S$

Figure 2-1. Signal and Noise Power Spectra

The sample MSCC is the sample magnitude-squared cross-correlation coefficient between $z_1(\ell)$ and $z_2(\ell)$ and is given by

$$\rho^2 = \frac{|a_{12}|^2}{a_{11}a_{22}} \quad . \tag{2.7}$$

The PDF of ρ^2 can be derived from the PDF of A by (1) performing the change of variables indicated in Eq. (2.7) and (2) integrating out the auxiliary variables a_{11}, a_{22}, and the phase angle of a_{12}.

According to the Nyquist sampling theorem, the minimum sampling rate is $2W_P$ samples/second so that $T_S \leq 1/2W_P$. Consequently, the $Z(\ell)$ are correlated because the signal component of $Z(\ell)$ is oversampled by the overcontainment ratio, OVC. Therefore, the PDF of A is difficult to derive from the joint PDF of the $Z(\ell)$ because the $Z(\ell)$ are dependent.

Let $Z(\hat{k})$ be a two-dimensional column vector denoting the vector of frequency coefficients from channels 1 and 2 at frequency k/T Hz for $k = 1,2,\ldots,N_P$ where $2W_P = N_P/T$ Hz. Since the minimum sampling frequency is $2W_P$, $N_T \geq N_P$. $Z(k)$ is computed as

$$\hat{Z}(k) = \frac{1}{N_T} \sum_{\ell=0}^{N_T-1} Z(\ell)\, e^{-j\frac{2\Pi\ell k}{N_T}} \tag{2.8}$$

for $k = 0,1,\ldots,N_P-1$. It is easily shown that $\hat{Z}(\ell)$ and $Z(k)$ are independent when $\ell \neq k$ for the strictly band-limited spectra and the frequency coefficients are spaced at intervals of 1/T Hz (Appendix A). Therefore, the power-spectral density matrix of $\hat{Z}(k)$ for the assumed power spectra is

$$R_z(\ell,k) = E\{\hat{Z}(k)\,\hat{Z}'(k)\}$$

$$= \begin{cases} R_{\hat{z}_0} = R_{\hat{N}} & , \quad \frac{N_S-1}{2} < |k| \leq \frac{N_P-1}{2} \\ R_{\hat{z}_1} = R_{\hat{S}} + R_{\hat{N}} & , \quad |k| \leq \frac{N_S-1}{2} \end{cases} \tag{2.9}$$

where R_S is the power-spectral density matrix of the signal; and $R_{\hat{N}}$ is the power-spectral density matrix of the noise which is diagonal. With the frequency spacing of 1/T Hz,

$$W_S T = N_S$$

and (2.10)

$$W_P T = N_P \quad .$$

N_S is the number of frequency coefficients or equivalently the degrees of freedom in the signal band. Similarly, N_P is the number of frequency coefficients or equivalently the degrees of freedom in the noise band. When the signal is overcontained, there are $M = N_P - N_S$ frequency coefficients containing ony noise. The overcontainment ratio can thus be expressed in terms of M and N_S:

$$\begin{aligned} OVC &= W_P/W_S \\ &= N_P/N_S \\ &= (N_S+M)/N_S \end{aligned} \tag{2.11}$$

The sample auto-correlation matrix defined in Eq. (2.5) can be computed with the frequency coefficients instead of the time samples. It is easily shown that

$$A = \sum_{k=1}^{N_P} \hat{Z}(k)\ \hat{Z}'(k) \tag{2.12}$$

The PDF of A is easily computed from the joint PDF of the Z(k) because the $\hat{Z}(k)$ are independent even when the observations are oversampled in the time domain.

2.2 CUMULATIVE AND PROBABILITY DENSITY FUNCTIONS

The probability density functions (PDF) of the sample magnitude-square correlation coefficient (MSCC) is easily computed from the PDF of the sample auto-correlation matrix, A. Since the frequency coefficients, $\hat{Z}(k)$, are independent, the characteristic function of A is easily derived, and the PDF of A is obtained by computing the Fourier inversion of the characteristic functions of A. Th PDF of A is derived in Section 2.2.1. The probability density function and the cumulative density function of the sample MSCC are computed and evaluated in Section 2.2.2 and 2.2.3, respectively.

2.2.1 Probability Density Function of the A Matrix

The characteristic function of A is

$$M_A(\Phi) = E\{e^{jTR(A\Phi)}\} \tag{2.13}$$

where TR(•) denotes the trace and Φ is a two-dimensional positive definite Hermitian matrix. Substituting Eq. (2.12) into Eq. (2.13) and using the fact that the $\hat{Z}(k)$ are Gaussian and independent, it is shown in Appendix B that

$$M_A(\Phi) = \frac{1}{|R_{\hat{z}_1}|^{N_S} \; |R_{\hat{z}_o}|^{M} \; |R_{\hat{z}_1}^{-1} - j\Phi|^{N_S} \; |R_{\hat{z}_1}^{-1} - j\Phi|^{M}} \tag{2.14}$$

where $|\cdot|$ denotes the determinant and $R_{\hat{z}_k}$, for k = 0 and 1, is defined in Eq. (2.9). The PDF of A is then given by

$$f(A) = \frac{1}{(2\Pi)^4} \int_{D_\Phi} M_A(\Phi) \; e^{-jTR(A\Phi)} d\Phi \tag{2.15}$$

where D_Φ is the domain of integration for two-dimensional positive definite Hermitian matrices. Substitute Eq. (2.14) into Eq. (2.15). It is shown in Appendix B that

$$f(A) = \frac{|A|^{N_P-2} \, e^{-TR(R_{\hat{z}_1}^{-1}A)}}{\Pi \, \Gamma(N_P) \, \Gamma(N_P-1) \, |R_{\hat{z}_o}|^M \, |R_{\hat{z}_1}|^{N_S}} \times {}_1\tilde{F}_1(M;N_P;\Delta RA) \qquad (2.16)$$

where ${}_1\tilde{F}_1(\cdot;\cdot;\cdot)$ is the confluent hypergeometric function of matrix argument (refs. 6 and 7); $\Gamma(\cdot)$ is the Gamma function (ref. 8) and

$$\Delta R = R_{\hat{z}_1}^{-1} - R_{\hat{z}_o}^{-1} \qquad (2.17)$$

Note that if M=0, $N_P=N_S$ and

$$f(A) = \frac{|A|^{N_S-2} \, e^{-TR(R_{\hat{z}_1}^{-1}A)}}{\Pi \, \Gamma(N_S) \, \Gamma(N_S-1) \, |R_{\hat{z}_1}|^{N_S}} \qquad (2.18)$$

which is the PDF of A for matched containment (ref. 1).

2.2.2 Probability Density Function of the Sample MSCC

The PDF of the sample MSCC is easily obtained from f(A) by the change of variables indicated in Eq. (2.7) and integrating out the auxiliary variables. Let

$$a_{12} = a_{11}a_{22} \; \rho \; e^{j\theta} \qquad (2.19)$$

where ρ is the sample correlation coefficient and θ is the phase angle of a_{12}. Then

$$\begin{aligned} f(a) &= f(a_{11}, a_{22}, a_{12}) \\ &= \frac{a_{11}a_{22}}{2} \, f(a_{11}, a_{22}, \rho^2, \theta) \qquad (2.20) \end{aligned}$$

The PDF of the sample MSCC is

$$f(\rho^2) = \frac{1}{2}\int_0^{\infty}\int\int_{-\Pi}^{\Pi} a_{11} \, a_{22} \, f(a_{11},a_{22},\rho^2,\theta) \, da_{11}da_{22}d\theta \qquad (2.21)$$

It is necessary to define the terms in the auto-spectral matrices before evaluating Eq. (2.21). The auto-spectral density matrices defined in Eq. (2.9) are:

$$R_{\hat{z}_o} = R_{\hat{N}} = \begin{bmatrix} N_{01} & 0 \\ 0 & N_{02} \end{bmatrix} \tag{2.22}$$

$$R_{\hat{S}} = \begin{bmatrix} S_{01} & \sqrt{S_{01}S_{02}}\ \rho_S\, e^{j\theta_S} \\ \sqrt{S_{01}S_{02}}\ \rho_S e^{-j\theta_S} & S_{02} \end{bmatrix} \tag{2.23}$$

and

$$R_{\hat{z}_1} = \begin{bmatrix} \sigma_1{}^2 & \sigma_{12} \\ \sigma_{12}^* & \sigma_2^2 \end{bmatrix} = \begin{bmatrix} \sigma_1^2 & \sigma_1\sigma_2\rho_T e^{j\theta} \\ \sigma_1\sigma_2\rho_T e^{-j\theta} & \sigma_2^2 \end{bmatrix}$$

$$= \begin{bmatrix} S_{01} + N_{01} & \sqrt{S_{01}S_{02}}\ \rho_S\, e^{j\theta_S} \\ \sqrt{S_{01}S_{02}}\ \rho_S\, e^{-j\theta_S} & S_{02} + N_{02} \end{bmatrix} \tag{2.24}$$

where N_{0k} is the noise spectral density in channel k, S_{0k} is the signal spectral density in channel k, ρ_S is the true correlation coefficient between the signal components, θ_S is the phase of the true signal correlation, ρ_T is the true correlation coefficient between the two channels, and θ is the phase of the true correlation between the channels. From Eq. (2.24), it follows that the true MSCC is

$$\rho_T^2 = \frac{SNR_1\ SNR_2}{(SNR_1+1)\ (SNR_2+1)}\ \rho^2{}_S \tag{2.25}$$

where

$$SNR_k = S_{0k}/N_{0k} \tag{2.26}$$

is the in-band signal-to-noise ratio (SNR) for channel k.

Substitute Eq. (2.22) - (2.26) into Eq. (2.21). The reader is referred to Appendix B for the details of evaluating Eq. (2.21). The PDF of the sample MSCC is

$$f(\rho^2|\rho_T^2,\ M,\ N_S) = \sum_{R=0}^{\infty} D(k{:}M,N_S)\ \left(SNR_1\ SNR_2(1-\rho_S^2)\right)^k\ f(\rho^2|k) \tag{2.27a}$$

where

$$f(\rho^2|k) = (1-\rho^2)^{N_P+k-2}(1-\rho_T^2)^{N_P}\ \frac{(SNR_2+1)^M}{(SNR_1)^k}\ \times$$

$$\sum_{\ell=0}^{\infty}(\rho^2\rho_T^2)^{\ell}A_k(\ell)\ {}_3F_1\Big(M+k,\ -N_P,\ N_P+k+\ell;$$

$$N_P+2K+2\ell;\ 1-\frac{1}{(SNR_1+1)(1-\rho_T^2)},\ 1-\frac{SNR_2+1}{SNR_1+1}\Big) \tag{2.27b}$$

$$D(k{:}M,N_S) = \frac{(-1)^k(M)_k(N_S)_k}{(N_P-1/2)_k} \tag{2.27c}$$

$$A_k(\ell) = \frac{\Gamma(N_P+2k)\ \Gamma(N_P+k+\ell)^2\ \Gamma(N_S+k+2\ell)}{\Gamma(N_P)\ \Gamma(N_P-1)\ \Gamma(N_S+k)\ \Gamma(N_P+2k+2\ell)(N_P)_{2k}(\ell!)^2} \tag{2.27d}$$

$(x)_n = \Gamma(x+n)/\Gamma(n)$ is Pochhammer's symbol (ref. 8).

${}_3F_1(\cdot,\cdot,\cdot;\cdot;\cdot,\cdot)$ is a three-one hypergeometric function of two arguments defined in Eq. (B.37).

If the signal components are perfectly correlated, $\rho_S^2 = 1$ and

$$f(\rho^2|\rho_T^2, M, N_S) = f(\rho^2|0) \tag{2.28}$$

Also, if there are equal channel conditions,

$$SNR = SNR_1 = SNR_2 \tag{2.29a}$$

and

$$\begin{aligned} & {}_3F_1\left(M+k,\ -N_P,\ N_P+k+\ell;\ N_P+2k+2\ell;\ 1 - \frac{1}{(SNR_1+1)(1-\rho_T^2)},\ 1 - \frac{SNR_2+1}{SNR_1+1}\right) \\ & = {}_2F_1\left(M+k,\ -N_P;\ N_P+2k+2\ell;\ 1 - \frac{1}{(SNR+1)(1-\rho_T^2)}\right) \end{aligned} \tag{2.29b}$$

It should be noted that ρ_T^2, SNR_1, SNR_2, and ρ_S^2 are related by Eq. (2.25) and that M and N_S are related by the overcontainment ratio, Eq. (2.11).

Eq. (2.27) does reduce to the well known expressions for the PDF of the sample MSCC for noise only and for matched containment (ref. 2). For matched containment, M = 0; $N_P = N_S$; and Eq. (2.22) becomes

$$\begin{aligned} f(\rho^2|\rho_T^2, 0, N_S) &= (N_S-1)(1-\rho_T^2)^{N_S}(1-\rho^2)^{N_S-2} \times \\ & \quad {}_2F_1(N_S, N_S;\ 1;\ \rho_T^2\rho^2) \\ &= (N_S-1)(1-\rho_T^2)^{N_S}(1-\rho^2)^{N_S-2} \times \\ & \quad (1-\rho_T^2\rho^2)^{1-2N_S}\ {}_2F_1(1-N_S,\ 1-N_S;\ 1;\ \rho_T^2\rho^2) \quad . \end{aligned} \tag{2.30}$$

Under noise only conditions, $SNR_1 = SNR_2 = 0$; $\rho_T^2 = 0$, and Eq. (2.22) reduces to

$$f(\rho^2|0,M,N_S) = (N_P-1)(1-\rho^2)^{N_P-2} \tag{2.31}$$

Example plots of th PDF of sample MSCC are shown in Figures 2-2 through 2-4 for equal channel conditions for several overcontainments. Figure 2-2 is the PDF of the sample MSCC for *noise only* and is provided as a point of comparison. Figures 2-3 and 2-4 are the PDF of the sample MSCC for signal present. By comparing Figures 2-3 and 2-4 to Figure 2-2, it is seen that the PDF of ρ^2 moves to the left and takes on "noise-like" characteristics as the overcontainment increases and as $\rho^2{}_T$ decreases.

2.2.3 Cumulative Density Function of the Sample MSCC

The cumulative density function of the sample MSCC is

$$F(\rho_t^2|(\rho_T^2,M,N_S) = \int_0^{\rho_t^2} f(\rho^2|\rho_T^2,M,N_S)\, d\rho^2 \tag{2.32}$$

where $\rho_t^2 \in [0,1]$ is the threshold on the sample MSCC. Substitute Eq. (2.22) into Eq. (2.32).

$$F(\rho_t^2|\rho_T^2,M,N_S) =$$

$$\sum_{k=0}^{\infty} D(k;M,N_S)\left(SNR_1 SNR_2(1-\rho_S^2)\right)^k F(\rho_t^2|k) \tag{2.33a}$$

where

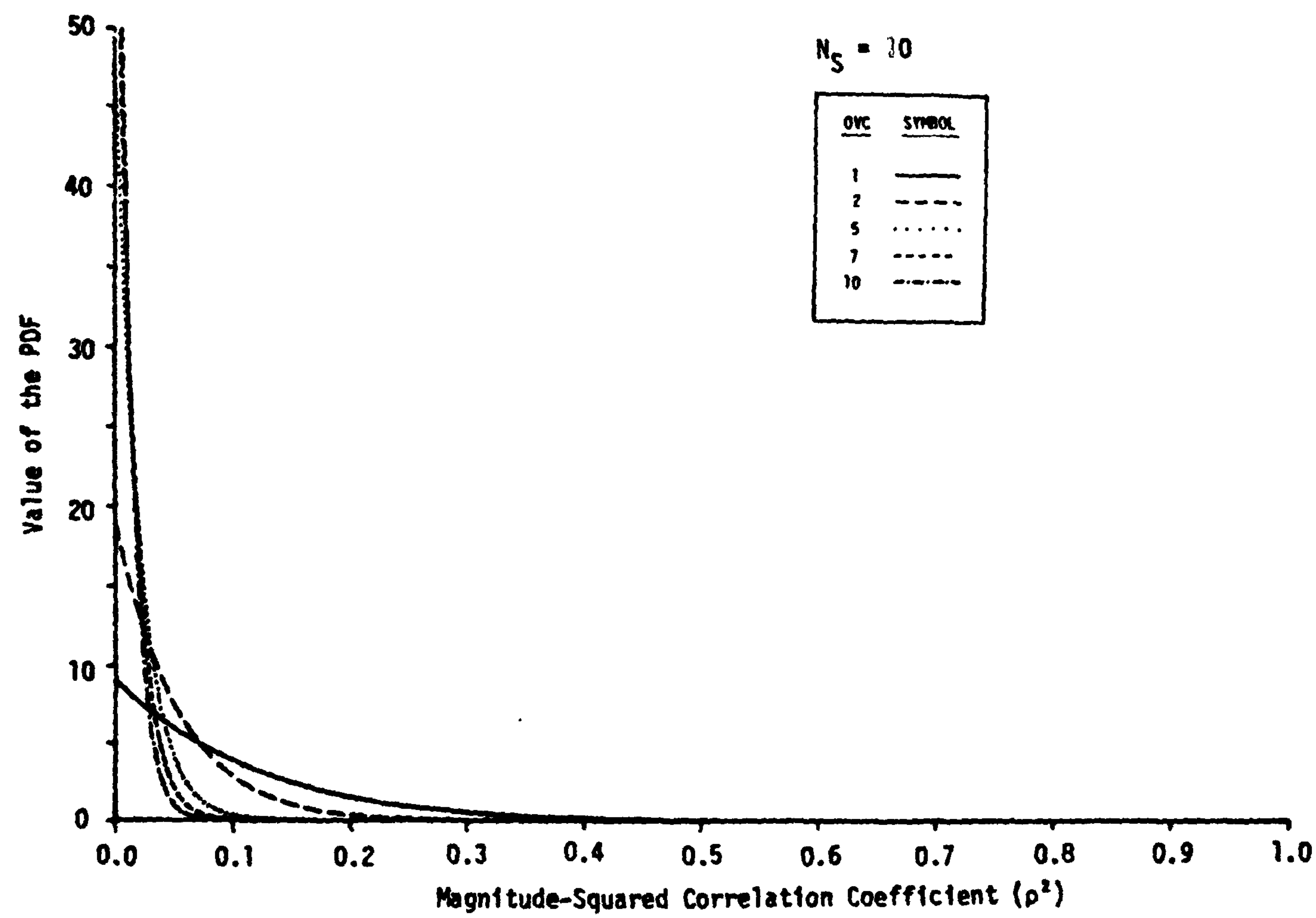

Figure 2-2. Probability Density Function of ρ^2 for $\rho_T^2 = 0.0$

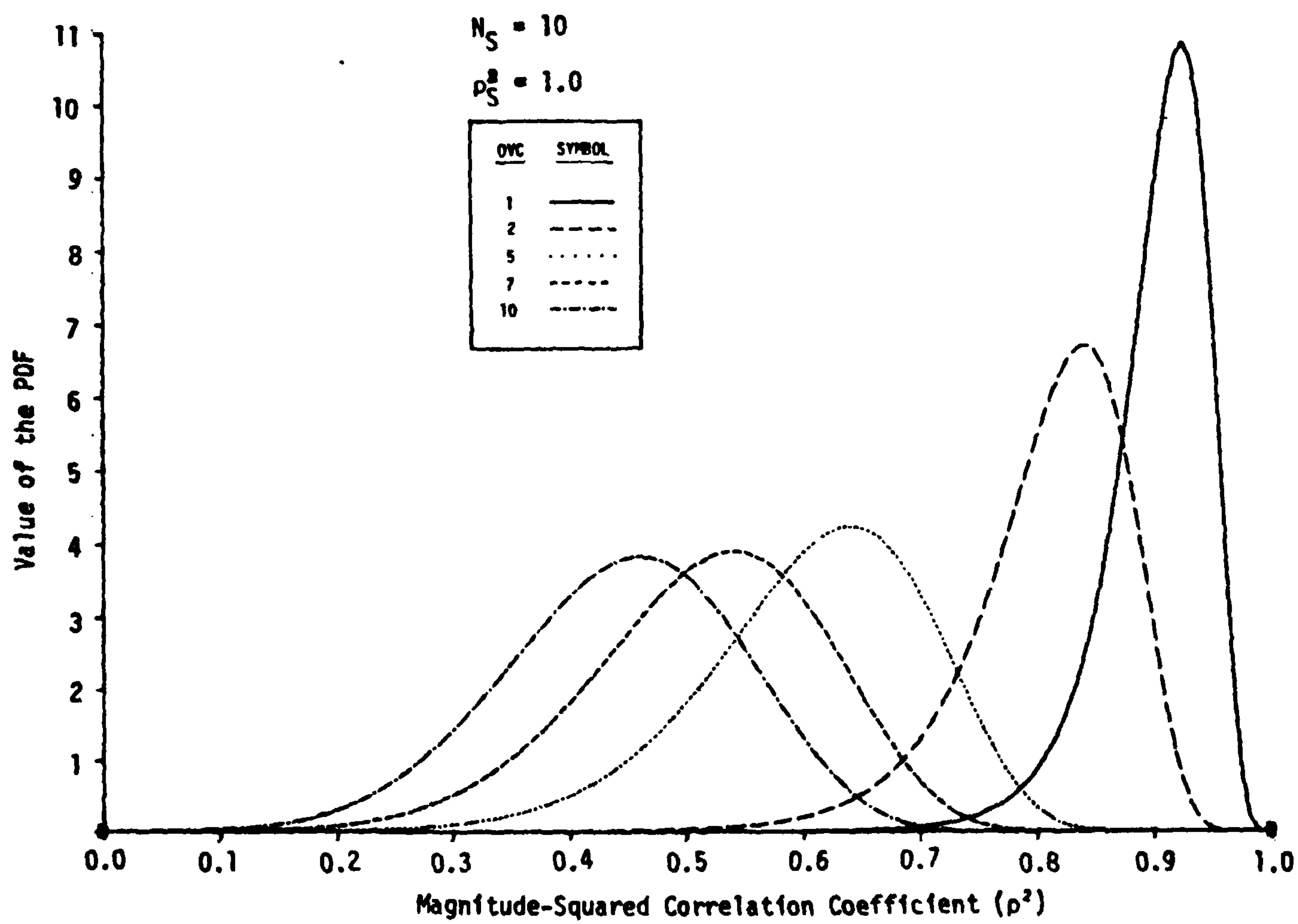

Figure 2-3. Probability Density Function of ρ^2 for $\rho_T^2 = 0.9$

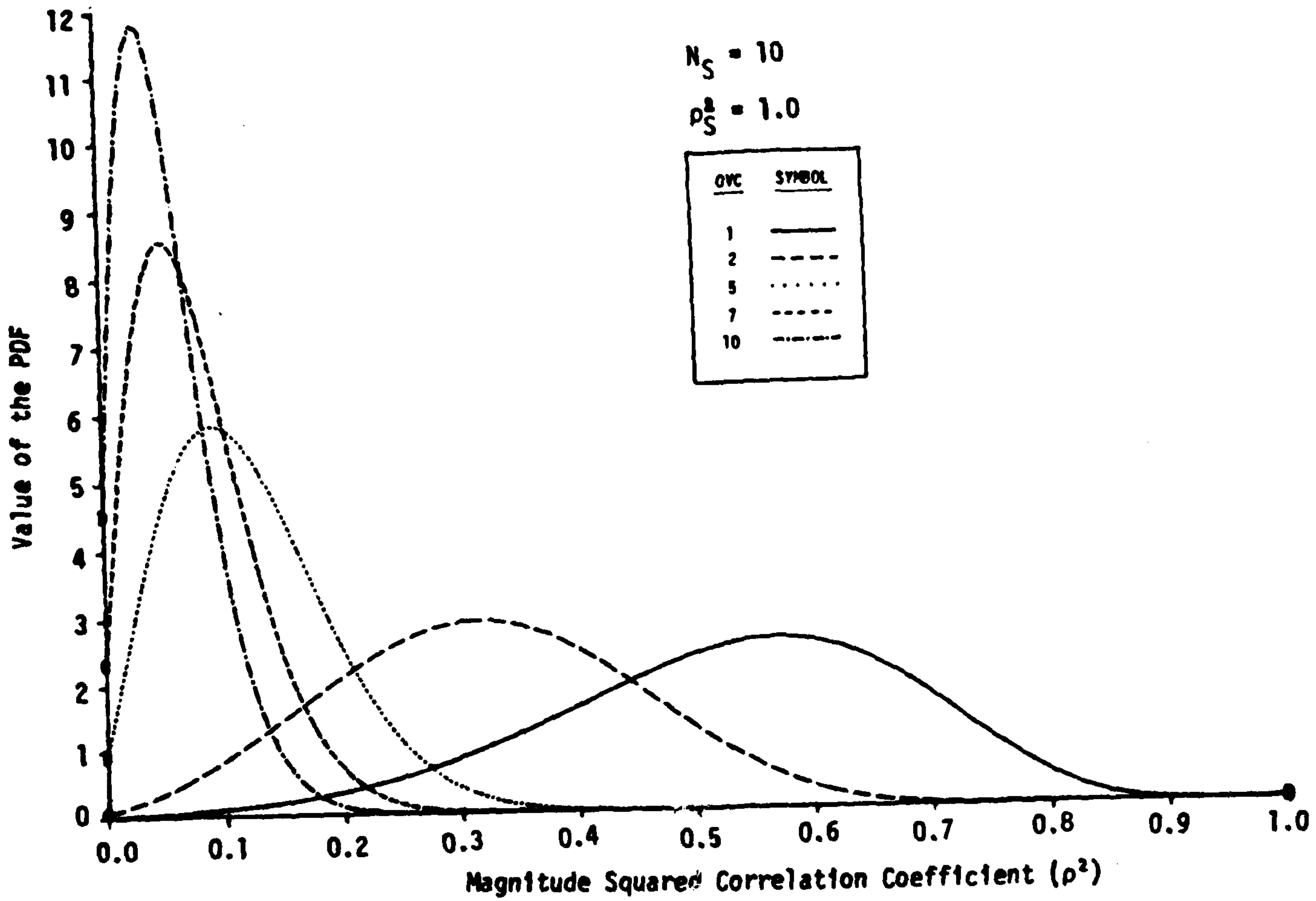

Figure 2-4. Probability Density Function of ρ^2 for $\rho_T^2 = 0.5$

$$F(\rho_t^2|k) = (1-\rho_T^2)^{N_P} \frac{(SNR_2+1)^M}{(SNR_2+1)^k} \sum_{\ell=0}^{\infty} \rho_T^{2\ell} B_k(\ell) \times$$

$$I_{\rho_t^2}(\ell+1, N_P+k-1)\ {}_3F_1\Big(M+k, -N_P, N_P+k+\ell;$$

$$N_P+2K+2\ell;\ 1 - \frac{1}{(SNR_1+1)(1-\rho_T^2)}, 1 - \frac{SNR_2+1}{SNR_1+1}\Big) \tag{2.33b}$$

where

$$B_k(\ell) = \frac{\Gamma(N_P+2K)\ \Gamma(n_P+k-1)\ \Gamma(N_P+k+\ell)\ \Gamma(N_S+k+2\ell)}{\Gamma(N_P)\ \Gamma(N_P-1)\ \Gamma(N_S+k)\ \Gamma(N_P+2k+2\ell)\ (N_P)_{2k}\ \ell!} \tag{2.33c}$$

$$I_x(a,b) = \frac{\Gamma(a+b)}{\Gamma(a)\ \Gamma(b)} \int_0^x a^{-1}(1-t)^{b-1}\ dt \tag{2.33d}$$

is the incomplete Beta Function (ref. 8). $D(k;M,N_S)$ is defined in Eq. (2.27c). As in the PDF of the sample MSCC, if $\rho_S = 1$,

$$F(\rho_t^2|\rho_T^2, M, N_S) = F(\rho_t^2|0) \tag{2.34}$$

For matched containment, $M = 0$, $N_P = N_S$, and Eq. (2.33) becomes

$$F(\rho_T^2|(\rho_T^2,0,N_S) = \sum_{\ell=0}^{\infty} \frac{\rho_T^{2\ell}\Gamma(N_S+\ell)}{(\ell!)^2\,\Gamma(N_S-1)} I_{\rho_t^2}(\ell+1,\ N_S-1)$$

$$= \rho_t^2\left[\frac{1-\rho_T^2}{1-\rho_t^2\rho_T^2}\right]^{N_S} \sum_{\ell=0}^{N_S-2}\left[\frac{1-\rho_t^2}{1-\rho_t^2\rho_T^2}\right]^{\ell} \times$$

$${}_2F_1(-\ell,\ 1-N_S;\ 1;\ \rho_t^2\rho_T^2) \qquad (2.35)$$

which is the well known equation for the CDF of the sample MSCC. Under noise-only conditions, $SNR_1 = SNR_2 = 0$; $\rho_T^2 = 0$; and

$$F(\rho_t^2) = 1 - (1-\rho_t^2)^{N_P-1} \qquad (2.36)$$

Example plots of the CDF of the sample MSCC are shown in Figures 2-5 through 2-8 for equal channel conditions for several overcontainments. The same conclusions that were drawn for the PDFs can be drawn for the CDFs. The CDF of the sample MSCC moves to the left and takes on "noise-like" characteristics as the overcontainment increases and as ρ_T^2 decreases.

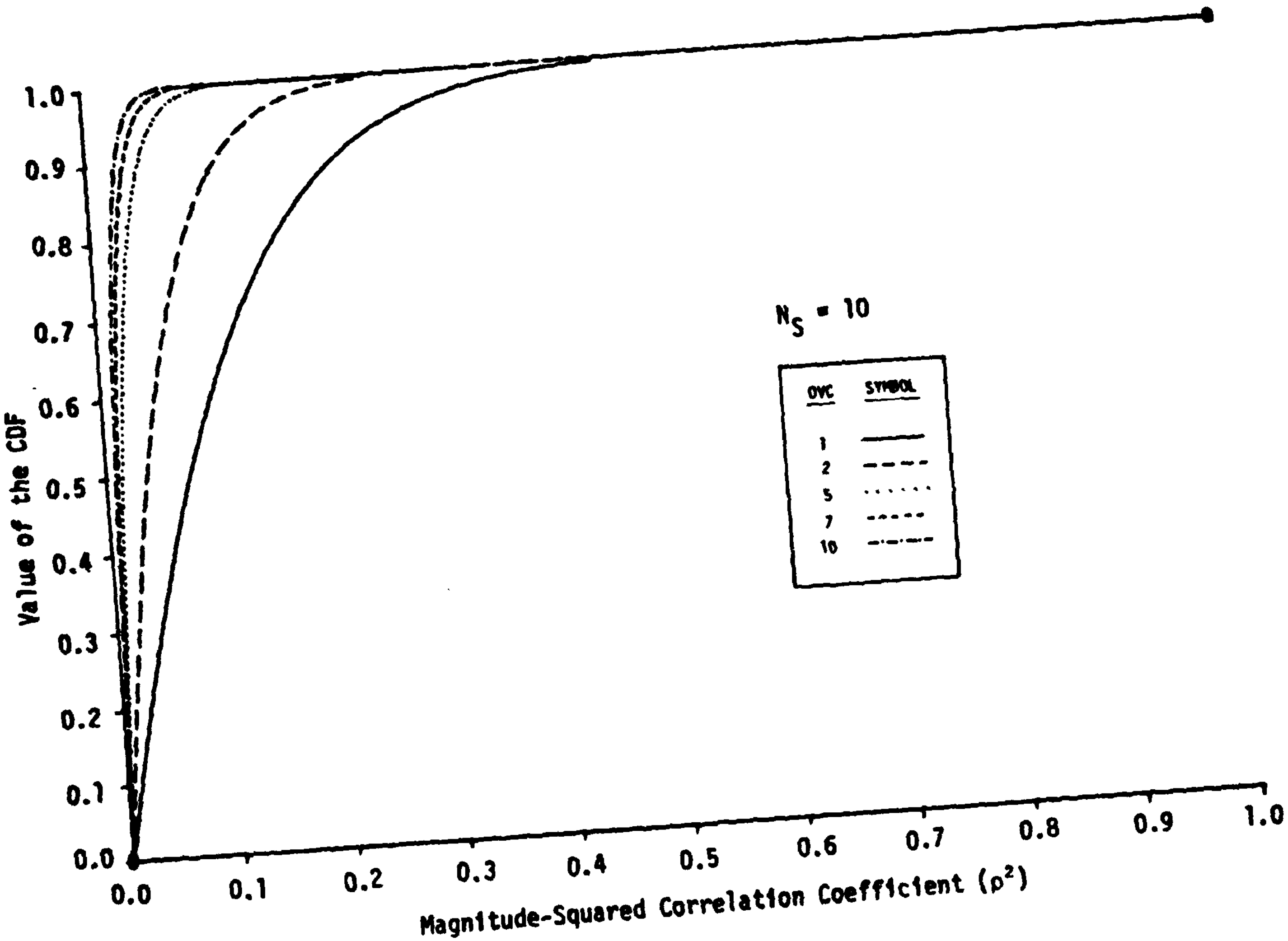

Figure 2-5. Cumulative Density Function of ρ^2 for $\rho_T^2 = 0.0$

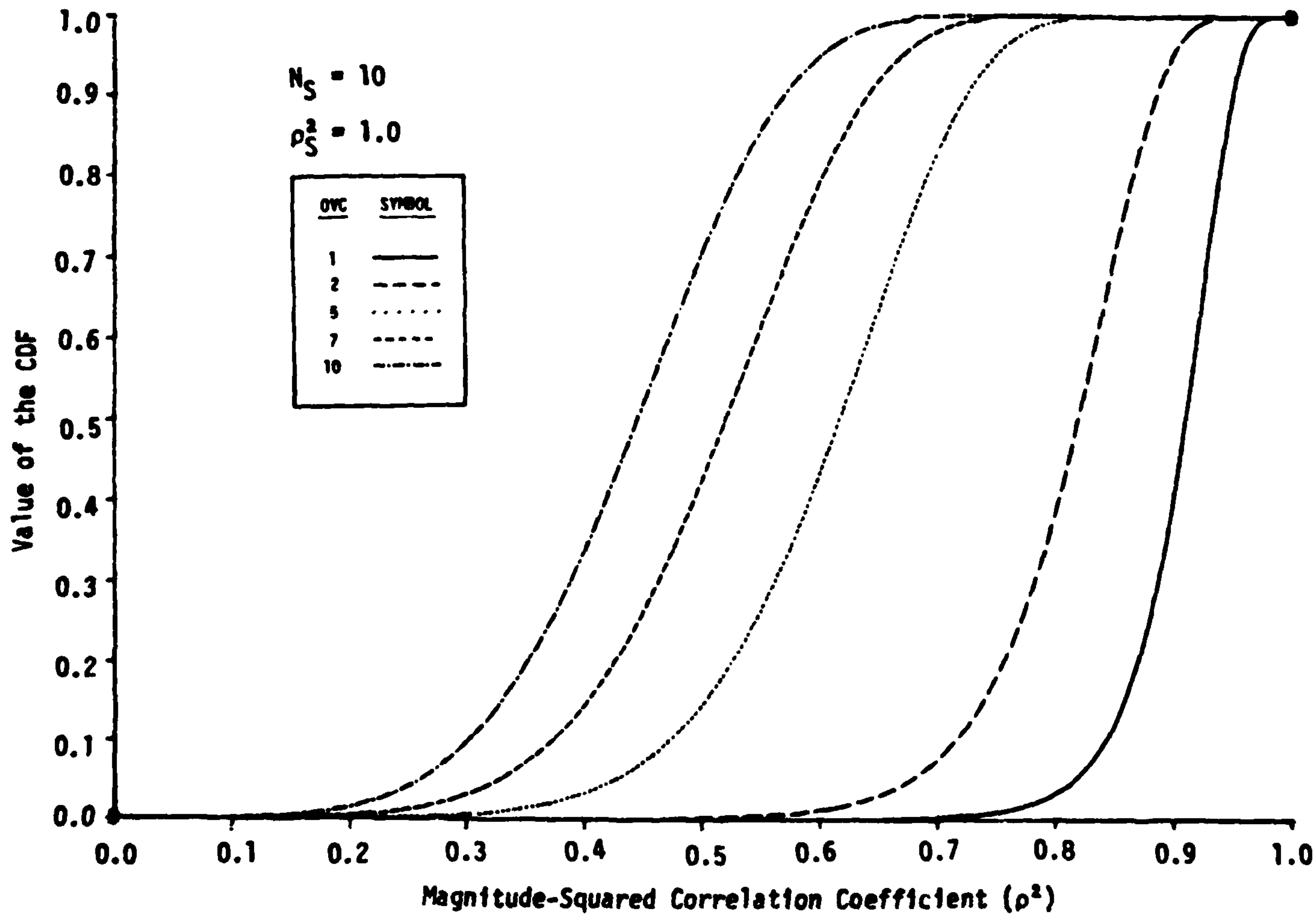

Figure 2-6. Cumulative Density Function of ρ^2 for $\rho_T^2 = 0.9$

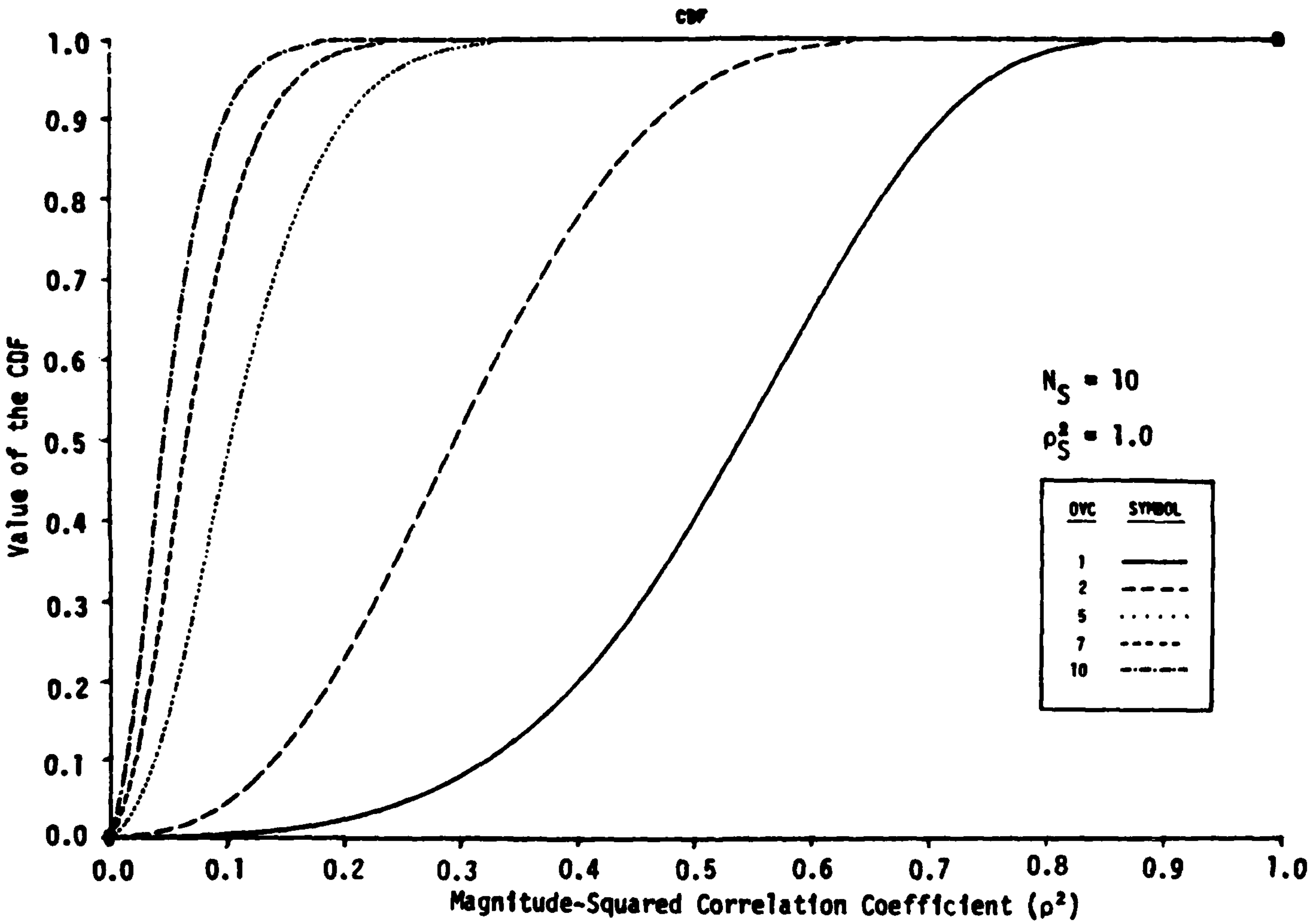

Figure 2-7. Cumulative Density Function of ρ^2 for $\rho_T^2 = 0.5$

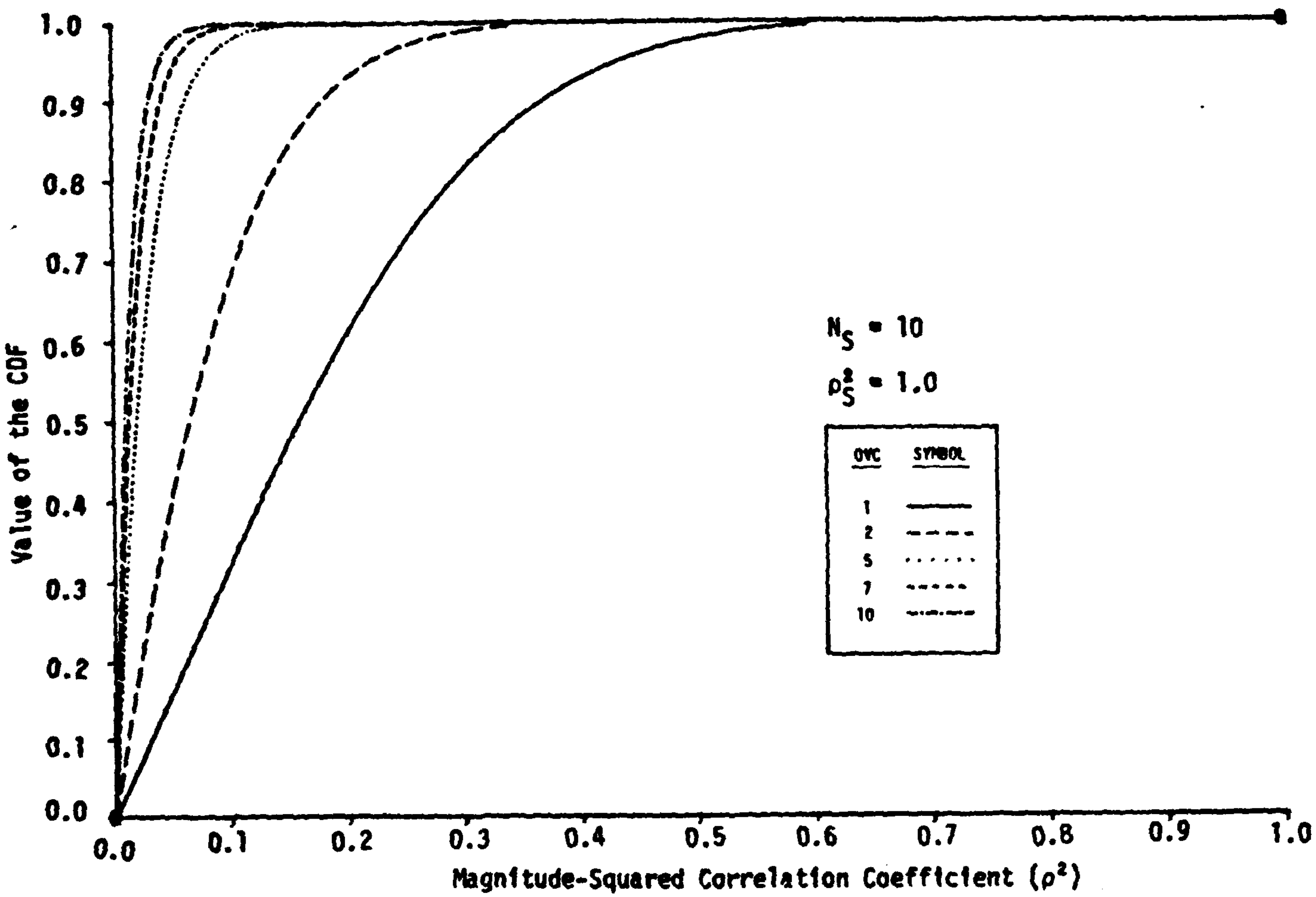

Figure 2-8. Cumulative Density Function of ρ^2 for $\rho_T^2 = 0.1$

2.3 DETECTION PERFORMANCE

The detection performance is defined as the in-band signal-to-noise power ratio (SNR) needed to achieve a specified Probability of Detection (P_D) and Probability of False Alarm (P_{FA}) for a set of operating parameters. SNR is defined as the in-band SNR in each channel for the equal channel case and the in-band SNR in the weakest channel for the unequal channel case. The operating parameters are the degrees of freedom in the signal band, the signal overcontainment, and the ratio of the SNRs in the two channels (DIF). The ratio of the SNRs is defined as

$$\mathrm{DIF} = \mathrm{SNR}_1/\mathrm{SNR} \tag{2.37}$$

where $\mathrm{SNR}_1 \geq \mathrm{SNR}$.

The P_{FA} and P_D are "one minus the CDF" evaluated under the appropriate conditions. From Eq. (2.36),

$$P_{FA} = (1 - \rho_t^2)^{N_P - 1} \tag{2.38}$$

Similarly, from Eq. (2.33),

$$P_D = 1 - F(\rho_t^2 | \rho_T^2, M, N_S) \tag{2.39}$$

for $\rho_T^2 \neq 0$. The procedure used to find the SNR needed to achieve a desired operating point is to (1) select a P_D, P_{FA}, N_S, ρ_S^2, DIF, and OVC, (2) use Eq. (2.38) to find the threshold, ρ_t^2, and (3) numerically solve Eq. (2.39) for the required SNR.

2.3.1 Equal Channel Performance

The matched containment equal channel SNR required to obtain a $P_{FA} = 10^{-4}$ and $P_D = 0.1$, 0.5, and 0.9 is shown in Figure 2-9 as a function of N_S. This

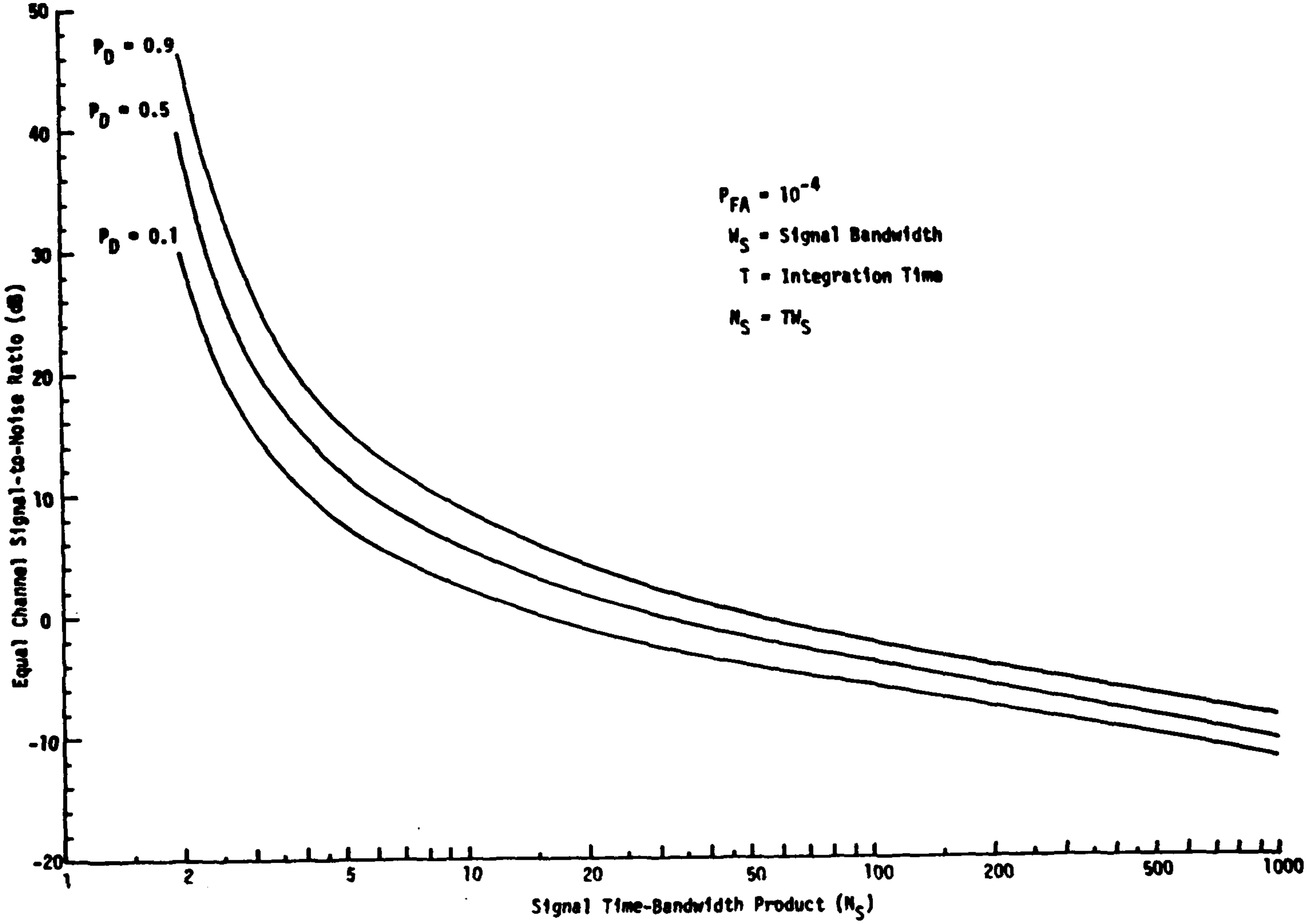

Figure 2-9. Equal Channel Matched Containment Detection Performance

figure is provided as a point of reference because the effects of overcontainment are presented by discussing the way this figure changes with overcontainment. As is well known, the SNR decreases 2 dB per doubling of N_S for $N_S > 64$. Overcontainment has two effects on the noise. The noise degrees of freedom is increased with respect to N_S, and the noise power is increased with respect to the matched containment noise power. The increase in both cases is equal to OVC. The effects of overcontainment on SNR is dependent on which of the two effects dominates.

The in-band equal channel SNR required to obtain an operating point of $P_D = 0.5$ and $P_{FA} = 10^{-4}$ as a function of OVC is shown in Figure 2-10 for $\rho_S^2 = 1.0$ and for a set of N_S's. It is immediately obvious that the SNR can be reduced by overcontaining the signal for small N_S. For a given N_S, there is a value of OVC, OVC_O, which minimizes the SNR. For OVC larger than OVC_O, the SNR increases at a rate of about 1 dB per doubling of OVC for the range of OVC shown in the figure. For $N_S \geq 12$, the SNR increases with OVC and also reaches an asymptote of 1 dB per doubling of OVC for the range of OVCs considered.

The reduction in SNR caused by overcontaining the signal for small N_S has been verified by two simulations developed to study the detection performance of surface filters (ref. 9 and 10). The simulation by Tetra-Tech consisted of two sine waves in Gaussian noise, while the Ensco simulation consisted of Gaussian signal in Gaussian noise. The effects of overcontainment for N_S in the range of 16 to 64 and OVC in the range of 2 to 8 has been verified with real ocean data in the MDS experiment conducted at the DARPA Acoustic Research Center in May 1981 (ref. 11).

Reducing the SNR by increasing the overcontainment is counterintuitive because increasing noise power is not expected to improve performance. However, for $N_S < 12$, N_P is small for matched containment; the sample MSCC is a poor measure of the true noise MSCC; and the threshold for $P_{FA} = 10^{-4}$ is large as shown in Figure 2-11 where the PDF of the sample MSCC is plotted for $N_S = 2$ and for several OVCs. Increasing OVC for these small N_S's increases the N_P which yields a better estimate of the true noise MSCC and results in a lower threshold. The PDF of the sample MSCC for the true MSCC needed to

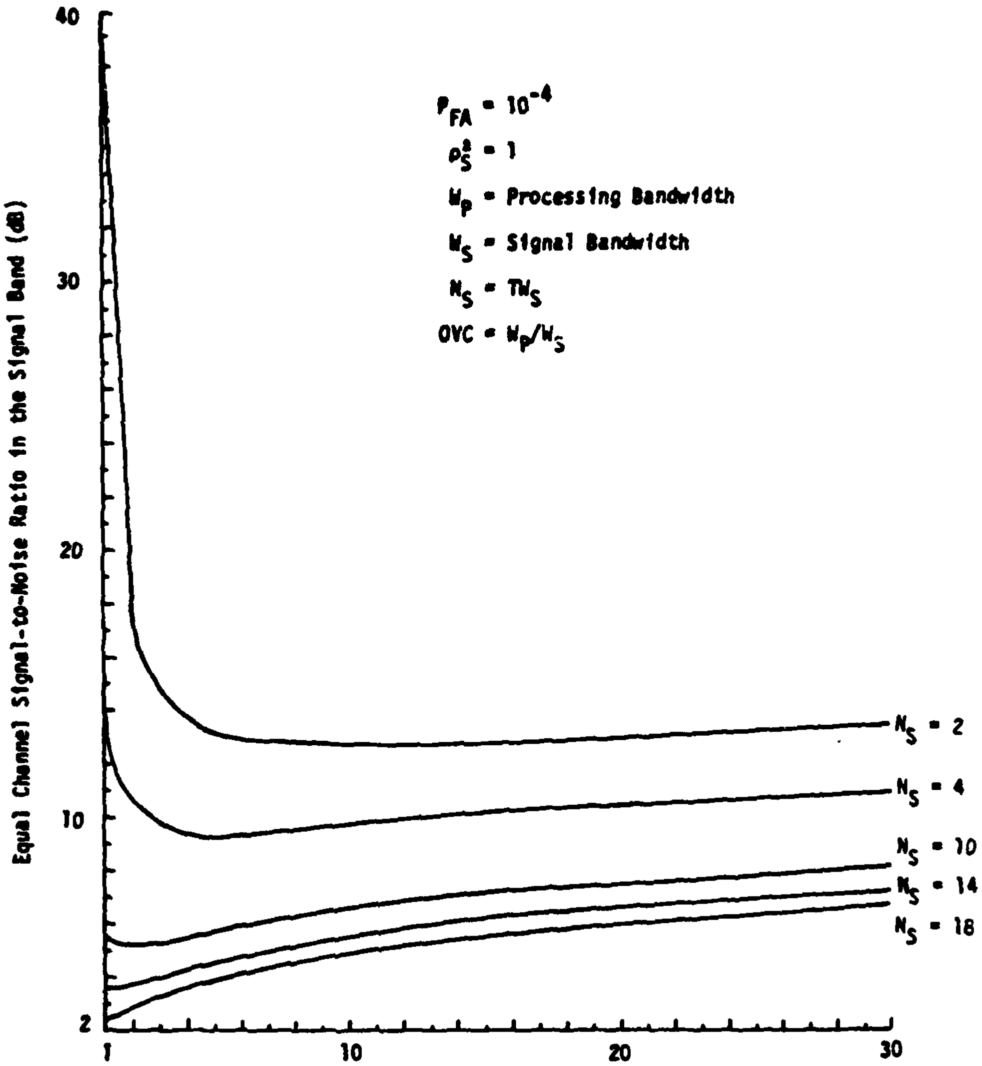

Figure 2-10. Effects of Overcontainment for $P_D = 0.5$

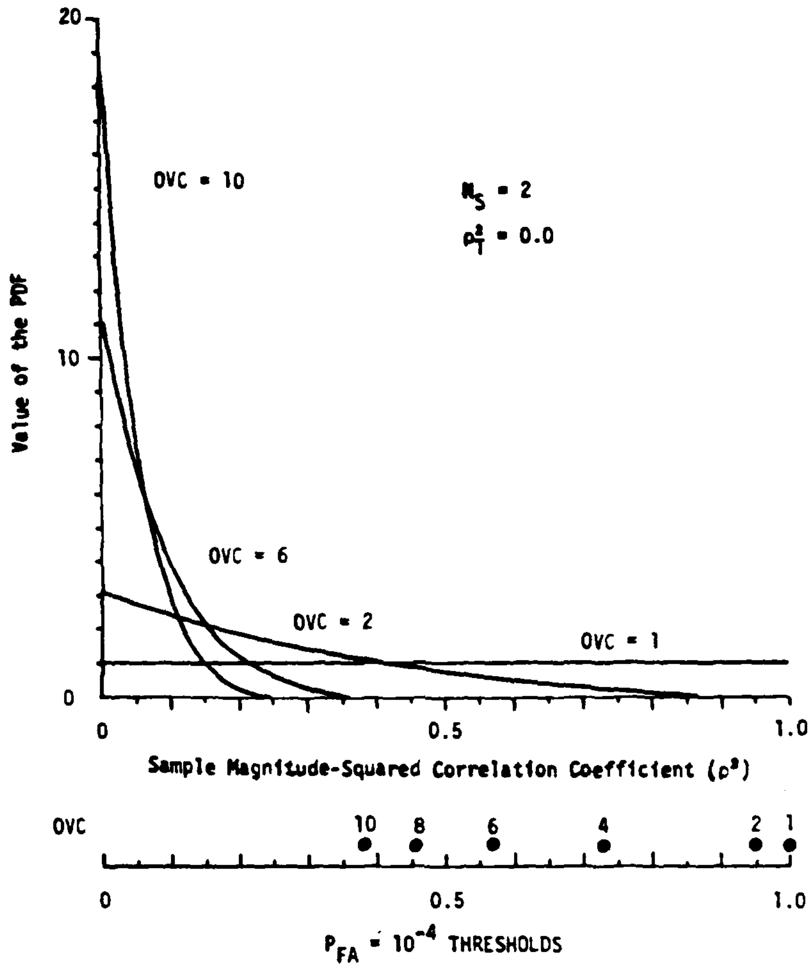

Figure 2-11. Probability Density Function for Noise

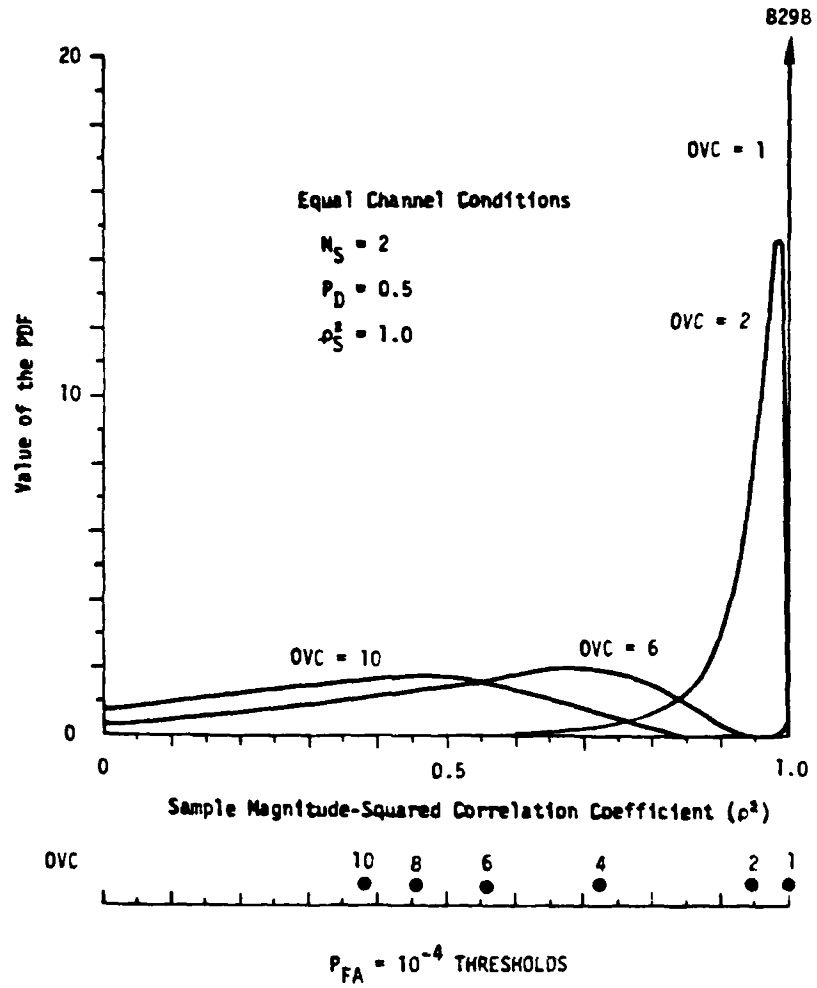

Figure 2-12. Probability Density Function of Signal and Noise

achieve a $P_{FA} = 10^{-4}$ and $P_D = 0.5$ is shown in Figure 2-12 for signal present, for $\rho_S^2 = 1.0$, and for the same OVCs used in Figure 2-11. It is seen that for matched containment, the signal PDF is impulsive because of the large threshold required by the small N_P. As OVC increases, the threshold is reduced; the signal PDF spreads out more; and the required SNR is reduced. However, when N_P is sufficiently large to produce an adequate estimate of the noise background, the SNR increases with OVC because the noise power dominates the performance.

The in-band equal channel SNRs for P_D of 0.1 and 0.9 and for $P_{FA} = 10^{-4}$ are shown in Figures 2-13 and 2-11, respectively, as a function of OVC. The decrease in SNR with increasing OVC that was observed for $P_D = 0.5$ is still retained for small N_S. There is still a value of OVC, OVC_o, that minimizes SNR. For OVCs larger than OVC_o,the SNR begins to increase at about 1 dB per doubling of OVC. When $N_S \geq 10$ for $P_D = 0.1$ and $N_S \geq 14$ for $P_D = 0.9$, the SNR increases for all overcontainments.

The in-band equal channel SNR does not continually increase at 1 dB per doubling of OVC as Figures 2-10, 2-13 and 2-14 seem to indicate. There is a value of OVC, OVC_T, for which SNR attains a maximum and retains the maximum value for all OVC $\geq OVC_T$. This effect is shown ion Figure 2-15 where N_S is sufficiently large to produce the effect for OVC ≤ 30. This effect is not very surprising because the PDFs and the CDFs under both hypotheses approach each other for sufficiently large overcontainment (Figures 2-2 through 2-4 and Figures 2-5 through 2-8). However, the presence of a small amount of coherence under H_1 prevents the PDFs and CDFs from becoming equal but cause a constant offset between the PDFs and CDFs for H_o and H_1.

2.3.2 Unequal Channel Performance

The unequal channel detection performance is only discussed for $P_D = 0.5$ and $P_{FA} = 10^{-4}$ because the effects of the unequal channels are the same for $P_D = 0.1$ and 0.9. In the unequal channel case, the true in-band MSCC is

$$\rho_T^2 = \frac{(DIF*SNR)SNR}{(DIF*SNR+1)(SNR+1)} \rho_S^2 \qquad (2.40)$$

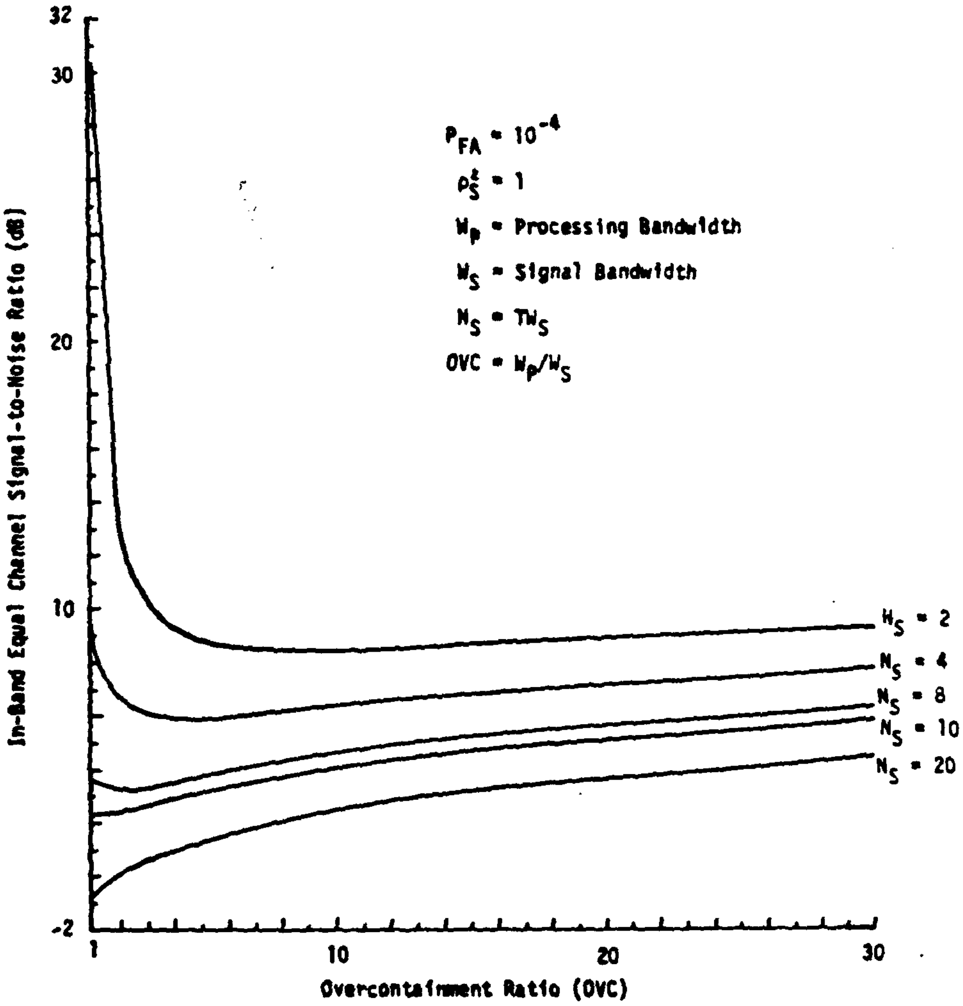

Figure 2-13. Effects of Overcontainment for $P_D = 0.1$

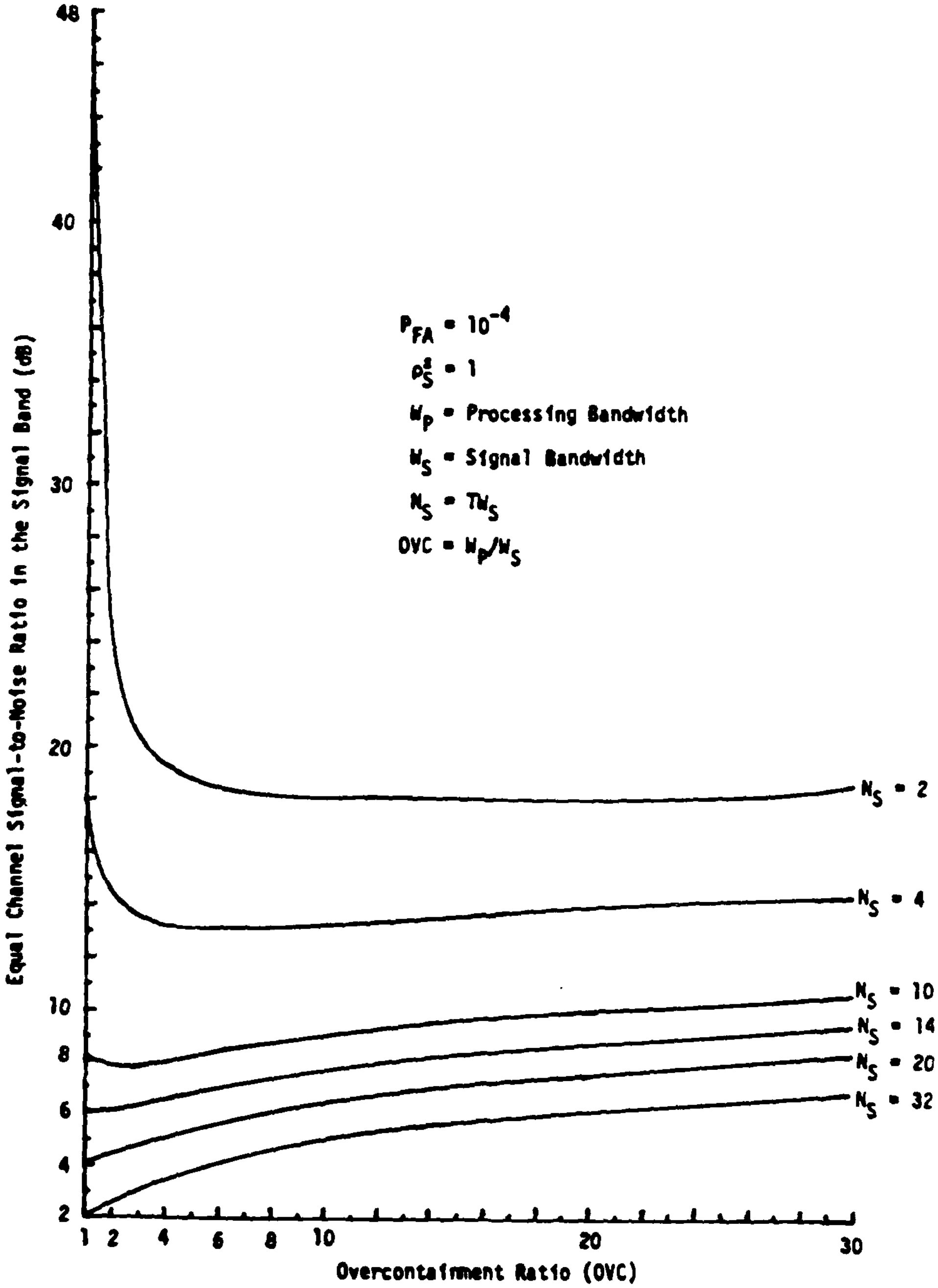

Figure 2-14. Effects of Overcontainment for $P_D = 0.9$

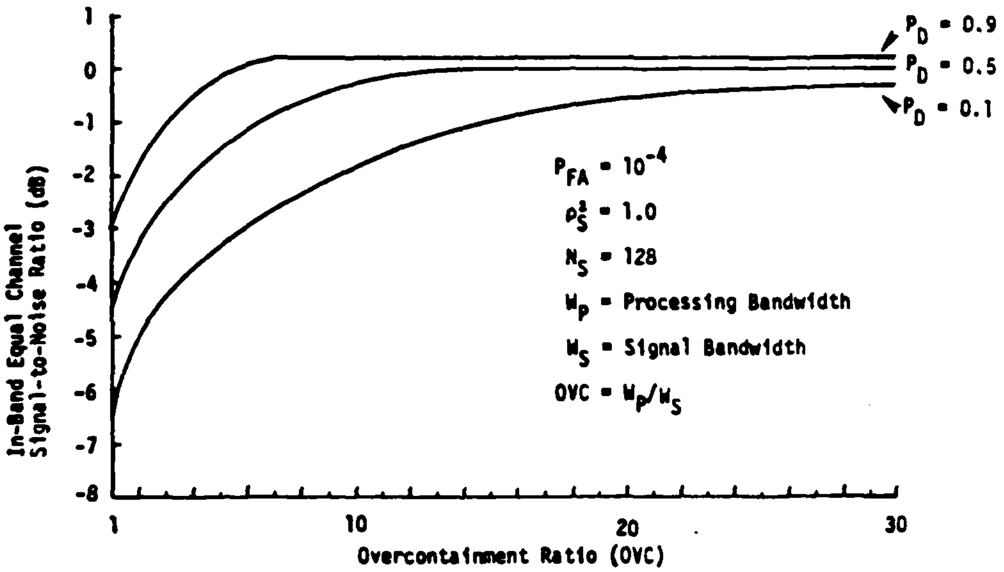

Figure 2-15. Effects of Overcontainment for Large N_S

where SNR_2 = SNR, SNR_1 = DIF*SNR, and $SNR_1 \geq SNR_2$. The equal channel case occurs for DIF = 0 dB. If SNR_1 is very large, DIF is very large and ρ_T^2 becomes

$$\rho_T^2 = \frac{SNR}{SNR + 1} \rho_S^2 \qquad (2.41)$$

Therefore, the equal channel case (DIF = 0 dB) provides the upper bound to SNR and the limiting case of unequal channels (DIF very large) provides the lower bound to SNR.

The unequal channel effects for N_S = 2 are shown in Figure 2-16 as a function of overcontainment. Therre is still some gain to be obtained by overcontaining. However, in the limiting case of unequal channels, SNR always decreases with OVC, but does reach a minimum value as will be seen for larger N_S. It is also apparent that the SNR in the weak channel can be decreased as the SNR in the strong channel is increased.

The unequal channel effects for other N_S are shown in Figure 2-17. For small N_S, overcontaining still produces gains. In the limiting case, the SNR reaches a minimum and maintains that value for further increases in OVC. However, for large N_S, SNR increases with OVC till a maximum value is reached. A small amount of gain can be produced for sufficiently large OVCs in the limiting case. The cause for this effect in unknown at this time. It can be concluded that for DIFs in the range of practical interest, the effects of overcontainment are the same for the equal and unequal channel cases.

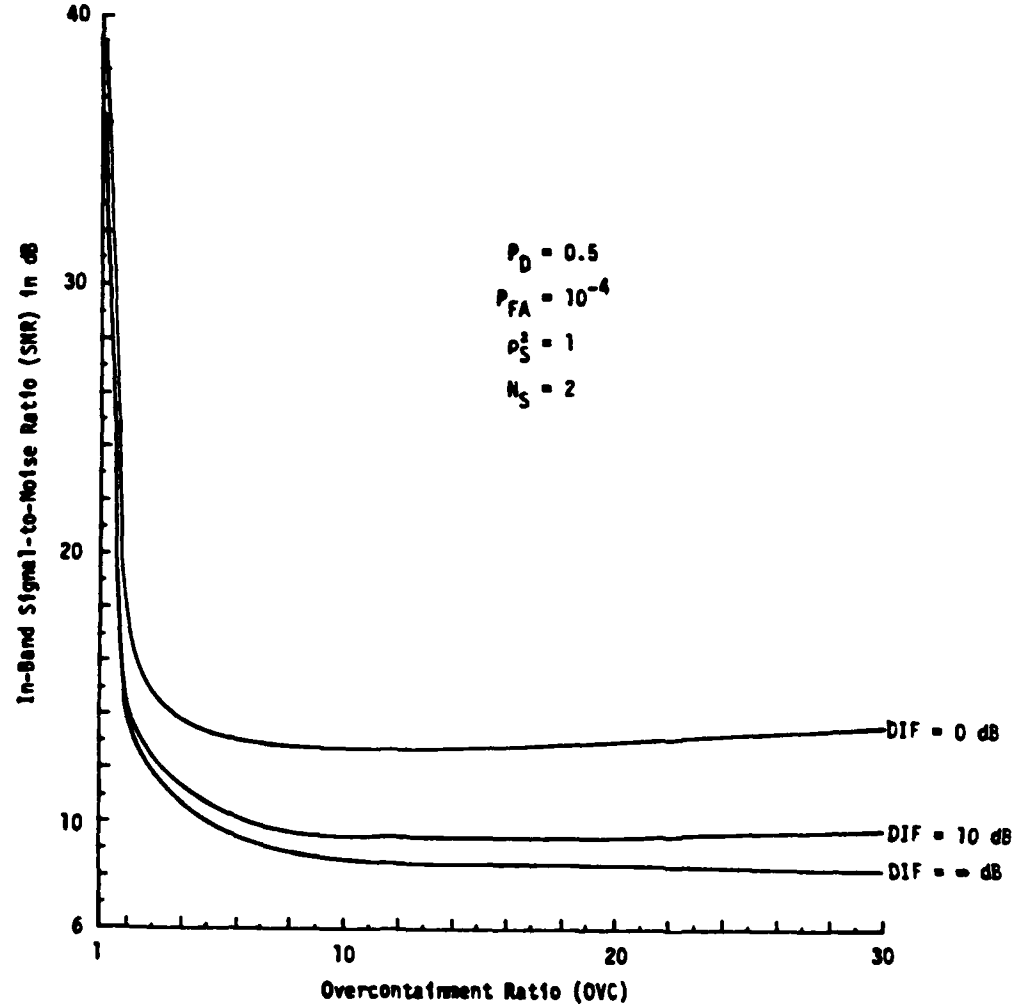

Figure 2-16. Effects of Unequal Channel Conditions

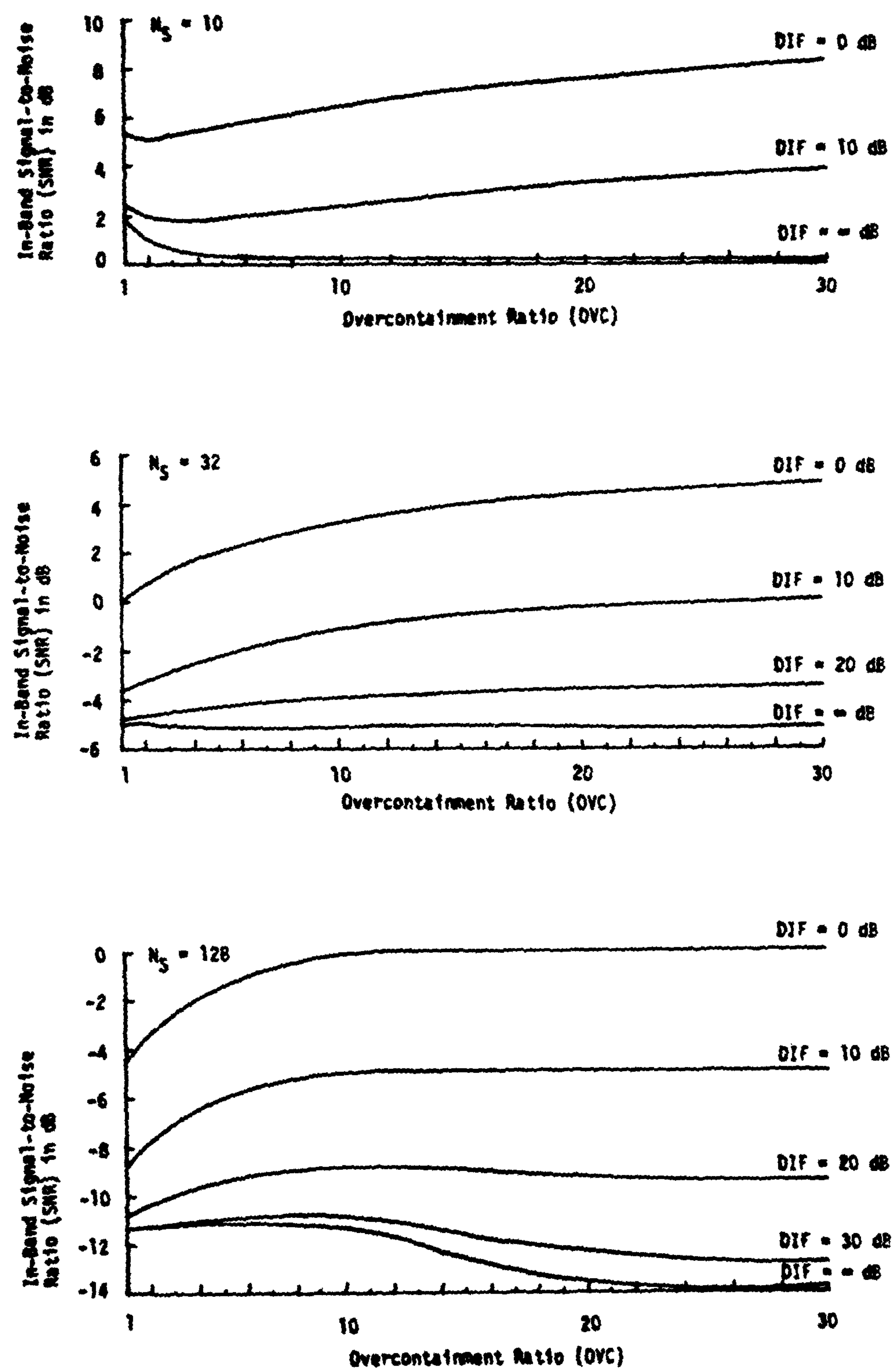

Figure 2-17. Effects of Unequal Channel Conditions for $P_D = 0.5$, $P_{FA} = 10^{-4}$ and $\rho_S^2 = 1.0$

2.4 DISCUSSION

The probability density and cumulative density functions of the sample MSCC were derived for the signal overcontainment case under conditions of known and flat signal and noise power spectra. As expected, the CDF and PDF took on "noise-like" characteristics when OVC became large.

The CDF was used to study the effects of signal overcontainment on the required in-band channel SNR to achieve a P_D = 0.1, 0.5 and 0.9 and a $P_{FA} = 10^{-4}$ for $\rho_S^2 = 1.0$. It was observed that for $N_S < N_{S_m}$ the SNR decreased with increasing OVC until a minimum was reached where N_{S_m} is 10, 12, and 14 for P_D = 0.1, 0.5 and 0.9, respectively. Once the minimum was reached, the SNR increased with increasing OVC. For $N_S \geq N_{S_m}$, the SNR always increased with OVC. For OVC sufficiently large, SNR reached a maximum value and SNR remained at that maximum value for all further increases in OVC.

III. APPROXIMATION TO THE DETECTION PERFORMANCE OF THE SAMPLE MAGNITUDE-SQUARED CORRELATION COEFFICIENT

The expressions developed in Chapter II for the probability density function (PDF) and the cumulative density function (CDF) of the sample magnitude-squared correlation coefficient (MSCC) are complex and difficult to evaluate numerically, Eq. (2.27) and (2.33). It is desirable to have an approximation of the PDF and CDF of the sample MSCC that is easy to use. Such an approximation based on the matched containment equations for the PDF and CDF is presented and evaluated in this section. Expressions for the PDF and CDF are derived and evaluated in Section 3.1. The equation for the CDF is then used to evaluate the detection performance in Section 3.2 where the approximation performance is compared to the exact performance.

3.1 CUMULATIVE AND PROBABILITY DENSITY FUNCTIONS

The approximation for the CDF and PDF of the sample MSCC is to use the matched containment expressions for the CDF and PDF given by Eq. (2.35) and (2.30), respectively, but to (1) use the degrees of freedom in the noise, and (2) use the true MSCC in the processing band for ρ_T^2. The true in-band MSCC is

$$\rho_T^2 = \frac{SNR_1 \; SNR_2}{(SNR_1+1)(SNR_2+1)} \, \rho_S^2 \tag{3.1}$$

where SNR_ℓ is the in-band signal-to-noise power ratio for channel ℓ and ρ_S^2 is the magnitude-squared correlation coefficient between the signal components. Define the SNR in the processing band to be

$$\overline{SNR_\ell} = SNR_\ell / OVC \tag{3.2}$$

where OVC is the overcontainment ratio. Then true MSCC in the processing band is

$$\rho_{TP}^2 = \frac{\overline{SNR}_1\ \overline{SNR}_2}{(\overline{SNR}_1+1)(\overline{SNR}_2+1)}\ \rho_S^2$$

$$= \frac{SNR_1\ SNR_2}{(SNR_1 + OVC)\ (SNR_2 + OVC)}\ \rho_S^2 \qquad (3.3)$$

Therefore, for a given ρ_S^2, SNR_1, and SNR_2, $\rho_{TP}^2 < \rho_T^2$. Finally, the degrees of freedom to use in the matched containment expression is not the signal degrees of freedom (N_S), but the noise degrees of freedom

$$N_P = N_S * OVC \qquad (3.4)$$

The approximation of the PDF of the sample MSCC in the signal overcontainment case is

$$f(\rho^2|\rho_T^2,M,N_S) \approx f(\rho^2|\rho_{TP}^2,0,N_P) =$$

$$(N_P-1)(1 - \rho_{TP}^2)(1-\rho^2)^{N_P-2} \times$$

$$(1 - \rho^2\rho_{TP}^2)^{1-2N_P}\ {}_2F_1(1-N_P,\ 1-N_P;\ 1;\ \rho^2\rho_{TP}^2) \qquad (3.5)$$

Example plots of the PDF of ρ^2 are shown in Figures 3-1 and 3-2 for equal channel conditions and $\rho_S^2 = 1.0$. It is seen that the PDF moves to the left and takes on "noise-like" characteristics as OVC increases. By comparing Figure 3-1 to Figure 2-3 and Figure 3-2 to Figure 2-4, it is seen that (1) the location of the peak for the approximate PDF is the same as the location of the peak for the true PDF for the same OVC, and (2) the approximate PDF is more concentrated than the true PDF for the same OVC.

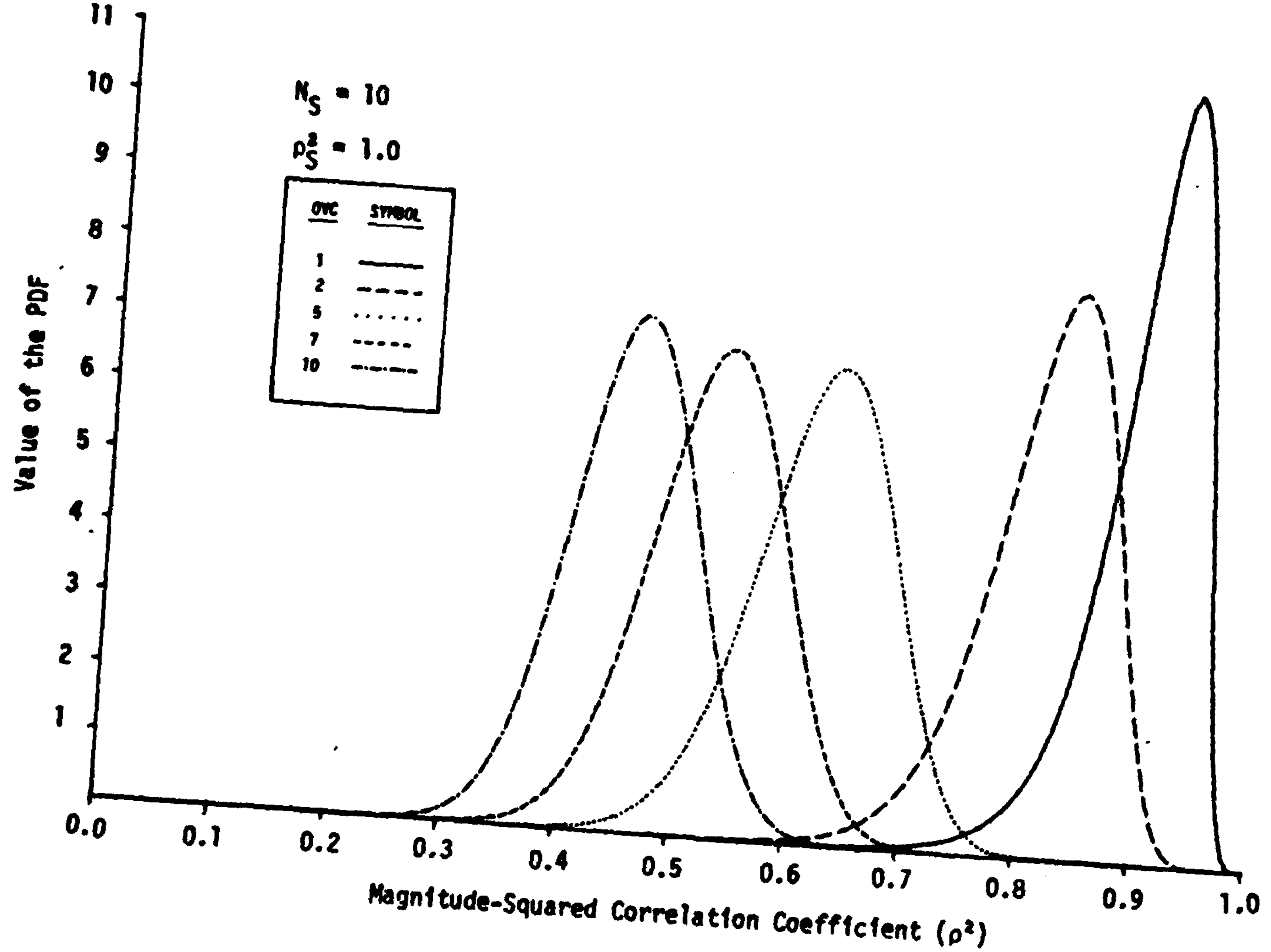

Figure 3-1. Approximate Probability Density Function of ρ^2 for $\rho_T^2 = 0.9$

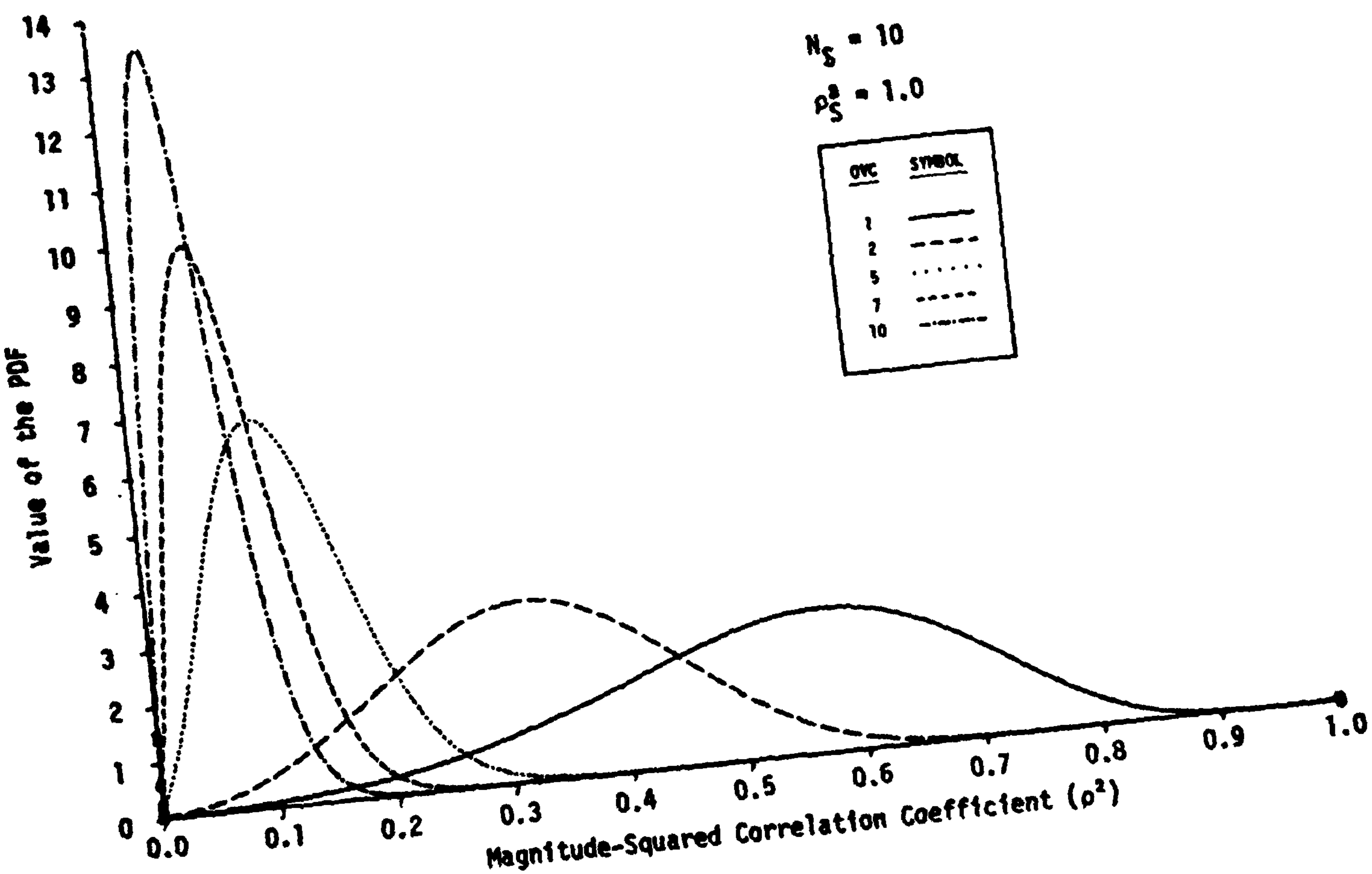

Figure 3-2. Approximate Probability Density Function of ρ^2 for $\rho_T^2 = 0.5$

The approximation of the CDF of the sample MSCC is

$$F(\rho_t^2|\rho_T^2,M,M_S) \approx F(\rho_t^2|\rho^2{}_{TP},0,N_P) =$$

$$\rho_t^2 \left[\frac{1-\rho_{TP}^2}{1-\rho_t^2\rho_{TP}^2}\right]^{N_P} \sum_{\ell=0}^{N_P-2} \left[\frac{1-\rho_t^2}{1-\rho_t^2\rho_{TP}^2}\right]^{\ell} \times$$

$$_2F_1(-\ell,\ 1-N_P;\ 1;\ \rho_t^2\rho_{TP}^2) \qquad (3.6)$$

where ρ_t^2 is the threshold. Example plots of the approximate CDF are shown in Figures 3-3 through 3-5 for equal channel conditions and for $\rho_S^2 = 1.0$. Upon comparing Figure 3-3 to Figure 2-6, Figure 3-4 to Figure 2-7, and Figure 3-5 to Figure 2-8, it is seen that the approximate CDF is less tilted than the true CDF and that the tails of the approximate CDF are more sharply defined.

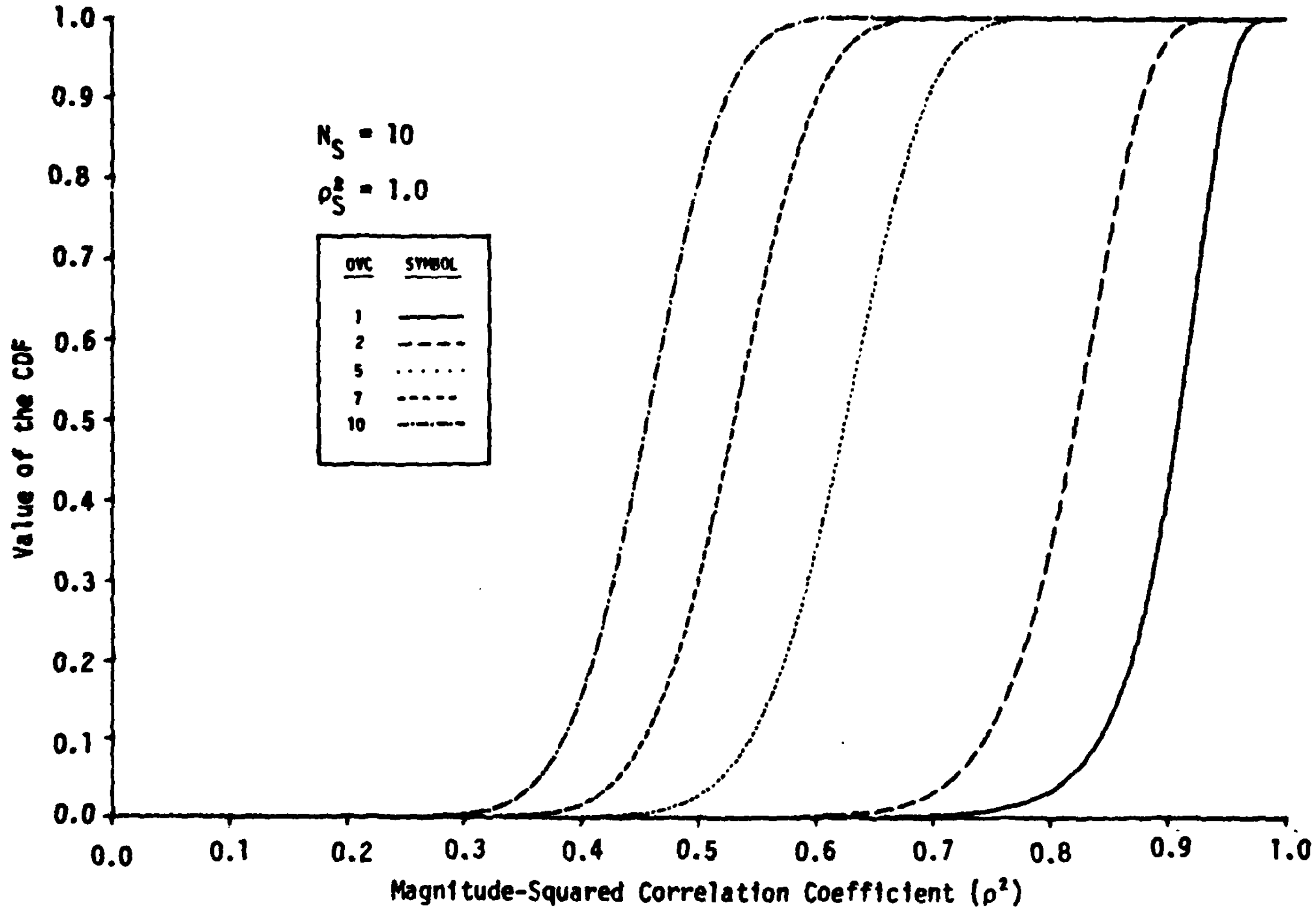

Figure 3-3. Approximate Cumulative Density Function of ρ^2 for $\rho_T^2 = 0.9$

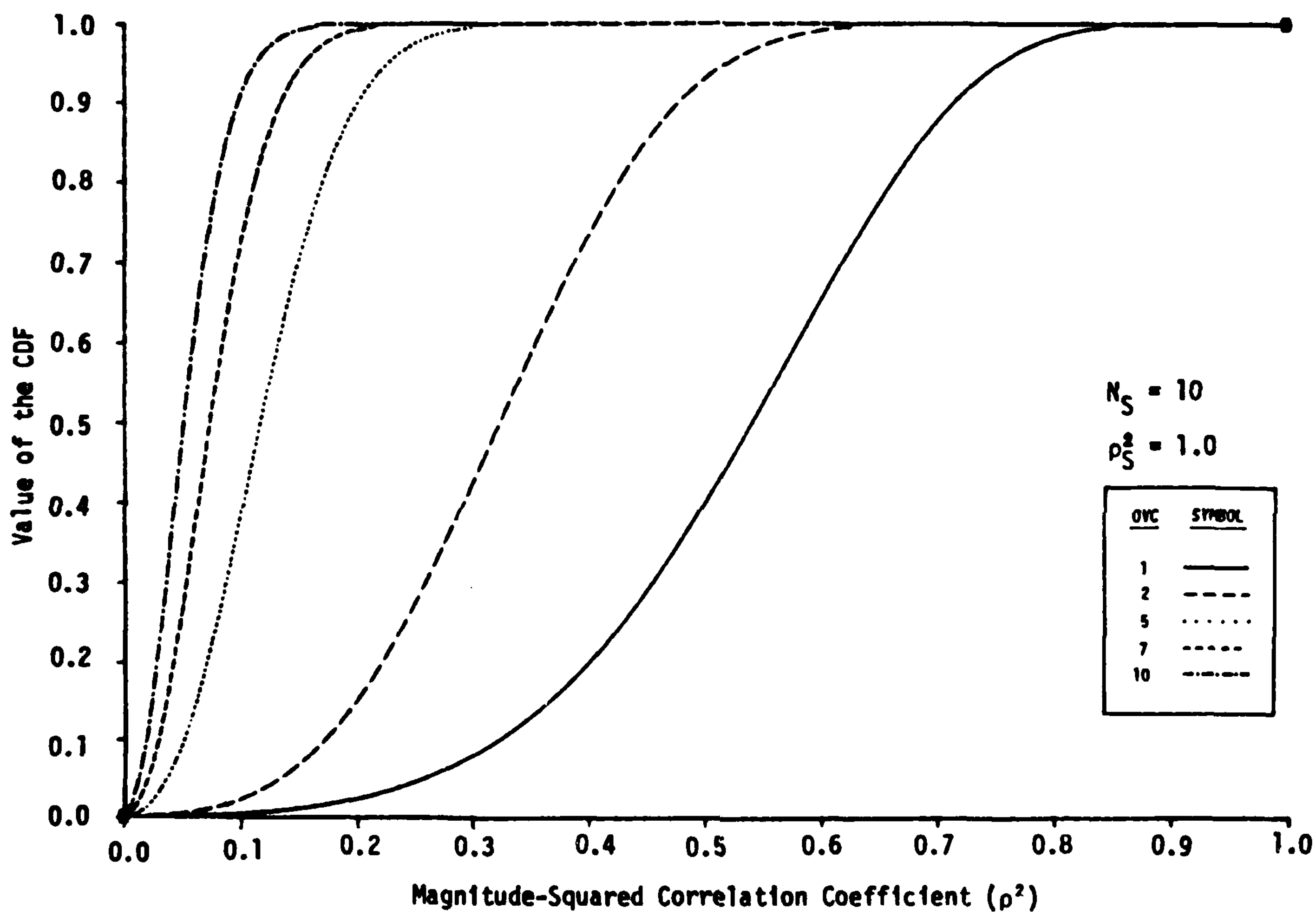

Figure 3-4. Approximate Cumulative Density Function of ρ^2 for $\rho_T^2 = 0.5$

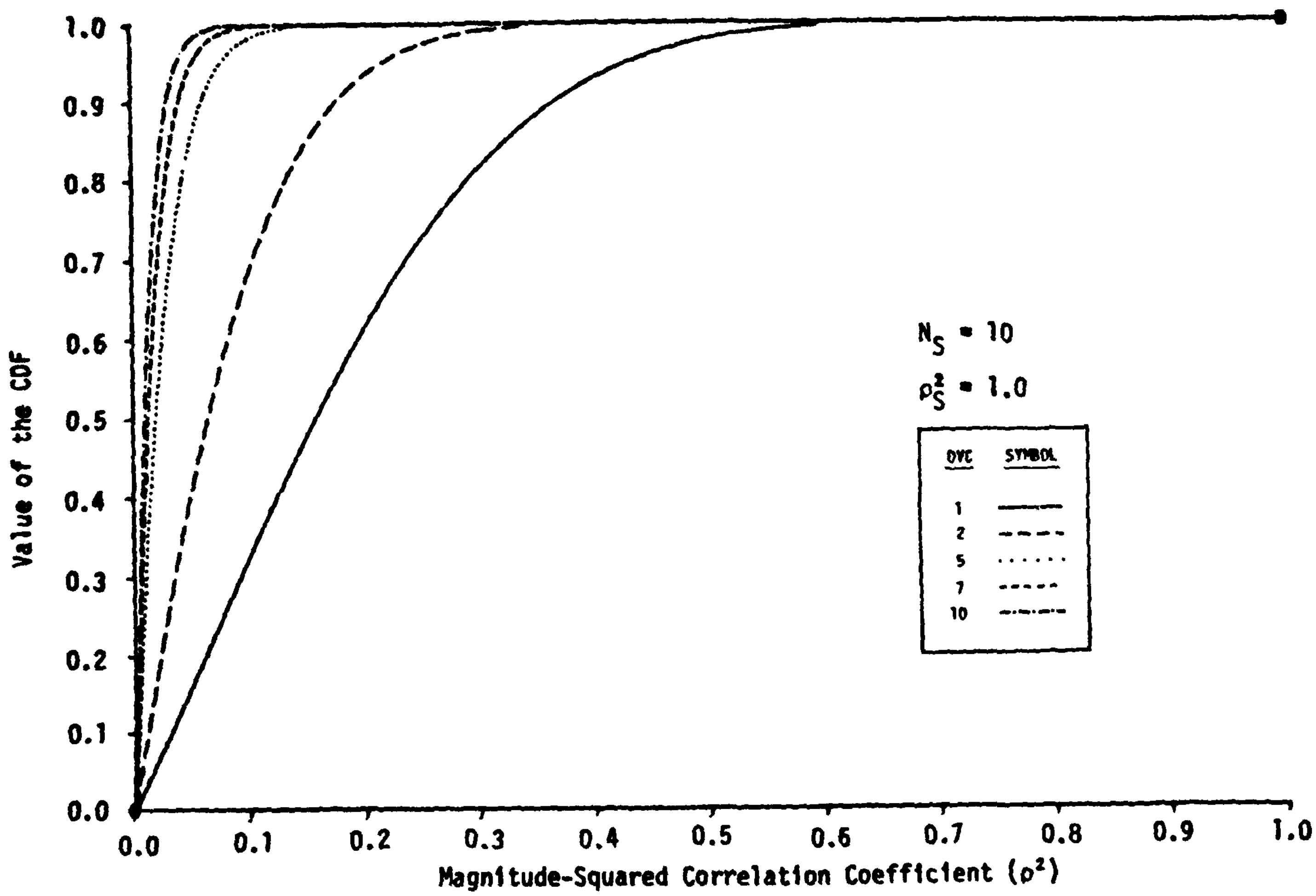

Figure 3-5. Approximate Cumulative Density Function of ρ^2 for $\rho_T^2 = 0.1$

3.2 APPROXIMATE DETECTION PERFORMANCE

The procedure for quantifying the detection performance with the approximate CDF is the same as used in Section 2.3 for the true CDF. The Probability of False Alarm is

$$P_{FA} = (1 - \rho_t^2)^{N_P - 1} \tag{3.7}$$

and the Probability of Detection is

$$P_D = 1 - \rho_t^2 \left[\frac{1 - \rho_{TP}^2}{1 - \rho_t^2 \rho_{TP}^2} \right] \sum_{\ell=0}^{N_P-2} \left[\frac{1 - \rho_t^2}{1 - \rho_t^2 \rho_{TP}^2} \right]^{\ell} \times$$

$$_2F_1(-\ell,\ 1-N_P;\ 1;\ \rho_t^2 \rho_{TP}^2) \tag{3.8}$$

where

$$\rho_{TP}^2 = \frac{(DIF*SNR)SNR}{(DIF*SNR+OVC)(SNR*OVC)} \quad . \tag{3.9}$$

SNR is the in-band SNR for the weakest channel, DIF $\geq$ 1, and DIF = 0 dB for equal channel conditions.

3.2.1 Equal Channel Performance

The approximate in-band equal channel SNRs for $P_{FA} = 10^{-4}$ are shown in Figures 3-6 through 3-8 as a function of OVC for P_D = 0.1, 0.5, and 0.9, respectively. Upon comparing Figures 3-6 through 3-8 to Figures 2-10, 2-13, and 2-14, it is seen that the approximate equal channel detection performance has the same characteristics as the true equal channel detection performance. The approximate SNRs for P_D = 0.1 closely match the true SNRs for all N_S, while the approximate SNRs for P_D = 0.9 are smaller than the true SNRs. However, when N_S is sufficiently large, the approximate and true SNRs closely agree for the range of OVC considered. It should be noted that the approximate detection performance predicts gains by overcontaining for larger N_S than does the true performance though the difference in N_S is slight.

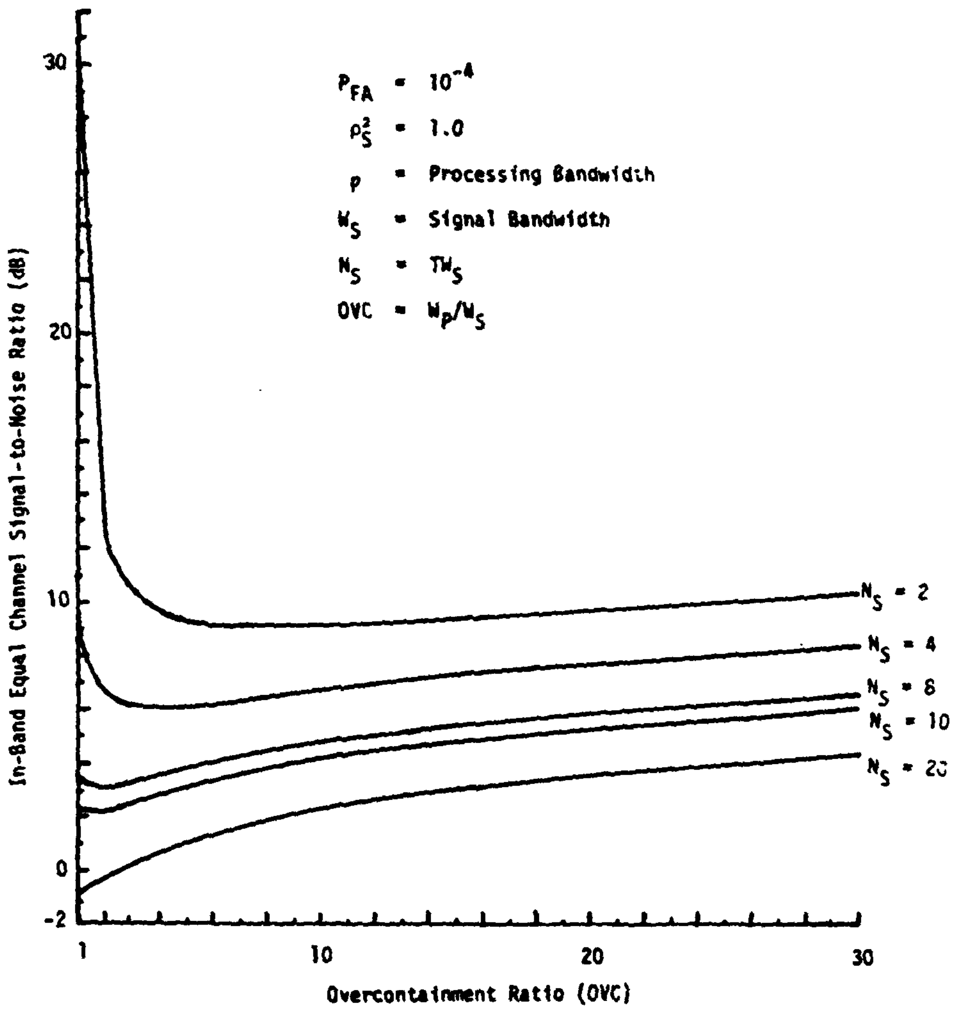

Figure 3 6. Approximate Effects of Overcontainment for P_D = 0.1

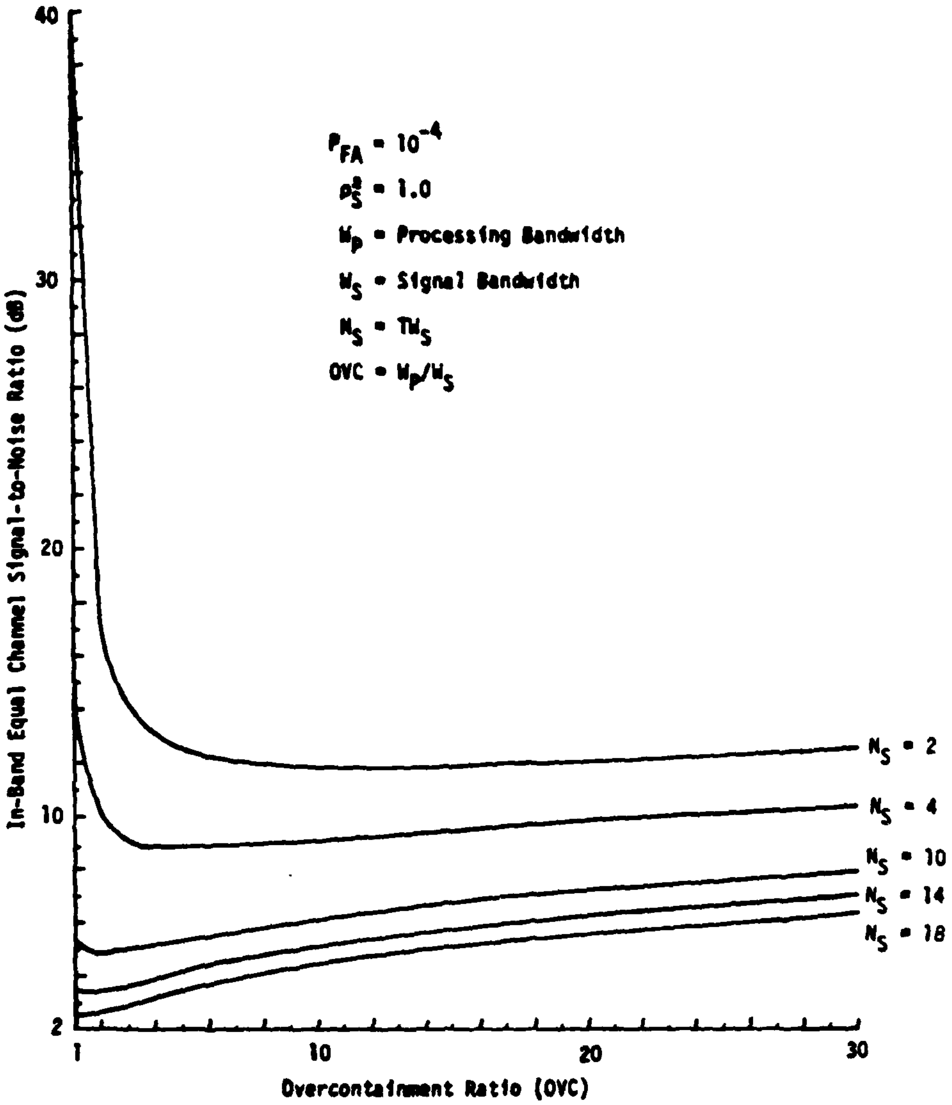

Figure 3 7. Approximate Effects of Overcontainment for $P_D = 0.5$

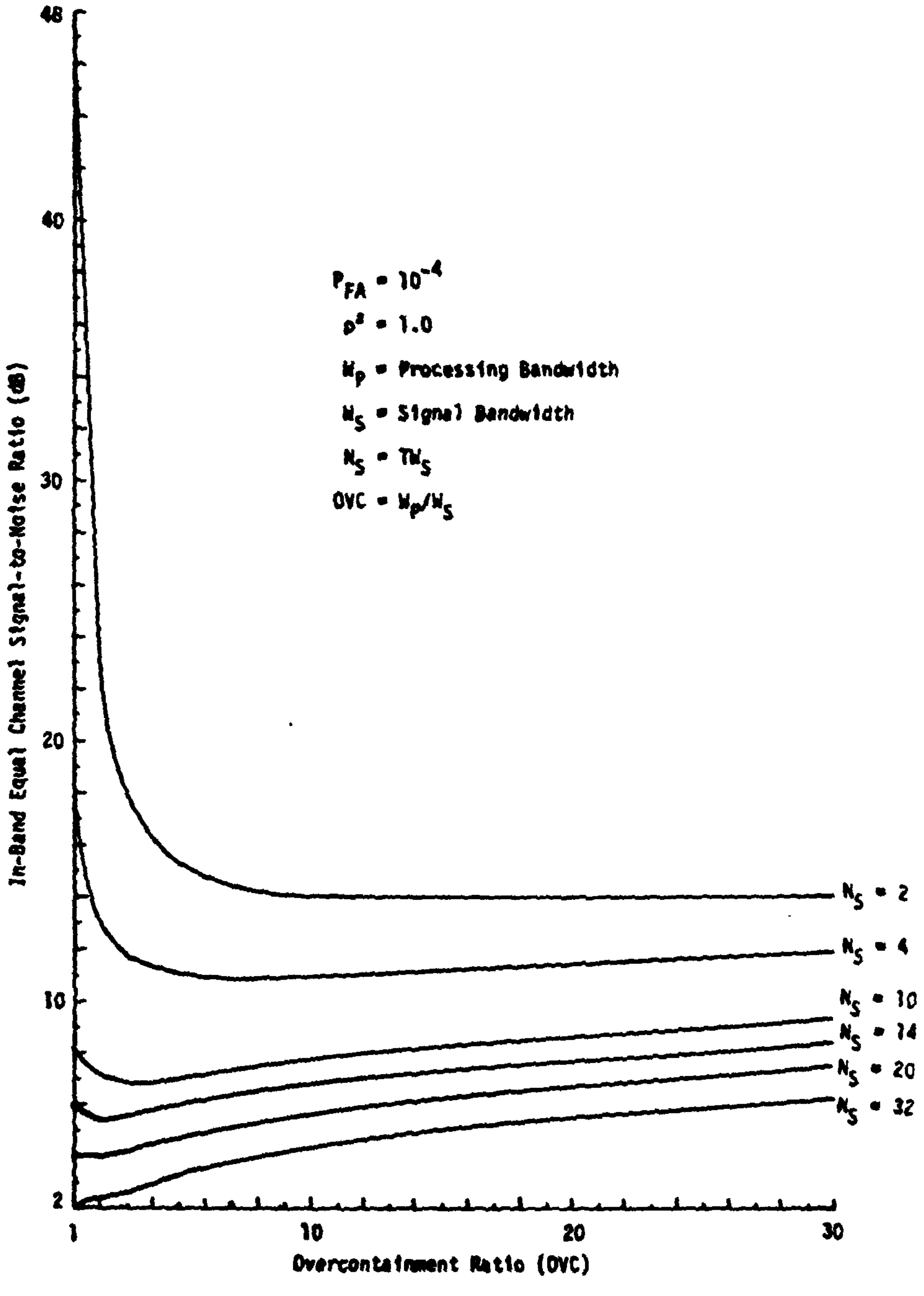

Figure 3 8. Approximate Effects of Overcontainment for $P_D = 0.9$

The approximate SNR does not reach a maximum value for sufficiently large OVC as does the true SNR as shown in Figure 3-9. The approximation indicates that SNR increases 1 dB per doubling of OVC for all OVC once OVC is sufficiently large.

3.2.2 Unequal Channel Performance

The matched containment detection performance equations are only dependent on the SNRs through the true MSCC, Eq. (3.8) and (3.9). It is then only necessary to use the ρ_{TP}^2 developed for the equal channel case and solve Eq. (3.19) for the SNR for a given DIF and OVC. If the SNR in one channel is much larger than in the other channel, Eq. (3.9) reduces to

$$\rho_{TP}^2 = \frac{SNR}{SNR + OVC} \rho_S^2 \quad . \qquad (3.10)$$

The approximate unequal channel detection performance is shown in Figure 3-10 for $P_D = 0.5$, $P_{FA} = 10^{-4}$, and $N_S = 2$. There is still some gain to be had by overcontaining but in the limiting case, SNR always decreases with OVC but reaches a minimum as will be seen for larger N_S. The approximate unequal channel SNRs are always smaller than the true unequal channel SNRs, but the difference is small for the range of OVCs considered (Figures 2-16 and 3-10).

The approximate unequal channel detection performance for other N_S is shown in Figure 3-11. There is still some gain obtainable by overcontaining for small N_S. In the limiting case, SNR reaches a minimum value and maintains that value for further increases in OVC. For large N_S, SNR always increases with OVC. In the limiting case, SNR is insensitive to OVC in contrast to the true performance where a small amount of gain can be obtained for sufficiently large OVCs (Figure 2-17). It can be concluded that for DIFs in the range of practical interest (0 dB - 30 dB), the effects of overcontainment are the same for the equal and unequal channel cases.

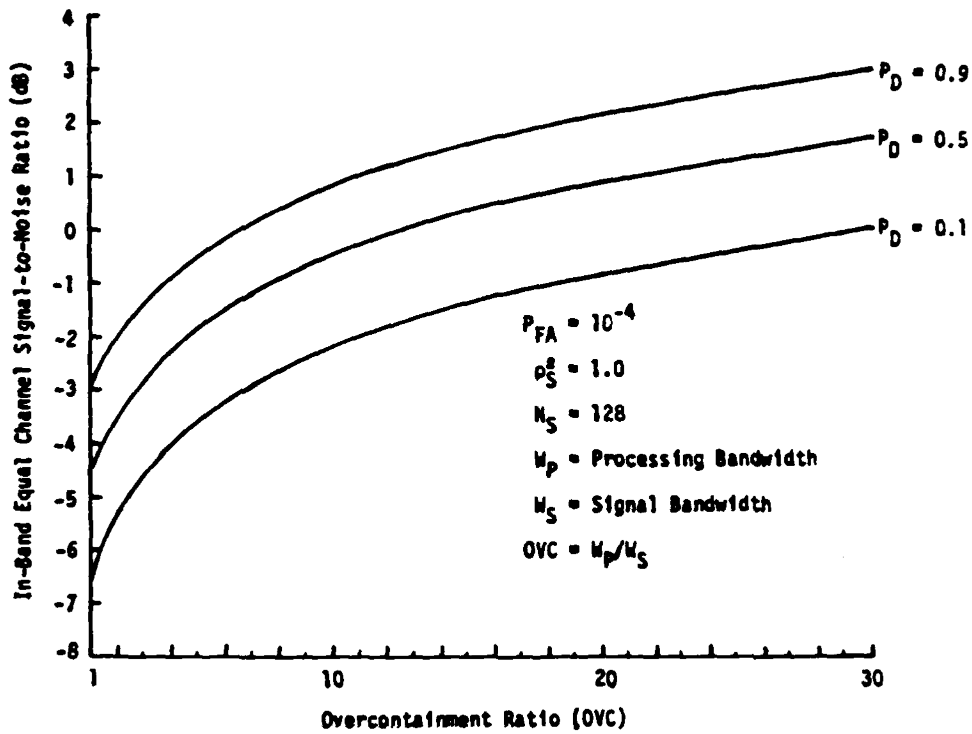

Figure 3-9. Approximate Effects of Overcontainment for Large N_S

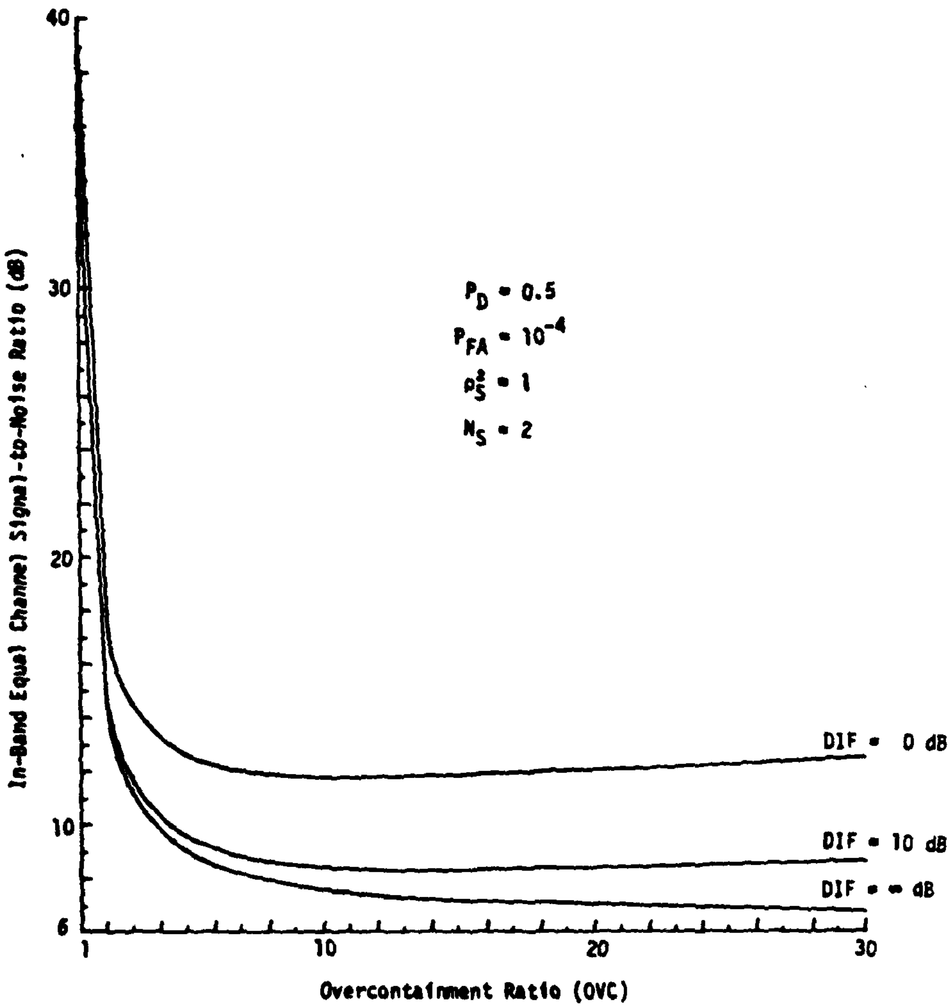

Figure 3-10. Approximate Effects of Unequal Channel Conditions

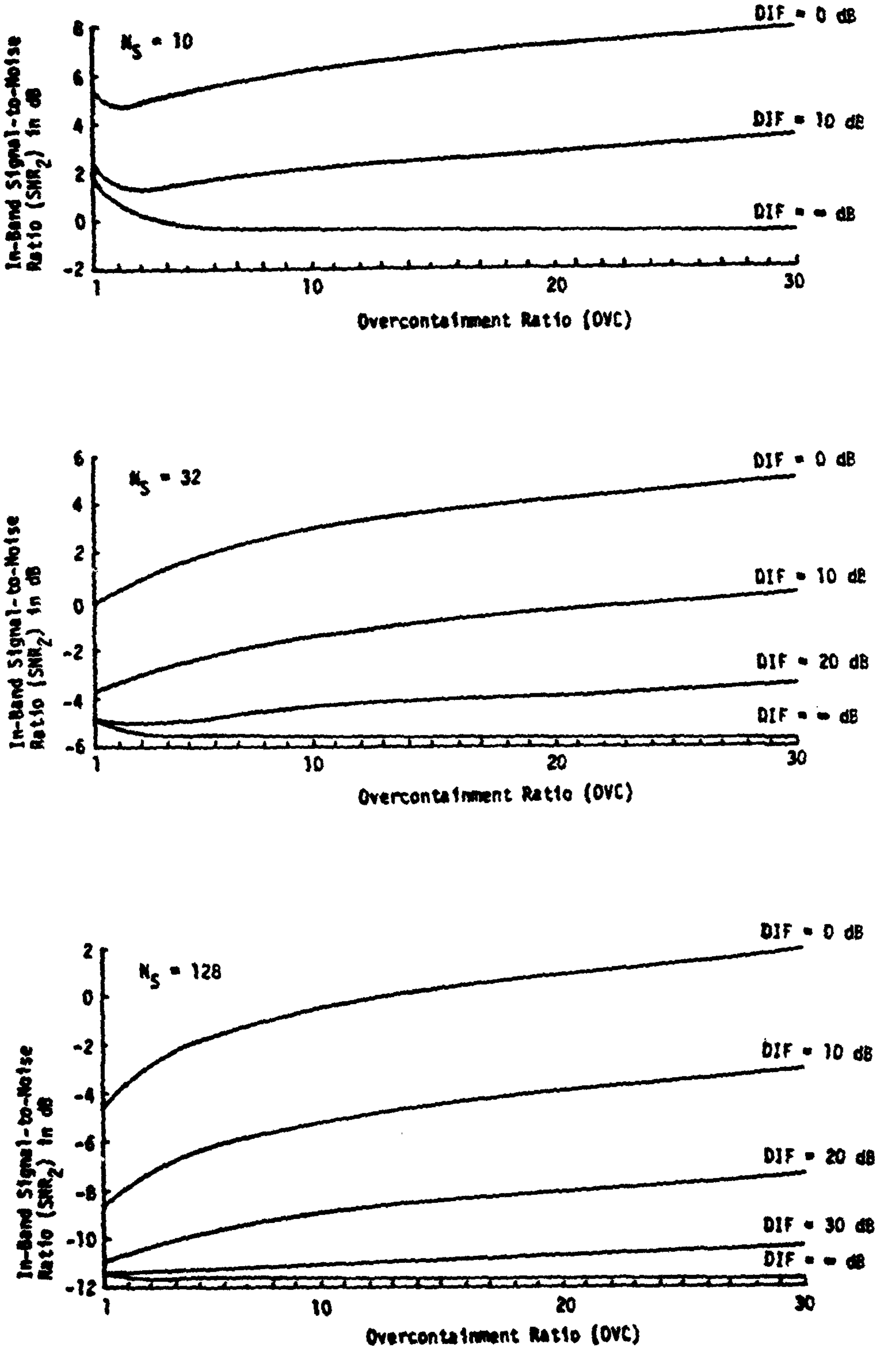

Figure 3-11. Approximate Effects of Unequal Channel Conditions for $P_D = 0.5$, $P_{FA} = 10^{-4}$ and $\rho_S^2 = 1.0$

3.3 DISCUSSION

An approximation to the detection performance for signal overcontainment was developed based on the matched containment equations for the CDF and PDF of the sample MSCC. This approximate CDF and PDF had the same characteristics as the true CDF and PDF.

The approximate detection performance based on the approximate CDF closely matched the true detection performance for sufficiently large N_S. For small N_S, the approximation predicted SNRs that were lower than the true SNRs. The approximation predicted that for sufficiently large OVC, SNR increased 1 dB per doubling of OVC for all OVC, whereas the true performance predicts that SNR will reach a maximum. Therefore, the approximation should be used with care to predict performance for large N_S's and large OVCs.

IV. DEPENDENCE BETWEEN CELLS IN AN AMBIGUITY SURFACE

The performance of algorithms that process an ambiguity surface as an image in order to enhance the detection performance or to enhance certain features is dependent on the statistics of the individual cells and the dependency between the cells. It is essential to understand the dependency between surface cells in order to quantify and understand the performance of these algorithms. The joint probability density between two cells is developed in Section 4.1. The correlation coefficient between two surface cells is derived and evaluated for the oversampled noise case in Section 4.2.

4.1 JOINT DENSITY FUNCTION

Each cell in an ambiguity surface is the sample MSCC between channel 1 and channel 2 for a specified time delay on channel 2. Consequently, the joint probability density functions between two cells is the joint PDF between two sample MSCCs for different time delays on channel 2. It is possible to define a three-dimensional observation vector containing a sample from channel 1, a sample from channel 2, and a delayed sample from channel 2, and to use the approach for deriving the single-cell PDF for deriving the joint PDF.

Let $Z(\ell)$ be a three-dimensional zero mean complex Gaussian random column vector with elements $z_1(\ell)$, $z_2(\ell)$, and $z_3(\ell)$ representing samples at time ℓT_S for $\ell = 1,2,\ldots,N_T$. T_S is the sampling interval, and $T = N_T T_S$ is the observation interval. The elements of $Z(\ell)$ map into time samples in the following manner: $z_1(\ell)$ is a sample from channel 1 at time ℓ; $z_2(\ell)$ is a sample from channel 2 at time ℓ; $z_3(\ell)$ is a sample from channel 2 at time $\ell+k_\Delta$ so that $z_3(\ell)$ is just a delayed version of $z_2(\ell)$. The sample auto-correlation matrix computed with the $z(\ell)$ is a three-dimensional matrix

PRECEDING PAGE BLANK-NOT FILMED

$$A = \sum_{\ell=1}^{N_T} Z(\ell)Z'(\ell) \tag{4.1}$$

$$= \begin{bmatrix} a_{11} & a_{12} & a_{13} \\ a_{12}^* & a_{22} & a_{23} \\ a_{13}^* & a_{23}^* & a_{33} \end{bmatrix} . \tag{4.2}$$

Since A is a three-dimensional matrix, it is possible to compute three sample MSCCs from A. The three sample MSCCs are:

$$\rho_{12}^2 = \frac{|a_{12}|^2}{a_{11}\ a_{12}} \tag{4.3}$$

$$\rho_{13}^2 = \frac{|a_{13}|^2}{a_{11}\ a_{33}} \tag{4.4}$$

$$\rho_{23}^2 = \frac{|a_{23}|^2}{a_{22}\ a_{33}} \tag{4.5}$$

where ρ_{12}^2 is the sample MSCC between channel 1 and channel 2; ρ_{13}^2 is the sample MSCC between channel 1 and the delayed channel 2, and ρ_{23}^2 is the sample MSCC between channel 2 and its delayed version. Since ρ_{23}^2 represents the normalized auto-correlation function of channel 2, the joint PDF between two cells in a surface is the joint PDF of ρ_{12}^2 and ρ_{13}^2, $f(\rho_{12}^2, \rho_{13}^2)$. Therefore, $f(\rho_{12}^2, \rho_{13}^2)$ can be computed from the PDF of A by a generalization of the approach used in Chapter II: (1) perform the change of variable indicated by Eqs. (4.3) through (4.5), and (2) integrate out the auxiliary variables a_{11}, a_{22}, a_{33}, ρ_{23}^2 and the phase angles of a_{12}, a_{13}, and a_{23}.

The PDF of A is derived by Fourier transforming the observations as done in Chapter II. Using the notation developed in Chapter II, the PDF of A in the three-dimensional case is

$$f(A) = \frac{|A|^{N_P-3} e^{-TR(R_{\hat{z}_1}^{-1} A)}}{\Pi^3 \, \Gamma(N_P) \, \Gamma(N_P-1) \, \Gamma(N_P-2) \, |R_{\hat{z}_1}|^{N_S} \, |R_{\hat{z}_o}|^{M}} \times$$

$$_1\widetilde{F}_1(M;\, N_P;\, \Delta RA) \qquad (4.6)$$

where $N_P = TW_P$ is the degrees of freedom in the noise; $N_S = 2TW_S$ is the degrees of freedom in the signal, R_{z_1} is the auto-spectral density matrix of the observations with signal present, R_{z_o} is the auto-spectral matrix of the noise, and ΔR is defined in Eq. (2.17). The auto-spectral density matrix for signal present is defined as

$$R_{\hat{z}_1} = \begin{bmatrix} \sigma_1^2 & \sigma_{12} & \sigma_{13} \\ \sigma_{12}^* & \sigma_2^2 & \sigma_{23} \\ \sigma_{13}^* & \sigma_{23}^* & \sigma_3^2 \end{bmatrix}$$

$$= \begin{bmatrix} \sigma_1^2 & \sigma_1\sigma_2\sigma_{T_{12}} e^{j\phi_{12}} & \sigma_1\sigma_3\sigma_{T_{13}} e^{j\phi_{13}} \\ \sigma_1\sigma_2\rho_{T_{12}} e^{-j\phi_{12}} & \sigma_2^2 & \sigma_2\sigma_3\rho_{T_{23}} e^{-\phi_{23}} \\ \sigma_1\sigma_3\rho_{T_{13}} e^{-j\phi_{13}} & \sigma_2\sigma_3\rho_{T_{23}} e^{-j\phi_{23}} & \sigma_3^2 \end{bmatrix}$$

where $\rho^2_{T_{nm}}$ is the true MSCC between channel n and m and ϕ_{nm} is the phase angle of σ_{nm}.

The joint PDF is only derived for the matched containment case (M=0) because of the difficulty in manipulating the mathematics. The detailed derivation of the joint PDF is presented in Appendix C and will not be repeated here. By performing the change of variables and integrating out the auxiliary variables discussed above, the joint PDF is

$$f(\rho_{12}^2,\rho_{13}^2) =$$

$$\frac{(1-\rho_{12}^2)^{N_P-2}(1-\rho_{13}^2)^{N_P-2}\left[1+2\rho_{T_{12}}\rho_{T_{13}}\rho_{T_{23}}\cos(\phi_{12}+\phi_{13}-\phi_{13})-\rho_{T_{12}}^2-\rho_{T_{13}}^2-\rho_{T_{23}}^2\right]^{2N_P}}{\Gamma(N_P)\ \Gamma(N_P-1)^2\left[(1-\rho_{T_{12}}^2)(1-\rho_{T_{23}}^2)(1-\rho_{T_{23}}^2)\right]^{N_P}} \times$$

$$\sum_{k=0}^{\infty} A(k)\ \cos k(\phi_{12}+\phi_{23}-\phi_{13}) \qquad (4.8a)$$

where

$$A(k) = (\rho_{12}^2\rho_{T_{12}}^2)^k(\rho_{13}^2\rho_{T_{13}}^2)^k(\rho_{T_{23}}^2)^k \times$$

$$\sum_{\ell,n,p=0}^{\infty} \frac{(\rho_{12}^2\rho_{T_{12}}^2)^n(\rho_{13}^2\rho^2_{T_{13}})^\ell(\rho_{12}^2\rho_{13}^2\rho_{T_{23}}^2)^p}{\ell!\ n!\ p!} \times$$

$$\frac{\Gamma(N_P+k+\ell+n)\ \Gamma(N_P+k+\ell+p)\ \Gamma(N_P+k+n+p)}{\Gamma(k+n+1)\ \Gamma(k+\ell+1)\ \Gamma(k+p+1)} \times$$

$${}_2F_1\left(N_P+k+\ell+p,\ N_P+k+n+p;\ N_P-1;\ (1-\rho_{12}^2)(1-\rho_{13}^2)\rho_{T_{23}}^2\right) . \qquad (4.8b)$$

In general the cells in a surface are not independent because the joint PDF does not factor. Before presenting the correlation coefficient between cells, it is instructive to consider the form of the joint PDF for some special cases. With the assumed flat power spectra, the auto- and cross-correlation functions have the form

$$R(\ell) = R(0)\,\frac{\sin(\Pi\ell/\alpha)}{\Pi\ell/\alpha} \qquad (4.9)$$

where ℓ is the time delay and $\alpha \geq 1$ is the ratio of the actual sampling rate to the Nyquist sampling rate.

Case I: Signal in Both Channels Sampled at Nyquist Rate

If the sampling is at the Nyquist rate, $\rho_{T_{13}}^2 = \rho_{T_{23}}^2 = 0$. In this case, the joint PDF becomes

$$f(\rho_{12}^2,\rho_{13}^2) = (N_p-1)(1-\rho_{13}^2)^{N_p-2} \times$$

$$(N_p-1)(1-\rho_{T_{12}}^2)^{N_p}(1-\rho_{12}^2)^{N_p-2} {}_2F_1(N_p,N_p;\ 1;\ \rho_{12}^2\rho_{T_{12}}^2) \tag{4.10}$$

which is the product of a "noise only" PDf for ρ_{13}^2 and a "signal plus noise" PDF for ρ_{12}^2 (Eqs. (2.30) and (2.31)). Therefore, the cells are independent in this case bacause the joint PDF factors.

Case II: Noise in Both channels Sampled at Nyquist Rate

Since the sampling is at the Nyquist rate, $\rho_{T_{23}}^2 = 0$. Also, $\rho_{T_{12}}^2 = \rho_{T_{13}}^2 = 0$ because the noise between channels 1 and 2 is spatially uncorrelated. The joint PDF is

$$f(\rho_{12}^2,\rho_{13}^2) = (N_p-1)(1-\rho_{12}^2)^{N_p-2} \times (N_p-1)(1-\rho_{13}^2)^{N_p-2} \quad . \tag{4.11}$$

Therefore, if the noise is sampled at the Nyquist rate, the cells are independent in the noise-only case.

Case III: Oversampled Noise in Both Channels

Since the noise between channels 1 and 2 is spatially uncorrelated, $\rho_{T_{12}}^2 = \rho_{T_{13}}^2 = 0$. However, because of the oversampling, $\rho_{T_{23}}^2 \neq 0$. The joint PDF is

$$f(\rho_{12}^2,\rho_{13}^2) = (N_P-1)^2(1-\rho_{12}^2)^{N_P-2}(1-\rho_{13}^2)^{N_P-2}(1-\rho_{T_{23}}^2)^{N_P} \times$$

$$\sum_{k=0}^{\infty} \frac{(\rho_{12}^2\rho^2{}_{13}\rho_{T_{23}}^2)^k}{(k!)^2} (N_P)_k \times$$

$${}_2F_1\left[N_P+k, N_P+k;\ N_P-1;\ (1-\rho_{12}^2)\ (1-\rho_{13}^2)\ \rho_{T_{23}}^2\right] \qquad (4.12)$$

As expected, the cells are dependent when the noise is oversampled.

4.2 CORRELATION COEFFICIENT BETWEEN CELLS

The correlation coefficient between two cells is a measure of the dependency between the cells. The correlation coefficient between ρ^2_{12} and ρ^2_{13} is defined as

$$\rho = \frac{E\{\rho^2_{12}\rho^2_{13}\} - E\{\rho^2_{12}\}\,E\{\rho^2_{13}\}}{\sqrt{\sigma^2_{\rho^2_{12}}\;\sigma^2_{\rho^2_{13}}}} \tag{4.13}$$

where $\sigma^2_{\rho^2_{12}}$ and $\sigma^2_{\rho^2_{13}}$ are the variance of ρ^2_{12} and ρ^2_{13} respectively.

According to ref. 1, the m^{th} moment of $\rho^2_{1\ell}$ for $\ell = 2$ and 3 is

$$E\{(\rho^2_{1\ell})^m\} = (1-\rho^2_{T_{1\ell}})^{N_p-1}\;\frac{\Gamma(N_p)\Gamma(m+1)}{\Gamma(N_p+m)} \times$$

$$_3F_2(m+1,\, N_p,\, N_p;\, m-N_p,\, 1;\, \rho^2_{T_{1\ell}}) \tag{4.14}$$

where $\rho^2_{T_{1\ell}}$ is the true MSCC of $\rho^2_{1\ell}$. The variance is then computed as

$$\sigma^2_{\rho^2_{1\ell}} = E\{(\rho^2_{1\ell})^2\} - E\{\rho^2_{1\ell}\}^{\,2} \quad . \tag{4.15}$$

The m^{th} joint moment between ρ^2_{12} and ρ^2_{13} is

$$E\{(\rho^2_{12}\rho^2_{13})^m\} = \int_0^1\!\int_0^1 (\rho^2_{12}\rho^2_{13})^m f(\rho^2_{12},\rho^2_{13})\; d\rho^2_{12}\,d\rho^2_{13} \quad . \tag{4.16}$$

It is shown in Appendix C that by substituting Eq. (4.8) into Eq. (4.16) that the m^{th} joint moment is

$$E\{(\rho_{12}^2\rho_{13}^2)^m\} = \frac{\left[1 + 2\rho_{T_{12}}\rho_{T_{13}}\rho_{T_{12}}\cos(\phi_{12}+\phi_{23}-\phi_{13}) - \rho_{T_{12}}^2 - \rho_{T_{13}}^2 - \rho_{T_{23}}^2\right]^{2N_p}}{\Gamma(N_p)\left[(1-\rho_{T_{12}}^2)(1-\rho_{T_{13}}^2)(1-\rho_{T_{23}}^2)\right]^{N_p}} \times$$

$$\sum_{k=0}^{\infty} B(k)\cos k\,(\phi_{12}+\phi_{23}-\phi_{13}) \tag{4.17a}$$

where

$$B(k) = \sum_{\ell,n,p=0}^{\infty} \frac{\rho_{T_{12}}^{k+2\ell}\,\rho_{T_{13}}^{k+2n}\,\rho_{T_{23}}^{k+2p}}{\ell!\;n!\;p!} \times$$

$$\frac{\Gamma(N_p+k+\ell+n)\,\Gamma(N_p+k+\ell+p)\,\Gamma(N_p+k+n+p)\,\Gamma(k+m+n+p+1)\,\Gamma(k+\ell+m+p+1)}{\Gamma(k+n+1)\,\Gamma(k+\ell+1)\,\Gamma(k+p+1)\,\Gamma(N_p+k+m+n+p)\,\Gamma(N_p+k+\ell+m+p)} \times$$

$$ {}_3F_2\left(N_p-1,\ N_p+k+\ell-p,\ N_p+k+n-p;\ N_p+k+\ell+m+n+1,\ N_p+k+m+n-p;\ \rho_{T_{23}}^2\right). \tag{4.17b}$$

The 1st joint moment is time consuming to evaluate because for each k there is a triple infinite sum involving a hypergeometric function with an infinite number of terms. The evaluation of the correlation coefficient is therefore restricted to the oversampled-noise-only case Case III in Section 4.12.

In the noise-only case

$$E\{\rho_{1\ell}^2\} = \frac{1}{N_p} \tag{4.18}$$

and

$$\sigma_{\rho_{1\ell}^2}^2 = \frac{N_p-1}{N_p^2(N_p+1)} \tag{4.19}$$

Letting $\rho^2_{T_{12}} = \rho^2_{T_{13}} = 0$,

$$E\{\rho^2_{12}\rho^2_{13}\} = (1 - \rho^2_{T_{23}})^{N_P} \sum_{k=0}^{\infty} \rho^{2k}_{T_{23}} \left(\frac{k+1}{N_P+k}\right)^2 \times$$

$$_3F_2(1,\ N_P-1,\ N_P+k;\ N_P+k+1,\ N_P+k+1;\ \rho^2_{T_{23}}) \qquad (4.20)$$

The correlation coefficient is then computed by substituting Eqs. (4.18) through (4.20) into Eq. (4.13). The correlation coefficient for the oversampled-noise-only case is plotted in Figure 4-1 as a function of N_P for several $\rho^2_{T_{23}}$.

It is seen that the correlation coefficient approaches the true value of the MSCC between the cells as N_P gets large. As an example of the use of Figure 4-1, consider the correlation between adjacent cells when the noise is oversampled by a factor of 2 and 4. For oversampling by 2 and 4, $\rho^2_{T_{23}}$ is 0.4 and 0.81, respectively, which indicates a significant correlation between cells. This type of behavior is also expected with signal present but the manner in which it approaches $\rho^2_{T_{23}}$ is more complex.

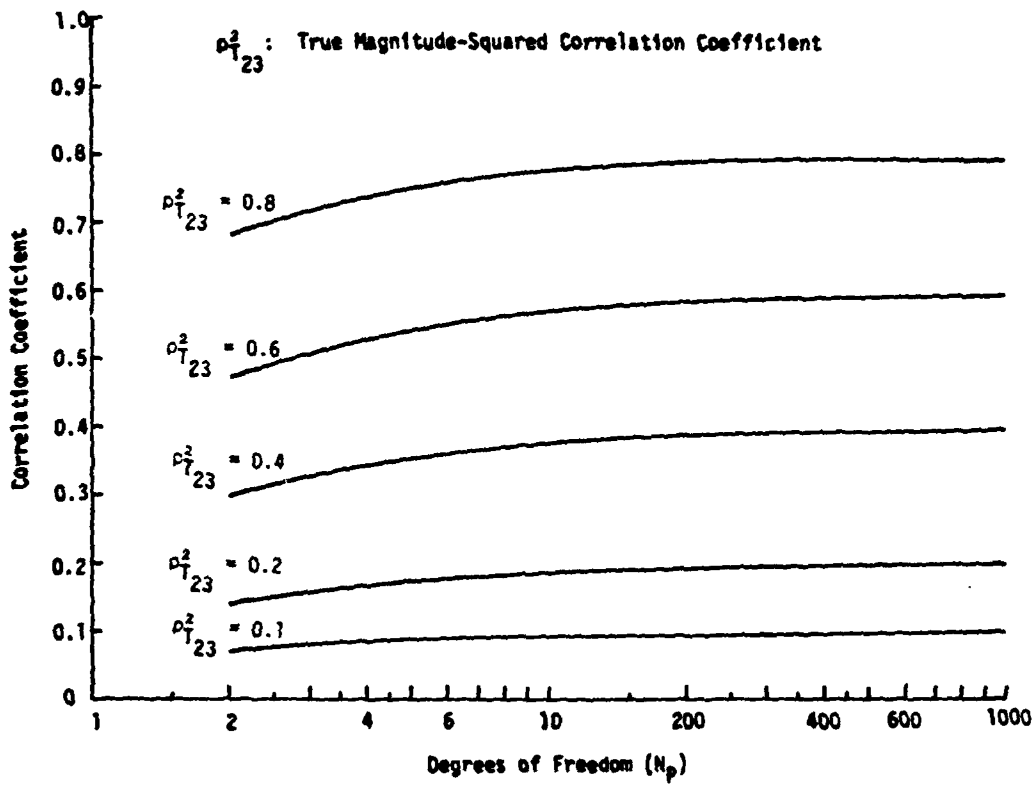

Figure 4-1. Correlation Coefficient for Oversampled Noise

4.3 DISCUSSION

The joint distribution between cells was derived for the matched containment case. It was shown that the cells are independent only when the data is sampled at the Nyquist rate. If the data is oversampled to produce surface feature magnification or to produce better estimates, the cells are dependent.

The correlation coefficient between cells was derived and evaluated for the oversampled noise case. It was shown that the correlation coefficient approaches the true MSCC between cells as N_p gets large. It is expected that the same will be observed with signal present.

V. CONCLUSIONS

A detailed analysis of the detection performance of the sample magnitude-squared correlation coefficient in the signal overcontainment case has been presented. The signal-to-noise power ratio (SNR) needed to detect a signal with a P_D of 0.1 - 0.9 can be reduced by increasing the signal overcontainment whenever the degrees of freedom in the signal (N_S) is small ($N_S \leq 12$). This gain is caused by decoupling N_S and the degrees of freedom in the noise (N_P) through overcontainment. In the matched containment case, whenever N_S is small, knowledge of the noise background is poor, high thresholds are needed for a specified P_{FA}, and large SNRs thereby are needed. By overcontaining, N_P is made larger, the P_{FA} threshold is reduced, and SNRs can be reduced. However, when N_S is large ($N_S > 12$), the SNR increases with increasing overcontainment because increases in noise power dominate the effects of increasing N_P. The gains caused by overcontainment for small N_S were verified by two independent simulations. The SNR increase with increasing overcontainment was verified for N_S in the range of 16 to 64 by the Minimum Detectable Signal Experiment conducted at the DARPA Acoustic Research Center in May, 1981.

An approximation to the exact detection performance was developed because the exact performance equations are complex and difficult to evaluate. The approximation is based on the well known matched containment performance equations. The approximate performance is very close to the exact performance for the ranges of overcontainment of practical interest though the approximate SNRs are slightly smaller than the exact SNRs. However, the approximation differs significantly from the exact performance for large OVC in that the exact SNRs reach a maximum value, while the approximate SNRs continually increase as the overcontainment increases. Therefore, the approximation is reasonably accurate for ranges of overcontainment of practical interest, but should be used with caution for large overcontainments.

The joint statistics of two cells in an ambiguity surface were developed and evaluated for the matched containment case. The cells in a surface are dependent whenever the data are sampled at a rate larger than the Nyquist rate, but are independent whenever the data is sampled at the Nyquist rate.

are independent, the well known equation relating P_{FA} to threshold can be used to set single-cell P_{FA}. If the data is oversampled to magnify surface features, there is no simple relation for selecting the threshold for a desired P_{FA}.

References

1. N.R. Goodman, "Statistical Analysis Based on a Certain Multivariate Complex Gaussian Distribution (An Introduction)," Annals of Math. Stat., vol. 34, 1963, pp. 152-177.

2. G.C. Carter, Estimation of the Magnitude-Squared Coherence Function (Spectrum), Report No. 7R4343, Naval Underwater Systems Center, New London, Conn., May 1972.

3. R.D. Trueblood and D.L. Alzrach, A Comparison of Incoherent and Coherent Test Statistics for Magnitude-Squared Coherence (U), Report No. TN1571, Naval Ocean Systems Center, San Diego, CA July 1975 (Secret).

4. G.C. Carter, "Receiver Operating Characteristics for a Linearly Thresholded Coherence Estimation Detector," IEEE Trans. Acoust., Speech, Signal Processing, vol. 25, pp. 90-92, February 1977.

5. The 1981 Naval Undersea Surveillance Symposium, Naval Postgraduate School, Monterey, CA, July 21-24, 1981.

6 C.S. Herz, "Bessel Functions of Matrix Argument," Annals of Math., vol. 61, May 1955, pp. 474-523.

7. A.J. Jones, "Distributions of Matrix Variates and Latest Rates Derived from Normal Samples," Annals of Math. Stat., vol. 35, 1964, pp. 475-501.

8 M. Abramowitz and I.A. Stegun (eds.), Handbook of Mathematical Functions with Formulas, Graphs, and Mathematical Tables, U.S. Government Printing Office, Washington, D.C., 1964.

9 Private conversation with G. Godshalk of ENSCO, Inc., Sunnyvale, CA.

10. Private conversations with B. Sharkey of Tetra-Tech, Inc., Arlington, VA.

11. G. Godshalk and J. LaPointe, Preliminary Minimum Detectable Signal (MDS) Experiment Report (U), Report No. VSD0183, ENSCO, Inc., Sunnyvale, CA, July 17, 1981 (Secret).

Appendix A

CROSS-COVARIANCE MATRIX OF THE FREQUENCY COEFFICIENTS

Let $Z(\ell)$ be a two-dimensional stationary zero mean complex random column vector with elements $z_1(\ell)$ and $z_2(\ell)$ which represent samples from two channels at time ℓT_S for $\ell = 1,2,\ldots,N_T$. T_S is the sampling interval and $T = N_T T_S$ is the observation interval. The cross-covariance matrix of $Z(\ell)$ is

$$R_z(k-\ell) = E\{Z(\ell)\, Z'(k)\} \tag{A.1}$$

where $\{\cdot\}$ denotes statiscal expectation and ' denotes the complex conjugate of the transpose. The elements of $R_z(k-\ell)$ are

$$R_z(k-\ell) = \begin{bmatrix} R_{z_1}(k-\ell) & R_{z_{12}}(k-\ell) \\ R_{z_{12}}^*(k-\ell) & R_{z_2}(k-\ell) \end{bmatrix}$$

$$= \begin{bmatrix} E\{z_1(\ell)\, z_1^*(k)\} & E\{z_1(\ell)\, z_2^*(k)\} \\ E\{z_2(\ell)\, z_1^*(k)\} & E\{z_2(\ell)\, z_2^*(k)\} \end{bmatrix} \tag{A.2}$$

where * denotes the complex conjugate.

Assume that the power spectral densities of $z_1(\ell)$ and $z_2(\ell)$ and the cross-spectral density between $z_1(\ell)$ and $z_2(\ell)$ have bandwidth $2W_P$ and are zero outside the interval $[-W_P, W_P]$. It is then possible to express the elements of $R_z(k-\ell)$ as

$$R_{z_1}(k) = \sum_{q=-N_F}^{N_F} S_1(q)\, e^{j\frac{2\Pi qk}{N_T}} \tag{A.3a}$$

$$R_{z_2}(k) = \sum_{q=-N_F}^{N_F} S_2(q)\, e^{j\frac{2\Pi qk}{N_T}} \tag{A.3b}$$

PRECEDING PAGE BLANK-NOT FILMED

$$R_{z_{12}}(k) = \sum_{q=-N_F}^{N_F} S_{12}(q)\, e^{j\frac{2\Pi qk}{N_T}} \qquad \text{(A.3c)}$$

where $S_1(q)$ and $S_2(q)$ are the power spectral densities of $z_1(\ell)$ and $z_2(\ell)$, respectively; $S_{12}(q)$ is the cross-power spectral density between $z_1(\ell)$ and $z_2(\ell)$; $2W_P = N_P/T = (2N_F+1)/T$; and the sampling rate $\geq 2W_P$.

Let $\hat{Z}(k)$ be the two-dimensional zero mean complex random column vector which represents the Fourier coefficients of the observation vector $Z(\ell)$ at frequency k/T for $k = 1,2,\ldots,N_P$. $\hat{Z}(k)$ is computed according to

$$\hat{Z}(k) = \frac{1}{N_T} \sum_{\ell=0}^{N_T-1} Z(\ell)\, e^{-j\frac{2\Pi \ell k}{N_T}} \qquad \text{(A.4)}$$

The cross-covariance matrix of $\hat{Z}(k)$ is

$$R_{\hat{Z}}(\ell,k) = E\{\hat{Z}(\ell)\ \hat{Z}(k)\}$$

$$= \begin{bmatrix} R_{\hat{Z}_1}(\ell,k) & R_{\hat{Z}_{12}}(\ell,k) \\ R^{*}_{\hat{Z}_{12}}(\ell,k) & R_{\hat{Z}_2}(\ell,k) \end{bmatrix} \qquad \text{(A.5)}$$

Substitute Eqs. (A.3) and (A.4) into Eq. (A.5).

$$R_{\hat{z}_1}(\ell,k) = E\{\hat{z}_1(\ell)\ \hat{z}_2^*(k)\}$$

$$= \frac{1}{N_T^2} \sum_{n,m=0}^{N_T-1} R_1(m-n)\, e^{-j\frac{2\Pi \ell n}{N_T}}\, e^{j\frac{2\Pi k m}{N_T}}$$

$$= \frac{1}{N_T^2} \sum_{q=-N_F}^{N_F} S_1(q) \sum_{n,m=0}^{N_T-1} e^{j\frac{2\Pi m(k-q)}{N_T}}\, e^{-j\frac{2\Pi n(\ell-q)}{N_T}}$$

$$= \sum_{q=-N_F}^{N_F} S_1(q)\, \frac{\sin \Pi(q-k)}{N_T \sin \Pi(\frac{q-k}{N_T})}\, \frac{\sin \Pi(q-\ell)}{N_T \sin \Pi(\frac{q-\ell}{N_T})}$$

$$= \begin{cases} 0 & , \ell \neq k \\ S_1(\ell) & , \ell = k \end{cases} \tag{A.6}$$

Similarly,

$$R_{\hat{z}_2}(\ell,k) = E\{\hat{z}_2(\ell)\ \hat{z}_2^*(k)\}$$

$$= \sum_{q=-N_F}^{N_F} S_2(q)\, \frac{\sin \Pi(q-k)}{N_T \sin \Pi\{\frac{q-\ell}{N_T}\}}\, \frac{\sin \Pi(q-\ell)}{N_T \sin \Pi\{\frac{q-\ell}{N_T}\}}$$

$$= \begin{cases} 0 & , \ell \neq k \\ S_2(\ell) & , \ell = k \end{cases} \tag{A.7}$$

and

$$R_{\hat{z}_{12}}(\ell,k) = E\{\hat{z}_1(\ell)\ \hat{z}_2^*(k)\}$$

$$= \sum_{q=-N_F}^{N_F} S_{12}(q) \frac{\sin \Pi(q-k)}{N_T \sin\{\frac{q-k}{N_T}\}} \frac{\sin \Pi(q-\ell)}{N_T \sin\{\frac{q-\ell}{N_T}\}}$$

$$= \begin{cases} 0 & , \ell \neq k \\ S_{12}(\ell) & , \ell = k \end{cases} \tag{A.8}$$

Therefore, for the strictly band-limited case,

$$R_z(\ell,k) = \begin{cases} 0 & , \ell \neq k \\ R_z(\ell) & , \ell = k \end{cases} \tag{A.9}$$

Appendix B

CUMULATIVE DENSITY AND PROBABILITY DENSITY FUNCTIONS OF THE SAMPLE MAGNITUDE-SQUARED CORRELATION COEFFICIENT

The derivation of the cumulative density function (CDF) and probability density function (PDF) of the sample magnitude-squared correlation coefficient (MSCC) is presented in this appendix for the signal overcontainment case under conditions of known but flat power spectra for the signal and noise. The PDF of the sampled MSCC is obtained by (1) deriving the PDF of the sampled auto-correlation matrix, and (2) making a change of variables and integrating out the auxiliary variables. the characteristic function of the sample auto-correlation matrix is derived in Section B.1. The Fourier inversion of the characteristic function to obtain the PDF of the sample auto-correlation matrix is presented in Section B.2. Finally, the derivation of the PDF and CDF of the sample MSCC is completed in Section B.3.

B.1 CHARACTERISTIC FUNCTION OF THE SAMPLE AUTO-CORRELATION MATRIX

Let $\hat{Z}(\ell)$ be a two-dimensional zero mean complex Gaussian random column vector at frequency ℓ with auto-spectral density matrix $R_Z(\ell,\ell)$ for $\ell = 1,\ldots,N_P$. Assume that $\hat{Z}(\ell)$ is independent of $\hat{Z}(k)$ for $k \neq \ell$. The sample auto-correlation matrix of the data is

$$A = \sum_{\ell=1}^{N_P} \hat{Z}(\ell)\, \hat{Z}'(\ell) \qquad (B.1)$$

where ' denotes complex conjugate.

The characteristic function of A is

$$M_A(\Phi) = E\left\{e^{jTR(A\Phi)}\right\}$$

$$= E\left\{e^{j\sum_{\ell=1}^{N_P} TR\left(\hat{Z}(\ell)\ \hat{Z}'(\ell)\ \Phi\right)}\right\}$$

$$= E\left\{e^{j\sum_{\ell=1}^{N_P} \hat{Z}'(\ell)\Phi\ \hat{Z}(\ell)}\right\}$$

$$= \prod_{\ell=1}^{N_P} E\left\{e^{j\hat{Z}'(\ell)\ \Phi\hat{Z}(\ell)}\right\} \qquad \text{(B.2)}$$

where TR(•) is the trace, Φ is a two-dimensional positive definite Hermitian matrix, and E{•} denotes statistical expectation. Since Φ is a positive definite Hermitian, there exists a *nonsingular matrix such that*

$$U'R_{\hat{Z}}(\ell,\ell)\ U = I \qquad \text{(B.3)}$$

$$U'\Phi U = W \qquad \text{(B.4)}$$

where W is a real diagonal matrix with $w_{11} > 0$ and $w_{22} > 0$. Let

$$\hat{Z}(\ell) = UY \quad . \qquad \text{(B.5)}$$

Then,

$$E\left\{e^{j\hat{Z}'(\ell)\Phi\hat{Z}(\ell)}\right\} = E\left\{e^{jY'U'\Phi UY}\right\}$$

$$= E\left\{e^{\,jY'WY}\right\}$$

$$= E\left\{e^{\,jw_{11}|y_1|^2}\right\} \quad E\left\{e^{\,jw_{22}|y_2|^2}\right\}$$

$$= \frac{1}{(1 - jw_{11})(1 - jw_{22})}$$

$$= |I - jW|^{-1}$$

$$= |U'R_{\hat{Z}}^{-1}(\ell,\ell)^{-1}U - jU'\Phi U|^{-1}$$

$$= |U'|^{-1} \; |R_{\hat{Z}}(\ell,\ell)^{-1} - j\Phi|^{-1} \; |U|^{-1} \tag{B.6}$$

where $|\cdot|$ denotes determinant.

From Eq. (B.3),

$$|U'| \; |R_{\hat{Z}}(\ell,\ell)| \; |U| = 1 \quad . \tag{B.7}$$

Thus, from Eqs. (B.2, (B.6), and B.7),

$$M_A(\Phi) = \prod_{\ell=1}^{N_P} |R_{\hat{Z}}(\ell,\ell)|^{-1} \; |R_{\hat{Z}}(\ell,\ell)^{-1} - j\Phi|^{-1} \quad . \tag{B.8}$$

In the signal overcontainment case, there are N_S frequency coefficients containing signal and noise and M frequency coefficients containing only noise, where

$$N_P = N_S + M \quad . \tag{B.9}$$

$M = 0$ if the processing bandwidth is matched to the signal bandwidth. Assume that signal and noise power spectra are flat. Then the auto-spectral density matrices become

$$R_z(\ell,\ell) = \begin{cases} R_{\hat{z}_o} = R_{\hat{N}_o} & \text{, noise only} \\ R_{\hat{z}_1} = R_{\hat{S}_o} + R_{\hat{N}_o} & \text{, signal + noise} \end{cases} \tag{B.10}$$

where R_{N_o} is the auto-spectral density matrix of the noise, and R_{S_o} is the auto-spectral density matrix of the signal. It then follows, from Eqs. (B.8), (B.9), and (B.10), that

$$M_A(\Phi) = |R_{\hat{z}_o}|^{-M} \, |R_{\hat{z}_1}|^{-N_S} \, |R_{\hat{z}_o} - j\Phi|^{-M} \, |R_{\hat{z}_1} - j\Phi|^{-N_S} \tag{B.11}$$

B.2 PROBABILITY DENSITY FUNCTION OF THE SAMPLE AUTO-CORRELATION MATRIX

The probability density function (PDF) of the sample auto-correlation matrix, A, is obtained by computing the inverse Fourier transform of $M_A(\Phi)$. The PDF of A is given by

$$f(A) = \frac{1}{(2\Pi)^4} \int_{D_\Phi} M_A(\Phi) \, e^{-jTR(A\Phi)} \, d\Phi \tag{B.12}$$

where D_Φ is the domain of integration for two-dimensional positive definite Hermitian matrices. Substitute Eq. (B.11) into Eq. (B.12),

$$f(A) = \frac{|R_{\hat{z}_o}|^{-M} \, |R_{\hat{z}_1}|^{-N_S}}{(2\Pi)^4} \int_{D_\Phi} \frac{e^{-jTR(A\Phi)}}{|R_{\hat{z}_o}^{-1} - j\Phi|^{M} \, |R_{\hat{z}_1}^{-1} - j\Phi|^{N_S}} \, d\Phi \tag{B.13}$$

The PDF of A can be computed either by computing the inverse Fourier transform of $M_A(\Phi)$ directly as given in Eq. (B.13), or by using the convolution property of Fourier transforms. At the time of this report, the only successful approach has been to use the convolution property of Fourier transforms. Let $f(A_1)$ be the PDF corresponding to the characteristic function

$$|R_{\hat{z}_o}|^{-M} \; |R_{\hat{z}_o}^{-1} - j\Phi|^{-M}$$

and $f(A_2)$ the PDF corresponding to the characteristic function

$$|R_{\hat{z}_1}|^{-M_S} \; |R_{\hat{z}_1}^{-1} - j\Phi|^{-M_S} \quad .$$

Then,

$$f(A) \;=\; f(A_1) * f(A_2) \tag{B.14}$$

where * denotes convolution. According to Goodman (ref. B1),

$$f(A_1) \;=\; \begin{cases} \dfrac{|A_1|^{M-2}\, e^{-TR(R_{\hat{z}_o}^{-1} A_1)}}{\Pi\;\Gamma(M)\;\Gamma(M-1)\;|R_{\hat{z}_o}|^{M}} & , \; |A_1| \geq 0 \\ 0 & , \; |A_1| < 0 \end{cases} \tag{B.15}$$

and

$$f(A_2) \;=\; \begin{cases} \dfrac{|A_2|^{N_S-2}\, e^{-TR(R_{\hat{z}_1}^{-1} A_2)}}{\Pi^2\Gamma(N_S)\;\Gamma(N_S-1)\;|R_{\hat{z}_1}|^{N_S}} & , \; |A_2| \geq 0 \\ 0 & , \; |A_2| < 0 \end{cases} \tag{B.16}$$

Substitute Eqs. (B.15) and (B.16) into Eq. (B.14).

$$f(A) = \frac{\int_{D_Y} |A-Y|^{N_S-2} |Y|^{M-2} e^{-TR(R_{\hat{z}_1}^{-1}A)} e^{-TR(R_{\hat{z}_o}^{-1}Y)} dY}{\Pi^2 \, \Gamma(N_S) \, \Gamma(N_S-1) \, \Gamma(M) \, \Gamma(M-1) \, |R_{\hat{z}_1}|^{N_S} \, |R_{\hat{z}_o}|^M}$$

$$= \frac{e^{-TR(R_{\hat{z}_1}^{-1}A)}}{\Pi^2 \, \Gamma(N_S) \, \Gamma(N_S-1) \, \Gamma(M) \, \Gamma(M-1) \, |R_{\hat{z}_1}|^{N_S} \, |R_{\hat{z}_o}|^M} \times$$

$$\int_{D_Y} |A-Y|^{N_S-2} |Y|^{M-2} e^{-TR((R_{\hat{z}_o}^{-1} - R_{\hat{z}_1}^{-1}))} dY \qquad \text{(B.17)}$$

where D_Y is the range of integration such that $|A-Y| \geq 0$ and $|Y| \geq 0$. Make a change of variables and use the definitions of the confluent hypergeometric functions of positive definite Hermitian matrices given in Eq. (2.9) of Ref. B2 or Eq. (47) of Ref. B3. Then,

$$f(A) = \frac{|A|^{N_S+M-2} e^{-TR(R_{\hat{z}_1}^{-1}A)}}{\Pi \, \Gamma(N_S+M) \, \Gamma(N_S+M-1) \, |R_{\hat{z}_o}|^M \, |R_{\hat{z}_1}|^{M_S}} \times {}_1\tilde{F}_1(M;M+M_S;\Delta RA) \qquad \text{(B.18)}$$

where

$$\Delta R = R_{\hat{z}_1}^{-1} - R_{\hat{z}_o}^{-1} \qquad \text{(B.19)}$$

and ${}_1\tilde{F}_1(\cdot;\cdot;\cdot)$ is the confluent hypergeometric function of matrix argument. According to Eq. (1.3) of Ref. B4, ${}_1\tilde{F}_1(\cdot;\cdot;\cdot)$ can be expressed as an infinite sum of confluent hypergeometric functions of a single dimensional variable. Thus,

$$
{}_1\tilde{F}_1(M;\ M+M_S;\ \Delta R\ A) =
$$

$$
\sum_{k=0}^{\infty} \frac{(-1)^k\ (M)_k (N_S)_k\ |\Delta R\ A|^k}{(M+M_S-\frac{1}{2})_k\ (M+M_S)_{2k}\ k!}\ {}_1F_1\left(M+k;\ M+M_S-2k;\ TR(\Delta R\ A)\right) \quad (B.20)
$$

where

$$
(\alpha)_x = \frac{\Gamma(\alpha + x)}{\Gamma(\alpha)} \quad .
$$

Therefore,

$$
f(A) = \frac{e^{-TR(R_{\hat{z}_1}^{-1}\ A)}}{\Pi\ \Gamma(N_S+M)\ \Gamma(N_S+M-1)\ |R_{\hat{z}_1}|^{N_S}\ |R_{\hat{z}_o}|^M} \times
$$

$$
= \sum_{k=0}^{\infty} \frac{(-1)^k\ (M)_k (N_S)_k\ |\Delta R|^k\ |A|^{M+N_S+k-2}}{(M+N_S-\frac{1}{2})_k\ (M+N_S)_{2k}\ k!} \times
$$

$$
{}_1F_1\left(M+k;\ M+N_S + 2k;\ TR(\Delta R\ A)\right) \quad . \quad (B.21)
$$

B.3 CUMULATIVE AND PROBABILITY DENSITY FUNCTIONS

The probability density function (PDF) of the sample magnitude-squared correlation coefficient (ρ^2) is obtained from the PDF of the sample auto-correlation matrix given in Eq. (B.21) by performing a change of variables and integrating out auxiliary variables. Let

$$A = \begin{bmatrix} a_{11} & a_{12} \\ a_{12}^* & a_{22} \end{bmatrix} \tag{B.22}$$

Let

$$a_{12} = \sqrt{a_{11}a_{22}}\ \rho\, e^{j\theta} \tag{B.23}$$

where ρ is the sample correlation coefficient. Then

$$\begin{aligned} f(A) &= f(a_{11}, a_{22}, a_{12}) \\ &= |a_{12}|\ f(a_{11}, a_{12}, |a_{12}|, \theta) \\ &= a_{11}\ a_{12}\ \rho\ f(a_{11}, a_{22}, \rho, \theta) \\ &= \frac{a_{11}\ a_{12}}{2}\ f(a_{11}, a_{22}, \rho^2, \theta) \quad . \end{aligned} \tag{B.24}$$

The PDF of the sample MSCC becomes

$$f(\rho^2) = \frac{1}{2} \int_0^\infty \int \int_{-\Pi}^{\Pi} a_{11}a_{22}\ f(a_{11}, a_{22}\ \rho^2, \theta)\ d\theta\ da_{11}\ da_{22}\ . \tag{B.25}$$

All that remains to derive $f(\rho^2)$ is to compute Eq. (B.25) using Eqs. (B.21) and (B.24). However, before proceeding, it is necessary to define the form of the quto-spectral density matrices. It is assumed that the noise is spatially uncorrelated. Then the auto-spectral density matrices defined in Eq. (B.10) become

$$R_{\hat{z}_o} = R_{\hat{N}_o} = \begin{bmatrix} N_{01} & 0 \\ 0 & N_{02} \end{bmatrix} \tag{B.26}$$

$$R_{\hat{S}_o} = \begin{bmatrix} S_{01} & \sqrt{S_{01}S_{02}}\,\rho_S\, e^{j\theta_S} \\ \sqrt{S_{01}S_{02}}\,\rho_S e^{-j\theta_S} & S_{02} \end{bmatrix} \tag{B.27}$$

and

$$R_{\hat{z}_1} = \begin{bmatrix} \sigma_1^2 & \sigma_{12} \\ \sigma_{12}^* & \sigma_2 \end{bmatrix} = \begin{bmatrix} \sigma_1^2 & \sigma_1\sigma_2\rho_T e^{j\theta} \\ \sigma_1\sigma_2\rho_T e^{-j\theta} & \sigma_2^2 \end{bmatrix}$$

$$= \begin{bmatrix} S_{01} + N_{01} & \sqrt{S_{01}S_{02}}\;\rho_S\; e^{j\theta_S} \\ \sqrt{S_{01}S_{02}}\;\rho_S\; e^{-j\theta_S} & S_{02} + N_{02} \end{bmatrix} \tag{B.28}$$

where N_{o_k} is the noise spectral density in channel k, S_{o_k} is the signal spectral density in channel k. ρ_S is the true correlation coefficient between the signal components, θ_S is the phase of the true signal correlation, ρ_T is the true correlation coefficient between the two channels, and θ is the phase of the true correlation between the channels. From Eq. (B.28), it follows that the true MSCC is

$$\rho_T^2 = \frac{SNR_1\ SNR_2}{(SNR_1)\ (SNR_2 + 1)}\ \rho_S^2 \tag{B.29}$$

where

$$SNR_k = S_{o_k} / N_{o_k} \tag{B.30}$$

is the in-band signal-to-noise ratio (SNR) for channel k. SNR_k is the actual in-band SNR because the spectra are flat.

With the above definitions, it is easily shown that

$$|R_{\hat{z}_1}| = (S_{01}+N_{01})\ (S_{02}+N_{02})\ (1 - \rho_T^2) \tag{B.31a}$$

$$|R_{\hat{z}_0}| = N_{01}\ N_{02} \tag{B.31b}$$

$$|\Delta R| = \frac{SNR_1\ SNR_2\ (1-\rho_S^2)}{|R_{\hat{z}_1}|} \tag{B.31c}$$

$$R_{\hat{z}_o}^{-1} = \begin{bmatrix} c_{11} & 0 \\ 0 & c_{22} \end{bmatrix} = \begin{bmatrix} 1/N_{01} & 0 \\ 0 & 1/N_{02} \end{bmatrix} \tag{B.31d}$$

$$R_{\hat{z}_1}^{-1} = \begin{bmatrix} b_{11} & b_{12} \\ b_{12}^* & b_{22} \end{bmatrix}$$

$$= \begin{bmatrix} \sigma_2^2 & -\sigma_1\sigma_2\rho_T e^{j\theta} \\ \sigma_1\sigma_2\rho_T d^{-j\theta} & \sigma_1^2 \end{bmatrix} \times |R_{\hat{z}_1}|^{-1} \quad . \tag{B.31e}$$

Substitute Eq. (B.31) into Eq. (B.21):

$$f(A) = \sum_{k=0}^{\infty} C(k;\ M,N_S)\ g(k,a_{11},a_{22},\rho^2,\phi;\ M,N_S) \tag{B.32}$$

where

$$C(k;\ M,M_S) = \frac{(-1)^k\ (M)_k\ (N_S)_k\ SNR_1^k\ SNR_2^k\ (1-\rho_S^2)^k}{\Gamma(N_S+M)\ \Gamma(N_S+M-1)(M+M_S-\frac{1}{2})_k(M+N_S)_{2k}\ |R_{z_o}|^M|R_{z_1}|^{N_S}} \tag{B.33}$$

and

$$g(k,\ a_{11},\ a_{22},\ \rho^2,\ \theta;\ M,\ N_S) = \frac{|A|^{M+N_S+k-2}}{\Pi}\ {}_1F_1\left(M+k;\ M+N_S+2k;\ TR(\Delta R\ A)\right)\ e^{-TR(R_{z_1}^{-1}A)} \tag{B.34}$$

Integrate Eq. (B.32) according to Eq. (B.25) so that

$$f(\rho^2) = \sum_{k=0}^{\infty} C(k;\ M,N_S)\ f(k,\rho^2;\ M,N_S) \tag{B.35}$$

where

$$f(k,\rho^2;\ M,N_S) = \frac{1}{2}\int_0^{\infty}\int\int_{-\Pi}^{\Pi} a_{11}a_{22}\ g(k,a_{11},a_{22},\rho^2,\theta;\ M,N_S)\ da_{11}da_{22}d\theta \tag{B.36}$$

Using the integral representation for the confluent hypergeometric function given in Eqs. (B.22) and (B.31) and Eq. (13.2.1) of ref. B5, and integrating over θ, we get

$$f(k,\rho^2;\ M,N_S) = \frac{(1-\rho^2)^{M+N_S+k-2}\ \Gamma(M+N_S+2k)}{\Gamma(M+k)\ \Gamma(N_S+k)} \times$$

$$\int_0^1 \int_0^\infty (a_{11}a_{22})^{M+N+k-1} I_o\left(2\sqrt{a_{11}a_{22}}\ |b_{12}|\ \rho\ (1-t)\right) \times$$

$$e^{-a_{11}(b_{11}-\Delta r_{11}t)}\ e^{-a_{22}(b_{22}-\Delta r_{22}t)}\ t^{M+k-1}\ (1-t)^{N_S+k-1}\ da_{11}da_{22}dt$$

(B.37)

Expand the Bessel function in a power series and integrate over a_{11} and a_{22}. Eq. (B.37) becomes

$$f(k,\rho^2;\ M,N_S) = \frac{(1-\rho^2)^{M+N_S+k-2}\ \Gamma(M+N_S+2k)}{\Gamma(M+k)\ \Gamma(N_S+k)} \times$$

$$\sum_{\ell=0}^{\infty} \frac{|b_{12}|^{2\ell}\ \rho^{2\ell}}{|\ell!|^2}\ \Gamma(M+N_S+k+\ell)^2 \times$$

$$\int_0^1 \frac{t^{M+k-1}\ (1-t)^{N_S+k+2\ell-1}}{\left((b_{11}-\Delta r_{11}t)\ (b_{22} - \Delta r_{22}t)\right)^{M+N_S+k+\ell}}\ dt \qquad (B.38)$$

According to Eqs. (3.21.1) and (9.183.1) of Ref. B6,

$$\int_0^1 \frac{t^{M+k-1}\,(1-t)^{N_S+k+2\ell-1}}{\left(b_{11}-\Delta r_{11}t)\,(b_{22}-\Delta r_{22}t)\right)^{M+N_S+k+\ell}}\,dt \quad =$$

$$\frac{\Gamma(N_S+k+2\ell)\;\Gamma(N_S+k)}{\Gamma(M+N_S+2k+2\ell)(b_{11}b_{22})^{M+N_S+k+\ell}}\quad \left(\frac{b_{11}}{c_{11}}\right)^{M+k} \quad \times$$

$${}_3F_1\left[M+k,-(M+N),M+N+k+\ell;\; M+N+2k+2\ell;\; 1-\frac{b_{11}}{c_{11}},\; \frac{\left(c_{11}/b_{11}\right)-\left(c_{22}/b_{21}\right)}{c_{11}/b_{11}}\right] \qquad (B.39)$$

where

$${}_3F_1(\alpha,\beta,\gamma;\;\theta;\;x,y) \quad = \quad \sum_{m,n=0}^{\infty}\frac{(\alpha)_{m+n}(\beta)_m(\gamma)_n}{(\theta)_{m+n}\;m!\;n!}\,x^m y^n \qquad (B.40)$$

Substitute Eq. (B.27), (B.28), (B.31), (B.32), (B.33), (B.38), and (B.39) into Eq. (B.35). Then

$$f(\rho^2|\rho_T^2,M,N_S) \quad = \quad \sum_{k=0}^{\infty} D(k;M,N_S)\left(SNR_1SNR_2(1-\rho^2)\right)^k\; f(\rho^2|k) \qquad (B.41a)$$

where

$$f(\rho^2|k) = (1-\rho^2)^{M+N_S+k-2}(1-\rho_T^2)^{M+N_S}\frac{R_2^M}{R_1^k} \times$$

$$\sum_{\ell=0}^{\infty}(\rho^2\rho_T^2)^{\ell}A_k(\ell)\ {}_3F_1\Big[M+k,\ -(M+N_S),\ M+N_S+k+\ell;\ M+N_S+2k+2\ell;$$

$$1-\frac{1}{R_1(1-\rho_T^2)},\ \ 1-R_2/R_1\Big] \tag{B.41b}$$

$$D(k;\ M,N_S) = \frac{(-1)^k\ (M)_k\ (N_S)_k}{(M+N_S-\frac{1}{2})_k} \tag{B.41c}$$

$$A_k(\ell) = \frac{\Gamma(M+N_S+2k)\ \Gamma(N+N_S+k+\ell)^2\ \Gamma(N_S+k+2\ell)}{\Gamma(M+N_S)\ \Gamma(M+N_S-1)\ \Gamma(N_S+k)\ \Gamma(N+N_S+2k+2\ell)\ (M+N_S)_{2k}\ (\ell!)^2} \tag{B.41d}$$

$$R_m = SNR_m + 1 \quad \text{for } m = 1 \text{ or } 2 \tag{B.41e}$$

It should be noted that if the SNRs in each channel are equal, $SNR_1 = SNR_2$, and

$${}_3F_1\Big(M+k,\ -(M+N_S),\ M+N_S+k+\ell;\ M+N_S+2k+2\ell; 1-\frac{1}{R_1(1-\rho_T^2)},\ 1\ \frac{R_2}{R_1}\Big) =$$

$${}_2F_1\Big(M+k,\ -(M+N_S);\ M+N_S+2k+2\ell;\ 1-\frac{1}{R_1(1-\rho_T^2)}\Big) \tag{B.42}$$

Finally, the cumulative density function is defined as

$$F(\rho_t^2|\rho_T^2,M,N_S) = \int_0^{\rho_t^2} f(\rho^2|\rho_T^2,M,N_S)\ d\rho^2 \tag{B.43}$$

AD-A108 762 ANALYTICAL TECHNOLOGY APPLICATIONS CORP SUNNYVALE CA F/G 12/1
AMBIGUITY SURFACE STATISTICS AND OVERCONTAINMENT.(U)
SEP 81 J LAPOINTE N00014-80-C-0698
UNCLASSIFIED ATAC-SV8007-1 NL

2 OF 2
AD A
108762

END
DATE
FILMED
02-82
DTIC

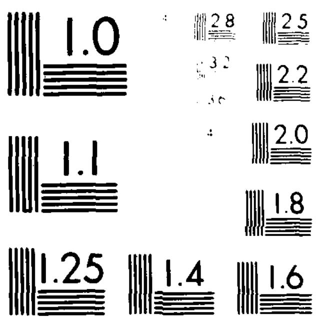

MICROCOPY RESOLUTION TEST CHART

Substitute Eq. (B.41) into Eq. (B.43). Then

$$F(\rho_t^2|\rho_T^2,M,N_S) =$$

$$\sum_{k=0}^{\infty} D(k;M,N_S) \left(SNR_1 SNR_2 (1-\rho_S^2)\right)^k F(\rho_t^2|k) \qquad \text{(B.44a)}$$

where

$$F(\rho_t^2|k) = (1-\rho_T^2)^{M+N_S} \frac{R_2^M}{R_1^k} \sum_{\ell=0}^{\infty} \rho_T^{2\ell} B_k(\ell)\, I_{\rho_t^2}(\ell+1, M+N_S+k-1) \times$$

$$_3F_1\left(M+k,\ -(M+N_S),\ M+N_S+k+\ell;\ M-N_S+2k+2\ell;\ 1-\frac{1}{R_1(1-\rho_T^2)},\ 1-\frac{R_2}{R_1}\right)$$

$$\text{(B.44b)}$$

$$B_k(\ell) = \frac{\Gamma(M+N_S+2k)\ \Gamma(M+N_S+k-1)\ \Gamma(M+N_S+k+\ell)\ \Gamma(M_S+k+2\ell)}{\Gamma(M+N_S)\ \Gamma(M+N_S-1)\ \Gamma(N_S+k)\ \Gamma(M+N_S+2k+2\ell)\ (M+N_S)_{2k}\ \ell!}$$

$$\text{(B.44c)}$$

$$I_x(a,b) = \frac{\Gamma(a+b)}{\Gamma(a)\ \Gamma(b)} \int_0^x t^{a-1}\ 1-t)^{b-1}\, dt \qquad \text{(B.44d)}$$

is the incomplete Beta function.

References for Appendix B

B1 N.R. Goodman, "Statistical Analysis Based on a Certain Multivariate Complex Gaussian Distribution (an Introduction)," Annals of Math. Stat., vol. 34, 1963, pp. 152-177.

B2 C.S. Herz, "Bessel Functions of Matrix Argument," Annals of Math. Stat., vol. 61, May 1955, pp. 474-523.

B3 A.T. Jones, "Distributions of Matrix Variates and Latent Roots Derived from Normal Samples," Annals of Math. Stat., vo. 35, 1964, pp. 475-501.

B4 R.J. Muirhead, "Expressions for Some Hypergeometrid Functions of Matrix Argument with Applications," J. Multivariate Analysis, vol. 5, 1975, pp. 283-293.

B5 M. Abramowitz and I.A. Stegun (eds.), Handbook of Mathematical Functiuons with Formulas, Graphs, and Mathematical Tables, U.S. Government Printing Office, Washington, D.C., 1964.

B6 I.S. Gradshteyn and I.M. Ryzhik, Tables of Integrals, Series and Products, Academic Press, New York, 1965.

Appendix C

CORRELATION COEFFICIENT BETWEEN TWO CELLS OF AN AMBIGUITY SURFACE FOR MATCHED CONTAINMENT

The derivation of the joint probability density function (PDF) of two cells in an ambiguity surface and the correlation coefficient between cells in an ambiguity surface is presented in this appendix for the matched containment case under conditions of known but flat power spectra for the signal and noise. The joint PDF of two cells is derived in Section C.1. The correlation coefficient is computed in Section C.2.

C.1 JOINT PROBABILITY DENSITY FUNCTION

Let $\hat{Z}(\ell)$ be a three-dimensional zero mean complex Gaussian random column vector at frequency ℓ with auto-spectral density matrix $\hat{R}_z$ for $\ell = 1,\ldots,N_P$ with elements $\hat{z}_k(\ell)$. Assume that $\hat{Z}(\ell)$ is independent of $Z(k)$ for $k \neq \ell$. The sample auto-covariance matrix of the data is

$$A = \sum_{\ell=1}^{N_P} Z(\ell)\, Z'(\ell) \qquad \text{(C.1)}$$

where ' denotes complex conjugate. The PDF of A is the complex Wishart PDF (Ref. C1) given by

$$f(A) = \begin{cases} \dfrac{|A|^{N_P-3}\, e^{-TR(R_{\hat{z}}^{-1}A)}}{\Pi^3\, \Gamma(N_P)\, \Gamma(N_P-1)\, \Gamma(N_P-2)\, |R_{\hat{z}}|^{N_P}} & , |A| \geq 0 \\ 0 & , |A| < 0 \end{cases} \qquad \text{(C.2)}$$

Let

$$A = \begin{bmatrix} a_{11} & a_{12} & a_{13} \\ a_{12}^{*} & a_{22} & a_{23} \\ a_{13}^{*} & a_{23}^{*} & a_{33} \end{bmatrix} \qquad \text{(C.3a)}$$

and

$$a_{mn} = \sqrt{a_{mm} a_{nn}} \; \hat{\rho}_{mn} \qquad \text{for } m,n = 1,2,3 \qquad \text{(C.3b)}$$

$$\hat{\rho}_{mn} = \rho_{mn} \, e^{j\theta_{mn}} \qquad \text{(C.3c)}$$

where ρ_{nm} is the sample corrlation coefficient between $\hat{z}_n(\ell)$ and $\hat{z}_m(\ell)$ and θ_{mn} is the phase of a_{mn}.

It is necessary to derive the joint PDF of ρ_{13}^2 and ρ_{23}^2 in order to compute the correlation coefficient. This can be accomplished by a change of variables in Eq. (C.2) and integrating out the auxiliary variables.

Consider the following transformation.

$$A = A_D \, P \, A_D$$

where

$$A_D = \begin{bmatrix} \sqrt{a_{11}} & 0 & 0 \\ 0 & \sqrt{a_{23}} & 0 \\ 0 & 0 & \sqrt{a_{33}} \end{bmatrix} \qquad \text{(C.4a)}$$

and

$$P = \begin{bmatrix} 1 & \hat{\rho}_{12} & \hat{\rho}_{13} \\ \hat{\rho}^2_{12} & 1 & \hat{\rho}^2_{23} \\ \hat{\rho}^*_{13} & \hat{\rho}^*_{23} & 1 \end{bmatrix} \qquad \text{(C.4b)}$$

Then

$$f(A) = f(A_D^2, P) \quad . \qquad \text{(C.5)}$$

Now it is possible to find an upper triangular positive definite matrix, T, such that

$$P = T\,T' \qquad \text{(C.6)}$$

where the diagonal elements are positive (Ref. C1). Then

$$T = \begin{bmatrix} t_{11} & t_{12} & t_{13} \\ 0 & t_{22} & t_{23} \\ 0 & 0 & t_{33} \end{bmatrix} \qquad \text{(C.7)}$$

where $t_{\ell\ell} > 0$ for $\ell = 1,2,3$. Substitute Eq. (C.7) into Eq. (C.6) and solve for the $t_{\ell k}$'s.

$$t_{11} = 1 \qquad \text{(C.8a)}$$

$$t_{12} = \hat{\rho}_{12} \qquad \text{(C.8b)}$$

$$t_{13} = \hat{\rho}_{13} \qquad \text{(C.8c)}$$

$$t_{22} = \sqrt{1 - |t_{12}|^2} \qquad \text{(C.8d)}$$

$$t_{23} = \frac{\hat{\rho}_{23} - t^*_{12} t_{13}}{t_{22}} \qquad \text{(C.8e)}$$

$$t_{33} = \sqrt{1 - |t_{23}|^2 - |t_{13}|^2} \qquad \text{(C.8f)}$$

The Jacobian is easily shown to be $(1 - |t_{12}|^2)$. Therefore,

$$f(A) = f(A_D^2,T)\,(1 - |t_{12}|^2) \quad . \qquad \text{(C.9)}$$

According to Eq. (C.8), ρ_{12} and ρ_{13} are directly related to t_{12} and t_{13}. Therefore,

$$f(\rho_{12}^2,\rho_{13}^2) = f\left(|t_{12}|^2, |t_{13}|^2\right) \quad . \qquad \text{(C.10)}$$

The derivation of the joint density between ρ_{12}^2 and ρ_{13}^2 is reduceable to computing the joint density between $|t_{12}|^2$ and $|t_{13}|^2$. Let

$$R_{\hat{z}}^{-1} = Q = \{q_{\ell k}\} \quad \text{for } \ell,k = 1,2,3 \qquad \text{(C.11a)}$$

where

$$q_{\ell k} = |q_{\ell k}|\, e^{j\phi_{\ell k}} \quad . \qquad \text{(C.11b)}$$

It then follows Eqs. (C.11) and (C.9) that

$$f(a_{11},a_{22},a_{33},|t_{12}|,|t_{13}|,|t_{23}|,\omega_{12},\omega_{13},\omega_{23}) =$$

$$\frac{(a_{11}a_{22}a_{33})^{N_p-1}\,|t_{12}||t_{13}||t_{23}|(1-|t_{23}|^2-|t_{13}|^2)^{N_p-3}(a-|t_{12}|^2)^{N_p-2}}{\Pi^3\,\Gamma(N_p)\,\Gamma(N_p-1)\,\Gamma(N_p-2)\,|R_{\hat{z}}|^{N_p}} \times$$

$$\exp\{-2(\sqrt{a_{11}a_{22}}\,|t_{12}||q_{12}|\cos(\omega_{12}-\phi_{12}) +$$

$$\sqrt{a_{11}a_{33}}\,|t_{13}||q_{13}|\cos(\omega_{13}-\phi_{13}) +$$

$$\sqrt{a_{22}a_{33}}\,(|t_{13}||t_{12}||q_{23}|\cos(\omega_{13}-\omega_{12}-\phi_{23}) +$$

$$\sqrt{1 - |t_{12}|^2}\,|t_{23}||q_{23}|\cos(\omega_{23}-\phi_{23})))\} \qquad \text{(C.12)}$$

where $\omega_{\ell k}$ is the phase angle of $t_{\ell k}$, $\ell \neq k$. Integrating out the phase angles and using the Neumann addition formula, one gets

$$f(a_{11}, a_{22}, a_{33}, |t_{12}|, |t_{13}|, |t_{23}|) =$$

$$\frac{8(a_{11}a_{23}a_{33})^{N_p-1} |t_{12}||t_{13}||t_{23}|(1-|t_{23}|^2-|t_{13}|^2)^{N_p-3}(1-|t_{12}|^2)^{N_p-2}}{\Gamma(N_p)\ \Gamma(N_p-1)\ \Gamma(N_p-2)\ |R_z|^{N_p}} \times$$

$$\exp\{-(a_{11}q_{11} + a_{22}q_{22} + a_{33}q_{33})\} \times$$

$$I_o(2\sqrt{a_{22}a_{33}}\sqrt{1-|t_{12}|^2}\ |t_{23}||q_{23}|) \sum_{k=0}^{\infty} \epsilon_k I_k(\sqrt{a_{11}a_{33}}\ |t_{13}||q_{13}|) \times$$

$$I_k(2\sqrt{a_{22}a_{33}}\ |t_{13}||t_{12}||q_{23}|)\ I_k(2\sqrt{a_{11}a_{22}}\ |t_{12}||q_{12}|) \times$$

$$\cos k(\phi_{12} + \phi_{23} - \phi_{13}) \qquad \text{(C.13)}$$

where $\epsilon_o = 1$, $\epsilon_k = 1$ for $k = 1,2,3\ldots$. Expand

$$I_o(2\sqrt{a_{22}a_{33}}\ \sqrt{1 - |t_{12}|^2}\ |t_{23}|\ |q_{23}|)$$

and integrate out $|t_{23}|$.

$$f(a_{11},a_{22},a_{33},|t_{12}|,|t_{13}|) =$$

$$\frac{4(a_{11}a_{22}a_{33})^{N_p-1}|t_{12}||t_{13}|(1-|t_{12}|^2)^{N_p-2}(1-|t_{13}|^2)^{N_p-2}}{\Gamma(N_p)\,\Gamma(N_p-1)\,|R_z|^{N_p}} \times$$

$${}_0F_1(N-1;\ a_{22}a_{33}(1-|t_{12}|^2)(1-|t_{13}|^2)\,|q_{33}|^2) \times$$

$$\exp\{-(a_{11}q_{11}+a_{22}q_{22}+a_{33}q_{33})\} \times$$

$$\sum_{k=0}^{\infty}\{\ e_k I_k(2\sqrt{a_{11}a_{33}}\,|t_{13}|\,|q_{23}|) \times$$

$$I_k(2\sqrt{a_{22}a_{33}}\,|t_{12}||t_{13}||q_{33}|)\ I_k(2\sqrt{a_{11}a_{22}}\,|t_{12}||q_{12}|) \times$$

$$\cos k\,(\phi_{12}+\phi_{23}-\phi_{13})\} \quad . \tag{C.14}$$

Expand the Bessel functions in an infinite series; integrate out a_{11}, a_{22}, a_{33}; and make a change of variables to ρ_{12}^2 and ρ_{13}^2. Then

$$f(\rho_{12}^2,\rho_{13}^2) = \frac{(1-\rho_{12}^2)^{N_p-1}(1-\rho_{13}^2)^{N_p-2}}{\Gamma(N_p)\,\Gamma(N_p-1)\,|R_z|^{N_p}\,(q_{11}q_{22}q_{33})^{N_p}} \times$$

$$\sum_{k=0}^{\infty} A(k)\cos k\,(\phi_{12}+\phi_{23}-\phi_{13}) \tag{C.15a}$$

where

$$A(k) = (\rho_{12}^2 \rho_{13}^2 \rho_{T_{12}} \rho_{T_{13}} \rho_{T_{23}})^k \times$$

$$\sum_{\ell,n,p=0}^{\infty} \frac{(\rho_{12}^2 \rho_{T_{12}}^2)^n (\rho_{13}^2 \rho_{T_{13}}^2)^\ell (\rho_{12}^2 \rho_{13}^2 \rho_{T_{23}}^2)^p}{\ell!\ n!\ p!} \times$$

$$\frac{\Gamma(N_p+k+\ell+n)\ \Gamma(N_p+k+\ell+p)\ \Gamma(N_p+k+n+p)}{\Gamma(k+n+1)\ \Gamma(k+\ell+1)\ \Gamma(k+p+1)} \times$$

$$_2F_1\left(N_p+k+\ell+p,\ N_p+k+n+p;\ N_p-1;\ (1-\rho_{12}^2)\ (1-\rho_{13}^2)(\rho_{T_{23}}^2)\right) \quad \text{(C.15b)}$$

$\rho_{T_{pn}}^2$ is the magnitude squared of the true correlation coefficient between $\hat{z}_p(\ell)$ and $\hat{z}_n(\ell)$ and $_2F_1(\cdot,\cdot;\ \cdot,\cdot)$ is the confluent hypergeometric function.

C.2 CORRELATION COEFFICIENT

The correlation coefficient between the magnitude-squared sample correlation coefficients ρ_{12}^2 and ρ_{13}^2 is defined as

$$\rho = \frac{E\left(\rho_{12}^2 \rho_{13}^2\right) - E\left(\rho_{12}^2\right) E\left(\rho_{13}^2\right)}{\sqrt{\sigma^2 \rho_{12}^2 \; \sigma^2 \rho_{13}^2}} \tag{C.16}$$

where $E(\cdot)$ denotes statistical expectation. According to Ref. C3,

$$E\left(\rho_{\ell k}^{2m}\right) = \left(1 - \rho_{T_{\ell m}}^2\right)^{N_p - 1} \frac{\Gamma(N_p)\,\Gamma(m+1)}{\Gamma(N_p + m)} \times$$

$$_3F_2\left(m+1, N_p, N_p;\ m+N_p,\ 1;\ \rho_{T_{\ell k}}^2\right) \tag{C.17a}$$

$$\sigma^2_{\rho_{\ell k}^2} = E\left(\rho_{\ell k}^4\right) - \left(E\left(\rho_{\ell k}^2\right)\right)^2 \tag{C.17b}$$

where $\rho_{T_{\ell k}}^2$ is the magnitude squared of the true correlation coefficients. All that remains is to compute the m^{th} joint moment.

$$E\left(\left(\rho_{12}^2 \rho_{13}^2\right)^m\right) = \int_0^1 \int \rho_{12}^{2m}\, \rho_{13}^{2m}\, f\left(\rho_{12}^2, \rho_{13}^2\right) d\rho_{12}^2 d\rho_{13}^2 \quad . \tag{C.18}$$

Substitute Eq. (C.15) into Eq. (C.18). It then becomes necessary to compute

$$\int_0^1 \int \rho_{12}^{2(k+m+n+p)}\, \rho_{13}^{2(k+\ell+m+p)} \left(1 - \rho_{12}^2\right)^{N_p - 2} \left(1 - \rho_{13}^2\right)^{N_p - 2} \times$$

$$_2F_1\left(N_p + k + \ell + p,\ N_p + k + n + p;\ N_p - 1;\right.$$

$$\left.\left(1 - \rho_{12}^2\right)\left(1 - \rho_{13}^2\right) \rho_{T_{23}}^2\right) d\rho_{12}^2\, d\rho_{13}^2 \quad . \tag{C.19}$$

According to Eqs. (7.512.11) and (7.512.12) of Ref. C2, Eq. (C.19) becomes

$$\frac{\Gamma(k+m+n+p+1)\ \Gamma(k+\ell+m+p+1)\ \Gamma(N_p-1)^2}{\Gamma(N_p+k+m+n+p)\ \Gamma(N_p+k+\ell+m+p)} \times$$

$$ {}_3F_2\left(N_p-1,\ N_p+k+\ell+p,\ N_p+k+n+p;\ N+k+m+p+1,\ N_p+k+m+n+p;\ \rho^2_{T_{23}}\right) \qquad \text{(C.20)}$$

The joint moment then becomes

$$E\left((\rho^2_{12}\rho^2_{13})^m\right) =$$

$$\frac{\left(1 + 2\rho_{T_{12}}\rho_{T_{13}}\rho_{t_{23}} \cos\left(\phi_{12}+\phi_{23}-\phi_{13}\right) - \rho^2_{T_{12}} - \rho^2_{T_{13}} - \rho^2{}_{T_{23}}\right)^{2N_p}}{\Gamma(N_p)\left((1-\rho^2_{T_{12}})(1-\rho^2_{T_{13}})(1-\rho^2_{T_{23}})\right)^{N_p}} \times$$

$$\sum_{k=0}^{\infty} B(k) \cos k \left(\phi_{12} + \phi_{23} - \phi_{13}\right) \qquad \text{(C.21a)}$$

where

$$B(k) = \sum_{\ell,n,p=0}^{\infty} \frac{\rho^{k+2\ell}_{T_{12}}\ \rho^{k+2n}_{T_{13}}\ \rho^{k+2p}_{T_{23}}}{\ell!\ n!\ p!} \times$$

$$\frac{\Gamma(N_p+k+\ell+n)\ \Gamma(N_p+k+\ell+1)\ \Gamma(N_p+k+n+p)\ \Gamma(k+m+n+p+1)\ \Gamma(k+\ell+m+p+1)}{\Gamma(k+n+1)\ \Gamma(k+\ell+1)\ \Gamma(k+p+1)\ \Gamma(N_p+k+m+n+p)\ \Gamma(N_p+k+\ell+m+p)} \times$$

$$ {}_3F_2\left(N_p-1,\ N_p+k+\ell+p,\ N_p+k+n+p;\ N_p+k+\ell+m+p+1,\ N_p+k+m+n+p;\ \rho^2_{T_{23}}\right)$$

(C.21b)

The correlation coefficient is then obtained by substituting Eqs. (C.17) and (C.21) into Eq. (C.16).

In the case of oversampled noise, the spatial correlation coefficients, $\rho^2_{T_{12}}$ and $\rho^2_{T_{13}}$, are zero. The m^{th} moment becomes

$$E\left((\rho_{12}^2\rho_{13}^2)^m\right) =$$

$$(1-\rho_{T_{23}}^2)^{N_p} \sum_{k=0}^{\infty} \frac{\rho_{T_{23}}^{2k}}{(k!)^2} \left(\frac{\Gamma(k+m+1)\,\Gamma(N_p+k)}{\Gamma(N_p+k+m)}\right)^2 \times$$

$$ {}_3F_2\left(m,\ N_p-1,\ N_p+k;\ N_p+k+m,\ N_p+k+m;\ \rho_{T_{23}}^2\right) \quad . \qquad (C.21)$$

The mean and variance of $\rho_{\ell k}^2$ are Y_{N_p} and $(N_p-1)/\left(N_p^2(N_p+1)\right)$, respectively.

Appendix C References

C1 N.R. Goodman, "Satistical Analysis Based on a Certain Multivariate Complex Gaussian Distribution (an Introduction)," Annals of Math. Stat., vol. 34, 1963, pp. 152-177.

C2 I.S. Gradshteyn and I.M. Ryzhik, Tables of Integrals, Sines and Products, Academic Press, New York, 1965.

C3 G.C. Carter, Estimation of the Magnitude-Squared Coherence Function (Spectrum), Report No. 7R4343, Naval Underwater Systems Center, New London, Conn., May 1972.

Distribution List

	No. of Copies
Defense Technical Information Center Bldg. 3, Cameron Station Alexandria, VA 22314	12
Office of Naval Research Department of the Navy Arlington, VA 22217 Attn: Mr. J. Smith (Code 411SP)	2
Office of Naval Research Branch Office Western Regional Office 1030 East Green Street Pasadena, CA 91106	1
Director Naval Research Laboratory Washington, D.C. 20375	
Attn: Code 2627	6
Naval Ocean Systems Center 271 Catalina Boulevard San Diego, CA 92152	
Attn: Dr. J. McCarthy (Code 7134)	1
Attn: Dr. C. Persons (Code 7133)	1
Naval Underwater Systems Center New London Laboratory New London, CT 06320	
Attn: Dr. G. Carter (Code 3331)	1
Attn: Dr. A. Nuttall (Code 3302)	1
Naval Sea Systems Command Navy Department Washington, D.C. 20360	
Attn: Mr. D. Porter (Code 63R11)	1
Naval Electronic Systems Command National Center Bulding No. 1 Washington, D.C. 20360	
Attn: Mr. J. Schuster (Code 612)	1
Acoustic Research Center Unit 1 Moffett Field, CA 94035	
Attn: Mr. R. Trueblood	1

Distribution List (cont.)

	No. of Copies
Naval Surface Weapons Center White Oak Laboratory Silver Spring, MD 20910 Attn: Code U-20	1
Defense Advanced Research Projects Agency 1400 Wilson Boulevard Arlington, VA 22209 Attn: Dr. T. Kooij	1
ENSCO, Inc. 5400 Port Royal Road Springfield, VA 22151 Attn: Dr. L. Parish	1
ENSCO, Inc. 1183 Bordeaux Drive, Suite 1 Sunnyvale, CA 94086 Attn: Mr. G. Godshalk	1
Orincon, Inc. 3366 North Torrey Prines Court Suite 320 San Diego, CA 92037 Attn: Dr. R. Himbarger	1
Tetra-Tech, Inc. 1911 N. Fort Meyer Drive Arlington, VA 22204 Attn: Mr. B. Sharkey	1
Bolt Beranek and Newman, Inc. 50 Moulton Street Cambridge, MA 02138 Attn: Mr. S. D. Milligan	1
Adaptronics, Inc. 1750 Meadow Road McLean, VA 22102 Attn: Dr. F. J. Cook	1
Systems Development Corporation P.O. Box 130 Moffett Field, CA 94035 Attn: Mr. P. Budnik	1

Distribution List (cont.)

	No. of Copies
Naval Underwater Systems Center Newport, RI 02840 Attn: Code 352	1
Naval Intelligence Support Center Suitland, MD 20390 Attn: Code 20C	1
Professor Marshall E. Frazer Applied Research Laboratories University of Texas P.O. Box 8029 Austin, TX 78712	1
Professor Donald W. Tufts Department of Electrical Engineering University of Rhode Island Kingston, RI 02881	1
Dr. Benjamin Friedlander Systems Control, Inc. 1801 Page Mill Road Palo Alto, CA 94304	1
Professor E. Masry Department of Applied Physics and Information Science University of California La Jolla, CA 92093	1
Professor M. J. Hinich Department of Economics Virginia Polytechnic Institute and State University Blacksburg, VA 24061	1
Professor S. C. Schwartz Department of Electrical Engineering and Computer Science Princeton University Princeton, NJ 08540	1
Professor Charles B. Bell Department of Biostatistics University of Washington Seattle, Washington 98195	1